DYNAMICS, DISTRIBUTION AND DEVELOPMENT OF SPECIALIZED METABOLISM IN GLANDULAR TRICHOME OF TOMATO AND ITS WILD RELATIVES

By

Zhenzhen Wang

A DISSERTATION

Submitted to
Michigan State University
in partial fulfillment of the requirements
for the degree of

Biochemistry and Molecular Biology - Doctor of Philosophy

2015

ABSTRACT

DYNAMICS, DISTRIBUTION AND DEVELOPMENT OF SPECIALIZED METABOLISM IN GLANDULAR TRICHOME OF TOMATO AND ITS WILD RELATIVES

By

Zhenzhen Wang

Glandular trichomes on the plant surface are specialized epidermal cells which can produce and store a variety of plant specialized metabolites. Specialized phytochemicals produced by trichome are extremely diverse among Solanaceae families and a lot of them have been characterized with the advance of plant omics. Due to their benefits for plant defense system and commercial values, biosynthesis and accumulation of trichome metabolites haven been intensively studied. In this study, analytical chemistry and genetic approaches were integrated to explore the remaining questions about mechanism for the production of specialized metabolites in Solanum trichomes.

In particular, this study included three studies addressing the dynamics, distribution and development of specialized metabolism in glandular trichomes from tomato and its relatives. This first study presented the development of analytical methods to profile localized metabolites in biological tissues through chemical imaging, and application of this method to investigations of glandular trichomes. Using this mass spectrometry imaging method, single-cell metabolic profiling and spatially preserved chemical information was achieved in tomato leaf trichomes for several type of trichome specialized metabolites, including acylsugar, flavonoids and terpenes. This work extended imaging mass spectrometry to specialized epidermal cells without using dissection or tissue fixation for the first time.

The second study described the isotope labeling methodology for tracing specialized metabolites flux in trichomes. In general, an integrated approach combining whole plant 13 CO₂ labeling and data-independent LC-MS quantitative profiling was developed to monitor the metabolic dynamic flux and turnover rate of protective plant specialized metabolites. This analytical strategy is applicable to a wide range of specialized metabolites.

The third study applied the isotopic labeling strategy to discover the dynamics of trichome specialized metabolites accumulation and the effect of developmental stage of tomato leaves. Using flux analysis method, we measured fluctuations in labeling enrichment and metabolite accumulation during different tomato leaf developmental stages, and demonstrated that total acylsugar accumulation reaches a steady state at early stage of development. Evidence was generated to support the concept that degradation of undetected metabolic intermediates provides a key regulatory point in the acylsugar metabolic network offers a new viewpoint for engineering plant metabolic networks for high levels of end product acylsugars. This novel regulation mechanism extends our understanding of catabolic activities of specialized metabolites.

ACKNOWLEDGMENTS

I would like to express the deepest appreciation and thanks to a number of people who have been very supportive during the years of my graduate school and towards finishing this dissertation. First and foremost, a special thanks to my advisor professor A. Daniel Jones for a supportive and patient mentor all the time. Thank you for being available almost 24/7 for any scientific problem we have in the lab, and all the late night and weekend meetings. Thank you for encouraging me on critical thinking and being passionate about my research project all the time. Thank you for truly caring about if the students are happy about their research and course work, with make the mentoring relationship very friendly and memorable. The most important lesson I learn from him is to explore and pursue a career that you feel excited all the time and wish to dedicate yourself with joy and passion. That and only that can make you a cheerful and helpful person to work with. In addition, I admire Dan's high standard on logic writing and telling an attractive scientific story of my research. Without his encouragement and mentoring, I cannot turn the "impossible" labeling project into "incredible" labeling project; turn the "frustrating" research into "fascinating" research. I consider myself very fortunate to have Dan as my mentor for both scientific career and persona life.

I would like to thank my committee member professor Yair Shachar-Hill, professor Gregg Howe, professor Dean DellaPenna and professor Min-Hao Kuo for their guidance and constructive criticism during my entire graduate school research, especially professor Yair Shachar-Hill for providing useful discussions and insights on my labeling project. I would also like to thank our trichome project collaborators from professor Robert Last's group and professor Cornelius Barry's group. It is honor to learn plant genetics and molecular biology

from them and work with them. I also would like to gratefully acknowledge the support the RTSF Mass Spectrometry Core at Michigan State University. My thanks go especially to Lijun Chen and Dr. Scott Smith for being very helpful on suggestion and help for various analyses.

Specially, I would like to extend my thanks to close friends at Michigan State University and beyond. I am glad that I have been working with a group of wonderful members from Dan's lab, especially Dr. Chao Li and Dr. Prabodha Ekanayaka, Chen Zhang, Sujana Pradhan, Xiaoxiao Liu and Afrand Kamali, which made my graduate school life full of memorable happiness. Without their great companion and friendship, graduate school would be difficult and boring. I would also like to make special mentions of Dr. Li Cui, Minyoung So and Dr. Li Zhou. Dr. Jing Ning and Jin Zhang for always being there backup me through the ups and downs of my graduate school life.

In the end, I sincerely thank my parents Yan Wang and Zhigang Wang for unconditional love. Their encouragement on pursing better education and a free life drives me this far from my hometown. My deep thanks go to my husband Long Han. I am very grateful for surviving many years of far separation with him and finally graduate from long distance relationship with his coming to the US. His understanding and tolerance through these years make me a confident, optimistic and open-minded person. Thank you for completing me.

TABLE OF CONTENTS

LIST OF TABLES	viii
LIST OF FIGURES	ix
Chapter 1. Introduction	
1.1 Importance of plant specialized metabolism	2
1.2 Growing interest and challenges in plant specialized metabolites	3
1.3 Solanum trichomes as a model system to study plant specialized metabolites	6
1.4 Introduction to acylsugars	
1.5 Analytical strategies for metabolite profiling and flux measurement	10
1.6 Summary of research	14
REFERENCES	17
Chapter 2. Chemical Imaging of Trichome Specialized Metabolites using Contact Printing	
and Laser Desorption/Ionization Mass Spectrometry	
2.1 Introduction	
2.2 Materials and methods	
2.2.1 Chemicals	
2.2.2 Plants	
2.2.3 Sample preparation	
2.2.3 LDI imaging	
2.2.4 LC/MS analysis	
2.3 Results and discussion	
2.3.1 Contact printing transfer of trichome metabolites	
2.3.2 Whole-leaf imaging using LDI from pencil lead surfaces	
2.3.3 Single-trichome imaging	46
2.3.4 Heterogeneity in localization and quantity of acylsugars in M82 leaf	
trichomes	
2.4 Conclusions	
REFERENCES	55
Chapter 3. Profiling of Stable Isotope Enrichment in Solanum Trichome Specialized	
Metabolites of Using Liquid Chromatography and Multiplexed Nonselective Collision-	
Induced Dissociation	
3.1 Introduction	
3.2 Materials and methods	
3.2.1 Chemicals	
3.2.2 ¹³ C labeling of plants	
3.2.3 Sample preparation	
3.2.4 UHPLC/MS analysis with Multiplexed collision-induced dissociation	
(CID)	67

3.2.5 Data processing	68
3.3 Results and discussion	68
3.3.1 Profiling and characterization of trichome metabolite diversity	68
3.3.2 Labeled acylsugar metabolites	
3.3.3 Enrichment calculation in metabolite Ions	
3.3.4 Assessment of isotope enrichments using Multiplexed CID	83
3.3.5 Advantages of Multiplexed CID for measuring stable isotope	
enrichments	86
3.3.6 Performance evaluation of LC/MS measurements	87
3.3.7 Comparisons of total metabolite and substructure enrichments	89
3.3.8 Comparison of ¹³ C enrichment in six acylsugars and their fragments	90
3.3.9 Labeling of other trichome metabolites species	
3.4 Conclusions	
REFERENCES	96
Chapter 4. Dynamics and Stable Isotope Labeling of Tomato Specialized Metabolites	101
4.1 Introduction	
4.2 Chamber design	107
4.2.1 Hardware setup	108
4.2.2 Power setup	109
4.2.3 System control setup	110
4.3 Methods and experiments	112
4.3.1 Materials and chemicals	112
4.3.2 Hydroponic growth of M82 and IL5-3 plants from seeds	113
4.3.3 ¹³ C Pulse-Chase labeling experiment	114
4.3.4 Leaf dip extract for trichome metabolites	
4.3.5 Quantitative LC-MS analysis and data processing	115
4.4 Results and discussion	
4.4.1 Diversity and accumulation of acylsugars in metabolites profiling	116
4.4.2 Leaf tissues sampled at different developmental stages	117
4.4.3 Rate of acylsugar biosynthesis	118
4.4.4 Rate of biosynthesis in acylsugar substructures	
4.4.5 Rate of acylsugar degradation	124
4.4.6 The effect of leaflet developmental stage on acylsugar metabolism	129
4.5 Conclusions	
REFERENCES	133
Chapter 5. Perspectives for Future Research	138

LIST OF TABLES

Table 2.1. The list of major ions observed in laser desorption/ionization spectra of <i>Solanum habrochaites</i> LA1777 trichome metabolites on pencil-lead-coated glass slides
Table 3.1. ¹³ C enrichments in tomato acylsugar S4:17 and substructure fragments after 5 Days of labeling using ¹³ CO ₂
Table 3.2. ¹³ C enrichments in various ions generated additional acylsugar metabolites extracted from a tomato leaflet after 5 days of labeling with ³ CO ₂ 80
Table 3.3. ¹³ C enrichments in tomatine and rutin metabolites from a tomato leaflet after 5 days of labeling with ³ CO ₂ and then 5 days growing in ambient atmosphere

LIST OF FIGURES

Figure 1.1. Acylsugar structural nomenclatures9
Figure 2.1. Optical images of a <i>S. habrochaites</i> LA1777 leaf showing trichomes on the adaxial (upper) leaf surface and stained type I and type IV trichomes
Figure 2.2. Schematic of the process used for contact printing of glandular trichomes from <i>S. habrochaites</i> LA1777 leaflets for laser desorption/ionization mass spectrometry imaging33
Figure 2.3. Transmitted light optical image of trichomes from the adaxial (upper) leaf surface of <i>S. habrochaites</i> LA1777 transferred to a glass microscope slide by contact printing36
Figure 2.4. The background matrix-assisted laser desorption/ionization (MALDI) and LDI mass spectra of 2,5-dihydroxybenzoic acid, α-cyano-4-hydroxycinnamic acid, and methanol-rinsed pencil lead in positive ion mode
Figure 2.5. LDI mass spectra of trichome extracts from <i>S. habrochaites</i> LA1777 spotted on pencil-lead-coated glass slides using positive ion mode and negative ion mode40
Figure 2.6. LDI mass spectrometry images of selected metabolic ions for contact-printed trichomes from an <i>S. habrochaites</i> LA1777 leaflet on pencil-lead-coated glass slides40
Figure 2.7. The hole-drilling on the leaf surface for validation of LDI metabolite profiling LC/MS and the ratio of the signal from sesquiterpene acid detected
Figure 2.8. Imaging of metabolites from <i>S. habrochaites</i> LA1777 leaf trichomes transferred into the 100 µm and 50 µm TEM grids
Figure 2.9. Mass spectrometry images and spectra of selected ions for <i>S. habrochaites</i> LA1777 trichomes transferred to glassy carbon

Figure 2.10. Reflected light LDI image and fluorescent image of a contact printing of <i>S. habrochaites</i> LA1777 trichomes on a glass slide
Figure 2.11. Localization of acylsugars in <i>S. lycopersicum</i> M82 leaf trichomes using contact printing and LDI imaging from carbon-coated slides
Figure 3.1. The workflow of nontargeted metabolomics approach for nonbiased quantitative assessments of labeling using nonselective multiplexed CID
Figure 3.2. UHPLC-TOF-MS based peak base peak intensity (BPI) chromatograms of (¹³ C labeled and unlabeled control tomato leaf dip extracts
Figure 3.3. Chemical structures of six most abundant acylsugars in extracts of tomato leaflet
Figure 3.4. UHPLC/MS total ion chromatogram (TIC) of leaflet dip extract sampled from <i>S. lycopersicum</i> M82 plant of 9 days post germination
Figure 3.5. Positive-ion mode electrospray ionization mass spectra of C6 containing acylsugars showing fragments generated using non-mass selective collision induced dissociation (CID)
Figure 3.6. Di- and tri- acylsugars with one C5 and one long chain identified in IL11-374
Figure 3.7. [M+formate] isotopologue ions of acylsugar S4:17 from control and 5-day ¹³ CO ₂ -labeled group in tomato leaflet trichome extract
Figure 3.8. Nonselective CID of acylsugar S4:17 and isotopologue distribution in molecular adduct ions and fragment ions
Figure 3.9. Precursor mass selection of labeled S4:17 [M+formate] by data-dependent mass-selective CID

Figure 3.10. Peak area relative standard deviations as a function of average extracted ion chromatogram (XIC) peak area values for all individual isotopologue ions of acylsugar S4:17 generated from 5 days of ¹³ CO ₂ labeling
Figure 3.11. Negative-ion mode mass spectra for tomatine and rutin from ¹³ C-labeled and unlabeled control M82 plants
Figure 4.1. Acylsucrose structure in <i>S. lycopersicum</i> and acyl chain substitution patterns104
Figure 4.2. Front of the labeling chamber and control system
Figure 4.3. Operation of the chamber for labeling experiments
Figure 4.4. Total acylsugar accumulation in M82 and IL5-3 leaf trichomes extracts at early developmental stages
Figure 4.5. Nomenclature for designating compound leaves and individual leaflets118
Figure 4.6. The slower biosynthesis rate of acylsugar from ¹³ CO ₂ in Leaflet A1 from IL5-3 correlated with lower total accumulation levels relative to M82
Figure 4.7. Incorporation of ¹³ C into long chain (C12) and short chain (C5) esters of acylsugars from M82 and IL5-3
Figure 4.8. Decay of ¹³ C content during the chase phase for long chain acylsugar end products S3:22, S4:24 and short chain acylsugar end product S4:17 in M82 and IL5-3124
Figure 4.9. The illustration of pathways for synthesis and degradation of long chain and short chain acylsugars from M82 and IL5-3
Figure 4.10. Decay of ¹³ C content during the chase phase for S3:22 in in younger leaflet trichomes of M82 and IL5-3 of leaflet A1 and C1

Figure 4.11. Accumulation of labeled, unlabeled	d and total acylsugar S3:22 in S. lycop	ersicum
M82 and IL5-3 showing levels in leaflets A1 a	and C1	133

Chapter 1. Introduction

"To such an extent does nature delight and abound in variety that among her trees there is not one plant to be found which is exactly like another; and not only among the plants, but among the boughs, the leaves and the fruits, you will not find one which is exactly similar to another." (Leonardo da Vinci)

1.1 Importance of plant specialized metabolism

Plants share and support this beautiful earth with humans and animals by providing not only nature's delights, but also renewable resources including foods, fuels, fibers, medicines and energy. The participation of the plant kingdom in achieving sustainability enables the earth to continue supporting the growing human population. In addition to advancement of agriculture for food products, a remarkable shift in plant breeding and cultivating practices has occurred over the past century in response to the necessity for various phytochemicals [1]. Engineering plant systems to produce more biochemical compounds has emerged as the driving force for understanding the biochemical and metabolic networks of plants [2, 3].

A great portion of the phytochemicals that we care about consists of specialized metabolites, which includes compounds humans use as medicines, drugs, flavorings, and cosmetics [4]. Plant specialized metabolites may facilitate primary metabolism for plant growth and development, but they are not like primary metabolites which are universal in the plant kingdom and produced from fundamental metabolic pathways or cycles [5-7]. A well-studied type of plant specialized metabolite is plant hormones, including terpenoids gibberellins, abscisic acid, and brassinosteroids, which regulate metabolic and developmental activities within the cells and tissues so that plants can adapt to changing environments [4, 8]. Beyond plant hormones, a common role of specialized metabolites is functioning in plant defense systems in the constant fight against herbivores, pests and pathogens [9, 10]. In recent decades, numerous studies of natural products have proved that these bioactive compounds are not "non-essential" or "secondary" as previously described in the definition of "secondary metabolites". Instead, these metabolites include valuable molecules that regulate plant growth

and as substances valued by human consumers [4, 11, 12]. A promising route for genetic engineers to develop more sustainable crop species lies in manipulating the synthesis and accumulation of these defensive specialized pathways within plant tissues to substitute for or diminish the use of pesticides [13, 14].

The 2015 Nobel Prize in Physiology or Medicine honored Youyou Tu, the first Chinese Nobel laureate in physiology or medicine and the first citizen of the People's Republic of China to receive the Nobel Prize in natural sciences, for discovering artemisinin (qinghaosu) and dihydroartemisinin from wormwood (Artemisia annua) trichomes. This important medicine is now used to treat malaria and has saved millions of lives. This is certainly a milestone for medicinal science development in China, but definitely not the first or only example showing that plant specialized metabolites remain exceptional sources of drug candidates and hold the promise to fight diseases and alleviate human suffering. In addition, plant specialized metabolites are popular in everyday life as food additives and ingredients including menthol and caffeine. The above reasons drive the expansion of research on plant specialized metabolism.

1.2 Growing interest and challenges in plant specialized metabolites

The exploration of secondary metabolites started with two hundred years of isolation and structure elucidation of active principles of plant-derived drugs, which provided the chemical basis for recent biochemical and genetic mechanistic research on functional and evolutionary aspects of plant secondary metabolism [4]. Starting in the middle of the 20th century, modern multidisciplinary approaches integrating traditional organic chemistry with genetics, biochemistry, and informatics techniques were used to investigate the biochemistry

and functions of plant specialized metabolism [15]. These investigations were soon followed by the first radioactive tracer labeling experiments in the 1950s [16], which revealed some of the biosynthetic pathways responsible for natural product formation. Recent interest has grown to identify the genes that control the production of newly discovered phytochemicals as drug candidates, pesticides and nutritional ingredients. By virtue of the high-throughput characterization and quantification of transcriptomes (mRNAs), proteomes (proteins) and metabolomes (metabolites) of plant tissues and cells, it became possible to define biochemical phenotypes on a large scale with the advent of plant "-omics" research [17, 18]. Such high-throughput analysis hastens the process of discovering the crucial genes needed to engineer biological systems to produce derived bioactive metabolites [19, 20].

One of the great challenges for discovery of genes involved in specialized metabolism is the uniqueness of metabolite classes and their biosynthetic pathways. Unlike central metabolism genes, which are conserved and consistent among species and cell/tissue types, the expression of specialized biosynthetic pathways is diverse and usually species- and/or cell type-specific [21, 22]. The chemical diversity of specialized metabolites among different species suggests complex networks of biosynthetic pathways. This taxonomically-restricted characteristic of plant specialized metabolites has presented barriers to referencing model plant species for investigation of novel metabolic mechanisms. Unlike central metabolism, limited genomic resources are available to investigate specialized metabolism in non-model plants.

Another challenge to investigations of plant specialized metabolism derives from the chemical complexity of the specialized metabolome, even within a single species. The evolutionary diversification of chemicals, enzymes and genes that plants create by gene

duplication is invaluable for plant adaption to changing environments, and is extremely pronounced in specific gene families. For example, divergence of terpene synthase (TPS) genes has created the vast complexity and variation of terpene metabolites and provides a well-defined example of evolutionary diversification of metabolic gene functions in plants [23, 24]. The variation of quantity and isomeric structures of specialized metabolites provides the complexity that must be addressed during phenotyping and gene discovery.

In addition, another challenge for secondary metabolism investigations lies in the dynamics of bioactive metabolites during plant growth and development. These substances are not inert end products but active components that interact with other metabolites and proteins. They can be transferred between compartments, cells, or tissues, turned over into other substances, or degraded upon specific triggers of environmental stress such as the induced production of defense compounds upon herbivore or microbial attack [25]. The catalytic machinery of specialized metabolism can be challenging to predict due to the plasticity and promiscuity of enzymatic reactions [26]. A typical example is the rapid formation and shifting of metabolic channeling metabolon during biosynthesis which is regarded as a tightly controlled mechanism [25, 27]. The lack of data regarding physiological levels and half-lives of specialized metabolites has led to few convincing reports regarding degradation pathways of specialized metabolites in plants. A rare example is the degradation of the cyanogenic glycoside dhurrin by beta-glucosidase upon tissue disruption by chewing insects. This degradation process releases toxic hydrogen cyanide in Sorghum defense to herbivory [28, 29]. This absence of knowledge regarding dynamics of specialized metabolites motivates a challenging but realistic facet for future research, especially for guiding molecular engineering of plants in medicinal and agricultural applications.

1.3 Solanum trichomes as a model system to study plant specialized metabolites

Trichomes are appendages of epidermal cells on plant surfaces such as leaf and stem. Uni- and multi-cellular trichomes are variable in morphology and cell type among plant species [30]. Glandular trichomes in some members of the Solanaceae (the nightshade family) have the remarkable capacity to synthesize, store, and secrete large quantities of specialized metabolites in different subtypes of glandular trichomes, which are proposed to play a critical role in plant protection against various biotic and abiotic stresses [13, 31]. Because of their remarkable biosynthetic capacity and morphological diversity [32], *Solanum* glandular trichomes provide an excellent model to study complex and specialized metabolic pathways that operate within a simple and accessible developmental structure [13, 19, 31]. In addition, the genus *Solanum* includes many commercially valuable crop species (*e.g.* tomato, pepper, potato, eggplant, and tobacco) with extensive genomic sequence database resources available for functional genomics. Such resources facilitate a system-wide understanding of metabolic networks involved in the development of glandular trichome chemistry.

The types of specialized metabolites produced by glandular trichomes in *Solanum* and other Solanaceous species include terpenes, phenylpropanoids, flavonoids and acylsugars [31]. Most function directly or indirectly in plant defenses. Terpenes, which are derived from assembly and modification of isoprene units, occur widely in plants and microorganisms, and research on terpene diversity and corresponding biosynthesis genes and pathways has been extensive [23, 24, 33]. The discovery of the methylerythritolphosphate (MEP) biosynthetic pathway in the 1990s [34] provided an alternative route for IPP and DMAPP biosynthesis, and is regarded as a recent milestone of terpene synthesis exploration. Tomato and its wild relatives produce various terpenes in their trichome glands, as has been summarized and

discussed by Matsuba *et al.* [23] and Falara *et al.* [33]. Phenylpropanoids synthesized from monolignol alcohol precursors are also frequently found in trichomes. For example, basil (*Ocimum basilicum*) glandular trichomes produce various phenylpropanoids, including eugenol, caffeic acid, and rosmarinic acid [35, 36]. Phenylpropanoids are well known for their versatile roles in defense against herbivores, as well as in attraction of pollinators [37, 38]. Flavonoids are derivatives from the phenylpropanoid pathway and are structurally diverse, though perhaps not as diverse as the terpenes. Accumulation of flavonoids in trichomes may serve to protect trichomes from UV radiation [39, 40]. In *Solanum* species, it was shown that type I, IV and VI glandular trichomes contain flavonoids including quercetin-trisaccharide, rutin, kaempferol-rhamnoside and 3-*O*-methylmyricetin [41]. Acylsugars are reported to accumulate in glandular trichomes of various *Solanum* species and will be introduced in more detail in the following sections.

Important genetic tools have been developed in recent decades that have accelerated functional characterization of enzymes, transporters, and regulators of branching biosynthetic pathways of plant specialized metabolism. For instance, chemical screening of *S. lycopersicum* M82 × *S. pennellii* LA0716 chromosomal substitution introgression lines (ILs) for changes in terpenes and acylsugars levels and compositions made it possible to identify genes that affect the accumulation levels of these metabolites [42, 43, 44, 45]. Together with silencing of candidate genes and state-of-art analytical analysis for chemical characterization, the functions of specific biosynthetic genes have been characterized for several trichome metabolites. Altogether, a complementary approach involving genetic tools and chemical profiling has been established and applied to exploration of chemical diversity in glandular trichome metabolism.

1.4 Introduction to acylsugars

Acylsugar metabolite diversity makes for complex chemical phenotypes among wild and cultivated tomato relatives, and acylsugars constitute a significant proportion of leaf biomass in some Solanaceous species [46]. The genetic mechanisms that control the chemical diversity of acylsugars have emerged as interesting models for exploring how evolutionary factors drive plant chemistry in cultivated and wild tomato accessions [47, 48]. The recognized insect resistance and repellent properties of acylsugars [49, 50] serve as primary reasons why quantities and chemotypes of acylsugar metabolites have been regarded as targets for tomato breeding efforts [51, 52, 53]. Acylsugars are also known to have commercial value as surfactants [54, 55], antimicrobials [56, 57] and pharmaceutical excipients [58] as well.

The structural and abundance diversity of acylsugar metabolites in some cultivated and wild tomato accessions has been demonstrated through deep profiling using mass spectrometry and NMR for structure elucidation [47]. Complex chemotypes were shown to vary in content of straight and/or branched aliphatic acid esters of different chain lengths attached to different hydroxyl group positions of sucrose or glucose [43, 47]. Because there may be hundreds of acylsugars in tomato and its wild relatives alone, a convenient nomenclature for acylsugars was developed, and is refined further here. For instance, the structure in Figure 1.1 shows the detailed nomenclature of substitution position and acyl chains type using the most abundant tomato acylsugar S4:17 (C2^{R2},aiC5^{R3},iC5^{R3},iC5^{R3}) as an example. For the nomenclature, 'S' refers to sucrose, '4' indicates the four acyl chains to make it a tetra-acylsugar, '17' is the total number of carbons in all four acyl chains. For *S. lycopersicum* acylsugars, positions of attachment of acyl chains are distributed among both

pyranose (carbon position labeled as number 1 to 6) and furanose (carbon position labeled as number 1 'to 6') rings. Superscripts R2, R3 and R4 here indicate acyl chains substituted at 2, 3, and 4 positions of pyranose ring hydroxyl groups, and superscript R3 'indicates acyl chains substituted at the 3 'position of the furanose ring. The acyl chain lengths typically vary from C2 (acetate) to C12. Differences in acyl group branching are labeled with abbreviations 'n' for straight chain, 'ai' for anteiso (branched at the *ante*-penultimate carbon, two carbons from the end), and 'i' for iso (branched at the penultimate carbon) chain.

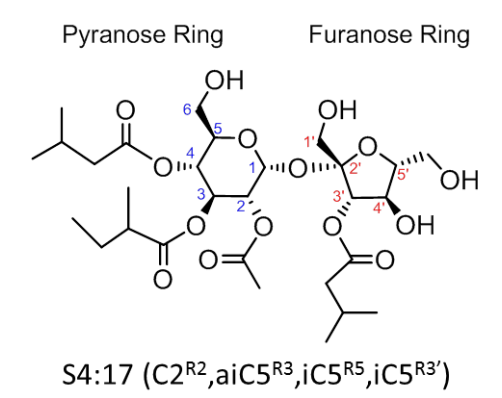


Figure 1.1. Acylsugar structure nomenclatures. The designation 'S' refers to sucrose, '4' indicates the total number of acyl chains, '17' is the total number of carbons in all acyl chains. Substitution of acyl chains at pyranose ring hydroxyls are labeled as carbon number 1 to 6, and at furanose hydroxyls are labeled as carbon number 1 'to 6'. Superscripts R2, R3 and R4 indicate acyl chains substituted at 2, 3, and 4 positions of pyranose ring, and superscript R3' indicates acyl chains substituted at the 3' position of furanose ring. The acyl chain lengths can vary from C2 (acetate) to C12. Differences in acyl group branching are labeled with abbreviations 'n' for straight chain, 'ai' for anteiso and 'i' for iso branched chain.

Given this diversity, a variety of synthetic and regulatory enzymes are expected to participate in complex metabolic networks that regulate abundance and chemical diversity of acylsugars. Recently, by virtue of cross-referencing genomic and genetic resources and advanced analytical tools for fast metabolic screening and metabolite identification, several trichome specific genes and enzymes were identified that catalyze acylsugar biosynthetic

steps and contribute to chemical diversity of acylsucroses that accumulate in cultivated and wild tomato species. Briefly, four acylsugar acyltransferase (ASAT) enzymes were characterized that sequentially add specific acyl chains onto sucrose cores to assemble a variety of *Solanum* acylsugars [45, 48, 59, 60]. More recently, AcylSugar acylHydrolase1 and 2 (ASH1 and ASH2) enzymes were shown to remove acyl chains from specific positions of certain types of acylsugars *in vitro* [Schilmiller *et al.*, 2015, *Plant Physiology*, submitted]. In addition, mutations in an isopropylmalate synthase 3 (IPMS3) recently discovered in cultivated tomato affect the proportions of 2-methylpropanoic acid (iC4) and 3-methylbutanoic acid (iC5) acyl chains in acylsugars from accessions of the wild tomato *Solanum pennellii* [44]. All of these genes and enzymes contribute to acylsugar chemical diversification and will be discussed in more detail in Chapter 4. The discoveries of genes involved in acylsugar biosynthesis and catabolism provide the basis for rational engineering of biosynthetic pathways for accumulation of desired amounts of chemical defense metabolites.

1.5 Analytical strategies for metabolite profiling and flux measurement

Definitions of precursors, intermediates and products of a biosynthetic pathway are prerequisites for a detailed characterization of the functions of enzymes in specialized metabolism. Recent improvements in comprehensive metabolite analysis, especially high-throughput mass spectrometry (MS) and nuclear magnetic resonance (NMR)-based strategies, when combined with chromatographic separation, have accelerated the detailed examination of chemical structure of specialized metabolites and outlined the biosynthetic routes for corresponding gene discovery [61]. Together with tracer techniques, annotation and

quantification of specialized metabolites has been largely relied on hyphenated techniques for fast metabolic profiling and chemical phenotyping, including gas chromatography-MS (GC-MS), liquid chromatography-MS (LC-MS), LC-NMR, LC-UV, LC-UV-MS and LC-NMR-MS [61-66].

GC-MS is suitable for profiling volatile metabolites including terpene compounds or non-volatile metabolites after derivatization to increase analyte volatility [67, 68]. Universal ionization, reproducible retention times, and available mass spectral databases make GC-MS a powerful analytical tool for plant specialized metabolite characterization [69, 70]. On the other hand, LC-MS is popular as a high-throughput technique with minimal sample preparation for non-volatile natural products that often cannot be analyzed using GC-MS. Recent LC column advancements have increased efficiency and flexibility and have made LC-MS a versatile approach that is suitable for broad ranges of metabolites [65, 71]. Ultrahigh performance liquid chromatography (UHPLC) coupled with high resolution mass spectrometry (HRMS) is emerging as a preferred tool in metabolomics research and addresses the necessity for deep profiling of complex mixtures of specialized metabolites, often documenting more than 1000 metabolites in a single LC/MS analysis [72, 73, 74].

NMR has been the gold standard for characterization of small molecules because of its capacity for absolute structure assignment when milligram quantities of metabolites are available from sample extracts. Compared to NMR, MS offers lower detection limits but often fails to provide detailed and comprehensive structure information. However, fragmentation in MS offers an approach to assign many features of a metabolite's structure and assist metabolite annotation. Tandem MS or MS/MS breaks intact ionized molecules of interest into substructure fragment ions, usually through collision with inert gas molecules (*e.g.* N₂, He)

inside a collision cell. Analysis of MS/MS spectra of metabolites using database searching and/or manual interpretation of the fragments often provides enough information to annotate metabolites in a profile, but since many specialized metabolites are taxonomically restricted in their range, the scope of spectrum databases remains limited. Together with chromatographic retention index values or comparisons with standard compounds, LC-MS/MS [75] and GC-MS/MS [76] have been widely employed in metabolite profiling to address questions of functional genomics and systems biology. Recently, improvements in mass resolution and mass measurement accuracy (*e.g.* using time-of-flight and Orbitrap mass analyzers) have been successfully applied to identify novel natural products in plants and bacteria, and are leading natural product research into the metabolomics era with explosive growth in chemical structural elucidation [61, 71].

Non-selective collision-induced dissociation of ions, including an approach known as MS^E, offers an option to generate spectra with non-fragmenting and fragmenting collision conditions in a single acquisition for nontargeted analysis [77], but this approach has not always provided sufficient information about energy-dependence of fragment ion formation and may not yield desired fragmentation for all metabolites [77, 78]. To address this issue, a data-independent and nonselective multiplexed CID fragmentation method was first developed by Dr. Feng Shi in the Jones laboratory at Michigan State University and was applied in many analyses of specialized metabolites [43]. This method takes advantage of the rapid acquisition capabilities of time-of-flight (TOF) mass spectrometry, which are capable of generating about 20,000 mass spectra per second, to generate energy-resolved fragmentation with accurate mass measurements by switching among four or five different CID voltages on

the chromatographic time scale. The advantage of this nontargeted approach is extended when isotope labeling is involved for non-target metabolite profiling and flux analysis [79].

Tracer techniques using labeling with radioisotope (such as ¹⁴C and ³H) or stable isotope (such as ¹³C) labeled compounds provided important foundations for research and development of natural product chemistry and paved the way for investigations into functional and evolutionary perspectives of specialized metabolism [4]. The outline of the Calvin cycle and MEP pathway of terpene biosynthesis through feeding studies are two of the pioneering examples showing the biosynthetic routes of plant central and specialized metabolism. The establishment of MS-based analytical tools has enabled the use of stable (non-radioactive) isotopes for biochemical pathway analysis since mass spectrometers have improved in sensitivity during recent years, and can resolve isotopically-labeled compounds based on mass differences. This method has been used to facilitate the emergence of metabolomics, a global approach to analysis of metabolites that encompasses metabolite identification and quantification, pathway discovery, and metabolic flux analysis [80-83]. Measurements of flux are essential for understanding the control and regulation of metabolic networks and to guide plant metabolic engineering [84, 85].

Beyond knowing the identities and amounts of metabolites, it is also useful to know where they are located among tissues and specific cell types. Spatially-resolved metabolite profiling using MS imaging has emerged as a complementary analytical strategy for measurements of spatio-temporal distributions of metabolites, lipids and proteins in plant and animal tissues [86, 87]. This technique provides fundamental and unique insights into plant specialized metabolism and fills the gap of limited understanding of physiological dynamics of natural product compounds within specialized cell/tissues of plant by defining the locations

of synthesis, storage and transportation of active plant specialized metabolites [88]. Related MS imaging applications in plant have been reviewed by Bjarnholt *et al.* [89] and will be discussed in more detail in Chapter 2.

1.6 Summary of research

The driving force behind this research comes from the ultimate goal of molecular engineering of plants to produce desired specialized metabolites. The challenge for synthetic biology and engineering of plants for secondary metabolite production lies with some of the unanswered questions within plant biology, including understanding when and where a specific biosynthetic or catabolic progress happens within a tissue, cell, or subcellular domain, and recognizing the factors that organize and regulate these progresses. To answer these key questions, biochemical, analytical, and genetic tools should be integrated to provide approaches for extensive understanding of the mechanisms that control plant specialized metabolism.

Toward this research goal, Chapter 2 addresses the 'where' question by describing chemical imaging of trichome specialized metabolites using laser desorption/ionization (LDI) mass spectrometry imaging. The contact printing scheme to transfer trichomes to a substrate for selective probing of the chemistry of trichomes successfully addresses the challenges (the fragile trichomes and their incompatibility with fixation) for imaging trichomes using mass spectrometry. Using this LDI-MS imaging method, single-cell metabolic profiling and spatially preserved chemical information was achieved for leaf trichomes of wild and cultivated tomato for several classes of trichome specialized metabolites, including acylsugars, flavonoids and terpenoids. This work extended imaging mass spectrometry to specialized

epidermal cells without using dissection or tissue fixation. The printed transfer method coupled with carbon based substrate provides a complementary sample preparation method for imaging mass spectrometry and provides potential novel applications.

Chapter 3 and 4 together address the 'when' and 'what regulates' questions through stable isotope labeling methodology for tracing specialized metabolite flux in trichomes. In Chapter 3, an integrated approach combining whole plant ¹³CO₂ labeling and data-independent LC-MS quantitative profiling is described to assess the dynamic biosynthetic and turnover rates of protective plant specialized metabolites. This chapter first describes the aim of the labeling study, followed by detailed description of the home-made growth chamber that was specially designed and made for whole plant ¹³C labeling. For methodology, special issues including hydroponic growth of tomato seedlings, growth condition controls (humidity, temperature, light and volatile) are explained and compared. Next, the LC-MS method and multiplexed nonselective collision induced dissociation (CID) on an orthogonal time of flight mass spectrometer is described for assessment of ¹³C incorporation in both molecular and fragment ions.

Using mass spectrometric profiling and ¹³C tracer methods described in Chapter 3, Chapter 4 describes the diversity and dynamics of trichome specialized metabolites and their relationships to developmental stages of tomato leaves. Quantification of stable isotope incorporation into both intact molecules and substructures of acylsugars were achieved. We measured fluctuations in labeling enrichment and metabolite accumulation during different tomato leaf developmental stages, and demonstrated that total acylsugar accumulation reaches a steady state at an early stage of leaf development. However, the steady state is dynamic at the same time, meaning biosynthesis, reassembly and degradation all occur at the same time.

In addition, different leaflets in a single plant have different developmental stages, and trichomes on younger leaflets are more active in acylsugar metabolism than on older leaflets. Thus harvesting time is important, and these findings suggest that metabolite profiling and labeling experiments might guide when to best collect specimens to assess gene expression levels and enzyme activities for both biosynthesis and degradation. One important finding has shown that ¹³C incorporation in acyl chains of acylsugars decreased faster than labeling in the whole molecule when plants were returned to ambient air (mostly ¹²CO₂) after five days of labeling. All above discoveries underscore the importance of developmental stage for metabolite turnover, degradation and reassembly.

The final chapter of this dissertation, Chapter 5, presents a brief summary of the above chapter and future perspectives for remaining questions. A reasonable hypothesis for fast biosynthesis and turnover indicates that plants have specific mechanisms to balance growth and self-defense with limited carbon resources. Using the methods developed and described in this dissertation, system-wide approaches can be applied to uncover the delicate regulation mechanisms that trigger and control the production of specialized metabolites, the sophisticated mechanisms that plants use to thrive in changing environments and produce substances valued by human populations.

REFERENCES

REFERENCES

- 1. Crosby, K., Jifon, J., Pike, L. & Yoo, K.S., Edn. 744 219-224 (International Society for Horticultural Science (ISHS), Leuven, Belgium, 2007).
- 2. Chattopadhyay, S., Srivastava, A.K. & Bisaria, V.S. Production of phytochemicals in plant cell bioreactors, in *Plant Biotechnology and Molecular Markers*. (eds. P.S. Srivastava, A. Narula & S. Srivastava) 117-128 (Springer Netherlands, 2005).
- 3. Schijlen, E. *et al.* Pathway engineering for healthy phytochemicals leading to the production of novel flavonoids in tomato fruit. *Plant biotechnology journal* **4**, 433-444 (2006).
- 4. Hartmann, T. From waste products to ecochemicals: Fifty years research of plant secondary metabolism. *Phytochemistry* **68**, 2831-2846 (2007).
- 5. Aharoni, A. & Galili, G. Metabolic engineering of the plant primary-secondary metabolism interface. *Current opinion in biotechnology* **22**, 239-244 (2011).
- 6. Schwab, W. Metabolome diversity: too few genes, too many metabolites? *Phytochemistry* **62**, 837-849 (2003).
- 7. Pichersky, E. & Gang, D.R. Genetics and biochemistry of secondary metabolites in plants: an evolutionary perspective. *Trends in Plant Science* **5**, 439-445 (2000).
- 8. Roberts, J. Srivastava, L. M. Plant growth and development. Hormones and the environment. *Annals of Botany* **92**, 846-846 (2003).
- 9. Iriti, M. & Faoro, F. Chemical diversity and defence metabolism: How plants cope with pathogens and ozone pollution. *International Journal of Molecular Sciences* **10**, 3371-3399 (2009).
- 10. Bennett, R.N. & Wallsgrove, R.M. Secondary metabolites in plant defence mechanisms. *New Phytologist* **127**, 617-633 (1994).
- 11. Pichersky, E. The validity and utility of classifying genes as 'essential'. *Trends in Plant Science* **14**, 412-413 (2009).
- 12. Petersen, M. Current status of metabolic phytochemistry. *Phytochemistry* **68**, 2847-2860 (2007).
- 13. Wilkens, R., Shea, G., Halbreich, S. & Stamp, N. Resource availability and the trichome defenses of tomato plants. *Oecologia* **106**, 181-191 (1996).

- 14. Treutter, D. Significance of flavonoids in plant resistance and enhancement of their biosynthesis. *Plant Biology* **7**, 581-591 (2005).
- 15. Mochida, K. & Shinozaki, K. Advances in omics and bioinformatics tools for systems analyses of plant functions. *Plant & cell physiology* **52**, 2017-2038 (2011).
- 16. Bjorkman, E. Monotropa hypopitys 1. an epiparasite on tree roots. *Physiologia Plantarum* **13**, 308-327 (1960).
- 17. Ohyanagi, H. *et al.* Plant Omics Data Center: an integrated web repository for interspecies gene expression networks with NLP-based curation. *Plant & cell physiology* **56**, e9 (2015).
- 18. Fukushima, A., Kusano, M., Redestig, H., Arita, M. & Saito, K. Integrated omics approaches in plant systems biology. *Current Opinion in Chemical Biology* **13**, 532-538 (2009).
- 19. Schilmiller, A.L., Pichersky, E. & Last, R.L. Taming the hydra of specialized metabolism: how systems biology and comparative approaches are revolutionizing plant biochemistry. *Current opinion in plant biology* **15**, 338-344 (2012).
- 20. Hall, R.D. Plant metabolomics in a nutshell: Potential and future challenges, in *Annual Plant Reviews Volume 43* 1-24 (Wiley-Blackwell, 2011).
- 21. Pichersky, E. & Gerats, T. The plant genome: an evolutionary perspective on structure and function. *The Plant Journal* **66**, 1-3 (2011).
- Weng, J.K., Philippe, R.N. & Noel, J.P. The rise of chemodiversity in plants. *Science* (New York, N.Y.) **336**, 1667-1670 (2012).
- 23. Matsuba, Y. *et al.* Evolution of a complex locus for terpene biosynthesis in solanum. *The Plant cell* **25**, 2022-2036 (2013).
- 24. Tholl, D. Terpene synthases and the regulation, diversity and biological roles of terpene metabolism. *Current opinion in plant biology* **9**, 297-304 (2006).
- 25. Laursen, T., Møller, B.L. & Bassard, J.-E. Plasticity of specialized metabolism as mediated by dynamic metabolons. *Trends in Plant Science* **20**, 20-32 (2015).
- 26. Weng, J.K. & Noel, J.P. The remarkable pliability and promiscuity of specialized metabolism. *Cold Spring Harbor symposia on quantitative biology* **77**, 309-320 (2012).
- 27. Jorgensen, K. *et al.* Metabolon formation and metabolic channeling in the biosynthesis of plant natural products. *Current opinion in plant biology* **8**, 280-291 (2005).

- 28. Morant, A.V. *et al.* The β -glucosidases responsible for bioactivation of hydroxynitrile glucosides in lotus japonicus. *Plant physiology* **147**, 1072-1091 (2008).
- 29. Bednarek, P. *et al.* A glucosinolate metabolism pathway in living plant cells mediates broad-spectrum antifungal defense. *Science (New York, N.Y.)* **323**, 101-106 (2009).
- 30. Wagner, G.J. Secreting glandular trichomes: More than just hairs. *Plant physiology* **96**, 675-679 (1991).
- 31. Schilmiller, A.L., Last, R.L. & Pichersky, E. Harnessing plant trichome biochemistry for the production of useful compounds. *The Plant Journal* **54**, 702-711 (2008).
- 32. Luckwill, L.C. *The genus lycopersicon : an historical, biological, and taxonomic survey of the wild and cultivated tomatoes.* (University Press, Aberdeen; 1943).
- 33. Falara, V. *et al.* The tomato terpene synthase gene family. *Plant physiology* **157**, 770-789 (2011).
- 34. Schwarz, M.a.A., D. Ginkgolide biosynthesis. In Comprehensive Natural Product Chemistry (Cane, D., ed), in *In Comprehensive Natural Product Chemistry* Vol. 2. (ed. D. Cane) 369-399 (Pergamon, Oxford, UK; 1999).
- 35. Gang, D.R. *et al.* An investigation of the storage and biosynthesis of phenylpropenes in sweet basil. *Plant physiology* **125**, 539-555 (2001).
- 36. Deschamps, C. & Simon, J.E. Phenylpropanoid biosynthesis in leaves and glandular trichomes of basil (Ocimum basilicum L.). *Methods in molecular biology (Clifton, N.J.)* **643**, 263-273 (2010).
- 37. Tan, K.H., Nishida, R. & Toong, Y.C. Floral synomone of a wild orchid, Bulbophyllum cheiri, lures Bactrocera fruit flies for pollination. *Journal of chemical ecology* **28**, 1161-1172 (2002).
- 38. Obeng-Ofori, D. & Reichmuth, C. Bioactivity of eugenol, a major component of essential oil of Ocimum suave (Wild.) against four species of stored-product Coleoptera. *International Journal of Pest Management* **43**, 89-94 (1997).
- 39. Karabourniotis, G., Kofidis, G., Fasseas, C., Liakoura, V. & Drossopoulos, I. Polyphenol deposition in leaf hairs of Olea europaea (Oleaceae) and Quercus ilex (Fagaceae). *American journal of botany* **85**, 1007 (1998).
- 40. Tattini, M. *et al.* On the role of flavonoids in the integrated mechanisms of response of Ligustrum vulgare and Phillyrea latifolia to high solar radiation. *The New phytologist* **167**, 457-470 (2005).

- 41. Schmidt, A., Li, C., Shi, F., Jones, A.D. & Pichersky, E. Polymethylated myricetin in trichomes of the wild tomato species Solanum habrochaites and characterization of trichome-specific 3'/5'- and 7/4'-myricetin O-methyltransferases. *Plant physiology* **155**, 1999-2009 (2011).
- 42. Eshed, Y. & Zamir, D. An introgression line population of Lycopersicon pennellii in the cultivated tomato enables the identification and fine mapping of yield-associated QTL. *Genetics* **141**, 1147-1162 (1995).
- 43. Schilmiller, A. *et al.* Mass spectrometry screening reveals widespread diversity in trichome specialized metabolites of tomato chromosomal substitution lines. *The Plant journal: for cell and molecular biology* **62**, 391-403 (2010).
- 44. Ning, J. *et al.* A feedback insensitive isopropylmalate synthase affects acylsugar composition in cultivated and wild tomato. *Plant physiology* (2015).
- 45. Schilmiller, A.L. & Moghe, G.D. Functionally divergent alleles and duplicated Loci encoding an acyltransferase contribute to acylsugar metabolite diversity in Solanum trichomes. **27**, 1002-1017 (2015).
- 46. Fobes, J.F., Mudd, J.B. & Marsden, M.P. Epicuticular Lipid Accumulation on the Leaves of Lycopersicon pennellii (Corr.) D'Arcy and Lycopersicon esculentum Mill. *Plant physiology* **77**, 567-570 (1985).
- 47. Ghosh, B., Westbrook, T.C. & Jones, A.D. Comparative structural profiling of trichome specialized metabolites in tomato (Solanum lycopersicum) and S. habrochaites: acylsugar profiles revealed by UHPLC/MS and NMR. *Metabolomics* 10, 496-507 (2014).
- 48. Kim, J. *et al.* Striking natural diversity in glandular trichome acylsugar composition is shaped by variation at the Acyltransferase2 locus in the wild tomato Solanum habrochaites. *Plant physiology* **160**, 1854-1870 (2012).
- 49. Simmons, A.T. & Gurr, G.M. Trichomes of Lycopersicon species and their hybrids: effects on pests and natural enemies. *Agricultural and Forest Entomology* **7**, 265-276 (2005).
- 50. Weinhold, A. & Baldwin, I.T. Trichome-derived O-acyl sugars are a first meal for caterpillars that tags them for predation. *Proceedings of the National Academy of Sciences of the United States of America* **108**, 7855-7859 (2011).
- 51. Glas, J. et al. Plant Glandular Trichomes as Targets for Breeding or Engineering of Resistance to Herbivores. *International Journal of Molecular Sciences* **13**, 17077 (2012).

- 52. Leckie, B., De Jong, D. & Mutschler, M. Quantitative trait loci increasing acylsugars in tomato breeding lines and their impacts on silverleaf whiteflies. *Mol Breeding* **30**, 1621-1634 (2012).
- 53. Leckie, B. *et al.* Quantitative trait loci regulating the fatty acid profile of acylsugars in tomato. *Mol Breeding* **34**, 1201-1213 (2014).
- 54. Hill, K. & Rhode, O. Sugar-based surfactants for consumer products and technical applications. *Lipid/Fett* **101**, 25-33 (1999).
- 55. Dembitsky, V.M. Astonishing diversity of natural surfactants: 1. Glycosides of fatty acids and alcohols. *Lipids* **39**, 933-953 (2004).
- 56. Chortyk, O.T., Kays, S.J. & Teng, Q. Characterization of Insecticidal Sugar Esters of Petunia. *Journal of agricultural and food chemistry* **45**, 270-275 (1997).
- 57. Ovenden, S.P. *et al.* Physaloside A, an acylated sucrose ester from Physalis viscosa. *Journal of natural products* **68**, 282-284 (2005).
- 58. Lerk, P.C., Sucker, H.H. & Eicke, H.F. Micellization and solubilization behavior of sucrose laurate, a new pharmaceutical excipient. *Pharmaceutical development and technology* **1**, 27-36 (1996).
- 59. Fan, P. *et al.* In vitro reconstruction and analysis of evolutionary variation of the tomato acylsucrose metabolic network *Sumited to PNAS* (2015).
- 60. Schilmiller, A.L., Charbonneau, A.L. & Last, R.L. Identification of a BAHD acetyltransferase that produces protective acyl sugars in tomato trichomes. *Proceedings of the National Academy of Sciences of the United States of America* **109**, 16377-16382 (2012).
- 61. Ryan, D. & Robards, K. Analytical chemistry considerations in plant metabolomics. *Sep Purif Rev* **35**, 319-356 (2006).
- 62. Ward, J.L., Baker, J.M. & Beale, M.H. Recent applications of NMR spectroscopy in plant metabolomics. *The FEBS journal* **274**, 1126-1131 (2007).
- 63. Ramautar, R., Somsen, G.W. & de Jong, G.J. CE-MS in metabolomics. *Electrophoresis* **30**, 276-291 (2009).
- 64. Nakabayashi, R. *et al.* Combination of Liquid Chromatography–Fourier Transform Ion Cyclotron Resonance-Mass Spectrometry with 13C-Labeling for Chemical Assignment of Sulfur-Containing Metabolites in Onion Bulbs. *Analytical Chemistry* **85**, 1310-1315 (2013).

- 65. Boughton, B., Thinagaran, D., Sarabia, D., Bacic, A. & Roessner, U. Mass spectrometry imaging for plant biology: a review. *Phytochem Rev*, 1-44 (2015).
- 66. Lisec, J., Schauer, N., Kopka, J., Willmitzer, L. & Fernie, A.R. Gas chromatography mass spectrometry-based metabolite profiling in plants. *Nature protocols* **1**, 387-396 (2006).
- 67. Schauer, N., Zamir, D. & Fernie, A.R. Metabolic profiling of leaves and fruit of wild species tomato: a survey of the Solanum lycopersicum complex. *Journal of experimental botany* **56**, 297-307 (2005).
- 68. Aprea, E. *et al.* Metabolite profiling on apple volatile content based on solid phase microextraction and gas-chromatography time of flight mass spectrometry. *Journal of chromatography*. A **1218**, 4517-4524 (2011).
- 69. Sawada, Y. *et al.* Widely targeted metabolomics based on large-scale MS/MS data for elucidating metabolite accumulation patterns in plants. *Plant & cell physiology* **50**, 37-47 (2009).
- 70. Ernst, M., Silva, D.B., Silva, R.R., Vencio, R.Z. & Lopes, N.P. Mass spectrometry in plant metabolomics strategies: from analytical platforms to data acquisition and processing. *Natural product reports* **31**, 784-806 (2014).
- 71. Tchoumtchoua, J., Njamen, D., Mbanya, J.C., Skaltsounis, A.-L. & Halabalaki, M. Structure-oriented UHPLC-LTQ Orbitrap-based approach as a dereplication strategy for the identification of isoflavonoids from Amphimas pterocarpoides crude extract. *Journal of Mass Spectrometry* **48**, 561-575 (2013).
- 72. Lin, L.Z., Sun, J., Chen, P. & Harnly, J. UHPLC-PDA-ESI/HRMS/MS(n) analysis of anthocyanins, flavonol glycosides, and hydroxycinnamic acid derivatives in red mustard greens (Brassica juncea Coss variety). *Journal of agricultural and food chemistry* **59**, 12059-12072 (2011).
- 73. Lin, L.-Z., Sun, J., Chen, P., Monagas, M.J. & Harnly, J.M. UHPLC-PDA-ESI/HRMS(n) Profiling Method To Identify and Quantify Oligomeric Proanthocyanidins in Plant Products. *Journal of agricultural and food chemistry* **62**, 9387-9400 (2014).
- 74. Sawada, Y. & Hirai, M.Y. Integrated LC-MS/MS system for plant metabolomics. *Computational and structural biotechnology journal* **4**, e201301011 (2013).
- 75. Muller, A., Duchting, P. & Weiler, E.W. A multiplex GC-MS/MS technique for the sensitive and quantitative single-run analysis of acidic phytohormones and related compounds, and its application to Arabidopsis thaliana. *Planta* **216**, 44-56 (2002).

- 76. Plumb, R.S. *et al.* UPLC/MSE; a new approach for generating molecular fragment information for biomarker structure elucidation. *Rapid Communications in Mass Spectrometry* **20**, 1989-1994 (2006).
- 77. Wrona, M., Mauriala, T., Bateman, K.P., Mortishire-Smith, R.J. & O'Connor, D. 'Allin-one' analysis for metabolite identification using liquid chromatography/hybrid quadrupole time-of-flight mass spectrometry with collision energy switching. *Rapid communications in mass spectrometry: RCM* **19**, 2597-2602 (2005).
- 78. Wang, Z. & Jones, A.D. Profiling of stable isotope enrichment in specialized metabolites using liquid chromatography and multiplexed nonselective collision-induced dissociation. *Anal Chem* **86**, 10600-10607 (2014).
- 79. Giavalisco, P., Köhl, K., Hummel, J., Seiwert, B. & Willmitzer, L. 13C Isotope-Labeled Metabolomes Allowing for Improved Compound Annotation and Relative Quantification in Liquid Chromatography-Mass Spectrometry-based Metabolomic Research. *Analytical Chemistry* 81, 6546-6551 (2009).
- 80. Wahl, S.A., Dauner, M. & Wiechert, W. New tools for mass isotopomer data evaluation in 13C flux analysis: Mass isotope correction, data consistency checking, and precursor relationships. *Biotechnology and Bioengineering* **85**, 259-268 (2004).
- 81. Kahn, M.L. *et al.* A mass spectrometry method for measuring 15N incorporation into pheophytin. *Anal Biochem* **307**, 219-225 (2002).
- 82. Romisch-Margl, W. *et al.* 13CO2 as a universal metabolic tracer in isotopologue perturbation experiments. *Phytochemistry* **68**, 2273-2289 (2007).
- 83. Shachar-Hill, Y. Metabolic network flux analysis for engineering plant systems. *Current opinion in biotechnology* **24**, 247-255 (2013).
- 84. Fernie, A.R., Geigenberger, P. & Stitt, M. Flux an important, but neglected, component of functional genomics. *Current opinion in plant biology* **8**, 174-182 (2005).
- 85. Martins, T.R., Berg, J.J., Blinka, S., Rausher, M.D. & Baum, D.A. Precise spatiotemporal regulation of the anthocyanin biosynthetic pathway leads to petal spot formation in Clarkia gracilis (Onagraceae). *The New phytologist* **197**, 958-969 (2013).
- 86. Li, C., Wang, Z. & Jones, A.D. Chemical imaging of trichome specialized metabolites using contact printing and laser desorption/ionization mass spectrometry. *Anal Bioanal Chem* **406**, 171-182 (2014).
- 87. Shitan, N., Hayashida, M. & Yazaki, K. Translocation and accumulation of nicotine via distinct spatio-temporal regulation of nicotine transporters in Nicotiana tabacum. *Plant signaling & behavior* **10**, e1035852 (2015).

88. Bjarnholt, N., Li, B., D'Alvise, J. & Janfelt, C. Mass spectrometry imaging of plant metabolites - principles and possibilities. *Natural product reports* **31**, 818-837 (2014).

Chapter 2. Chemical Imaging of Trichome Specialized Metabolites using Contact Printing and Laser Desorption/Ionization Mass Spectrometry

This chapter presents an extended version of research described in the following journal article: C. Li, Z. Wang, and A. D. Jones, Chemical imaging of trichome specialized metabolites using contact printing and laser desorption/ionization mass spectrometry. *Analytical and Bioanalytical Chemistry*. January 2014, Volume 406, Issue 1, pp 171-182 (Paper In Forefront).

2.1 Introduction

The application of metabolomics tools to plant research is accelerating engineering of stronger plants that can better resist disease and predation, improving nutritional quality of plant-derived foods and increasing yields of valuable feed-stocks, including biofuels and medicines [1]. Most investigations of plant metabolite profiles have focused on whole-tissue or whole-organism levels, and for these studies, metabolite information represents averages over many cells and tissues. Such profiles are usually dominated by contributions from the most abundant cell types, and this hinders understanding of less abundant specialized cells [2]. However, to investigate the functional roles of specialized cells and address the important questions about the mechanisms of development, cell differentiation, and cell-cell signaling, understanding the biochemical functions of individual cells is necessary. Among the approximately 40 different cell types encountered in the plant kingdom [3], glandular trichomes are renowned as prolific "chemical factories" for either synthesizing or storing plant metabolites as chemical defenses [4]. Such trichomes are the repositories of valuable food chemicals (e.g., flavors from mint, basil, and hops) as well as being pharmacologically active substances (e.g., cannabis) [5, 6]. In the plant family Solanaceae, which includes tomato, potato, eggplant, pepper, petunia, and tobacco, trichomes are abundant and have multiple morphological types, as observed on the leaf surfaces of the wild tomato Solanum habrochaites (Figure 2.1) [7]. In some wild tomatoes, trichome metabolites account for a substantial proportion of dry leaf weight. Owing to substantial genetic and genomic resources in this plant family and the physical accessibility of trichomes, investigations of trichome chemistry offer a unique and powerful model for understanding biosynthesis of specialized metabolites.

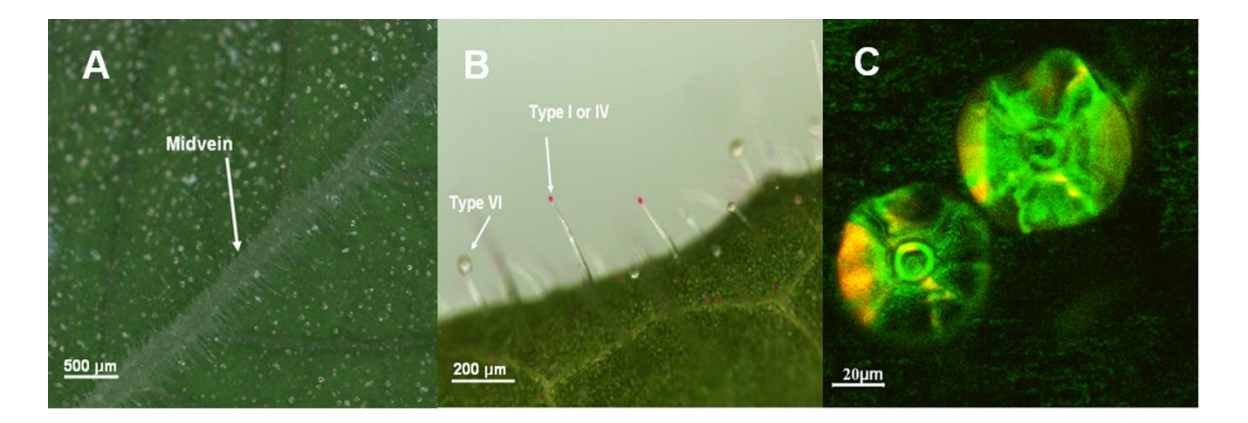


Figure 2.1. Optical images of a *S. habrochaites* LA1777 leaf showing trichomes on the adaxial (upper) leaf surface and stained type I and type IV trichomes. (A) trichomes on the adaxial (upper) leaf surface; (B) type I and type IV trichomes selectively stained by rhodamine B; (C) Two type VI trichomes under a fluorescence microscope after contact printing transfer to a ground glass microscope slide. Fluorescence was acquired using 488-nm excitation and a 505-530-nm band-pass filter.

A variety of approaches have been explored to address the challenges of sampling and detecting analytes in single cells [8-16], with the low levels of metabolites dictating a targeted approach to specific metabolites. Recently, mass spectrometry imaging (MSI) has provided an approach for multiplexing cellular profiling by fast scanning across an area of tissue, acquiring chemical information for individual pixels across the entire area. Several MSI approaches have been demonstrated in recent years, with matrix-assisted laser desorption/ionization (MALDI) imaging finding extensive use in profiling proteins, lipids, and other metabolites in animal tissues [17, 18]. More recently, a few examples have been reported for localization of natural products in biological tissues from a range of organisms [19-21]. Water has been developed as an alternative option as an endogenous matrix for MSI [22, 23]. Recently, an infrared laser ablation electrospray ionization system was developed that uses a fiber tip to focus radiation onto a small (approximately 30 µm) spot followed by electrospray-assisted ionization of desorbed neutrals, and this approach has been applied for profiling of constituents in single cells [24, 25]. Desorption electrospray ionization has been touted as a

new alternative approach for MSI. To our knowledge, this approach has yet to demonstrate resolution of single cells [26], but nanospray desorption electrospray ionization has achieved resolution of lipids in animal tissues with spatial resolution down to 12 µm [27].

The diversity of epidermal cell types on leaves and stems of tomato and its wild relatives presents challenges for sampling trichome chemistry at the level of individual trichomes. Complicating matters further are trichome fragility, morphological differences between trichome types, close proximity of individual trichomes that often precludes micropipette sampling without contamination, and the irregular distances of trichomes above the leaf surface. In the wild tomato *S. habrochaites*, examination of the leaf surface reveals the long hair-like trichomes defined as type I or type IV (Figure 2.1) [7]. Closer examination at higher magnification reveals the type VI glands, which consist of bundles of four cells on a short stalk. Although these glands might be probed using optical or ion beams, avoidance of sampling from multiple cells at different heights can only be minimized if the incident angle of the beam is zero; otherwise, spatial information is compromised. Furthermore, owing to the variation of the stalk height of trichomes, laser or ion beams might probe taller trichomes, but this interaction could block sampling of those below. In addition, ions ejected from shorter trichomes may also be blocked from detection by adjacent taller trichomes.

When imaging of trichomes is conducted using a laser for metabolite ionization and volatilization, no single laser focal plane will be optimal for all trichomes on a tissue surface. Although long focal lengths may be exploited to improve the depth of field, a more promising approach involves physical transfer of trichomes onto a single horizontal plane, presented in the form of a substrate that absorbs the laser radiation and uses this energy for analyte vaporization and ionization. A similar strategy for "tissue printing" of cells from various plant

and animal tissues onto polymer surfaces was reviewed, and included optical and electron microscope detection methods, often using selective staining [28]. Even subcellular printing resolution has been achieved [29]. Tissue printing has also been successfully applied to live neuronal cells for investigation of synaptic communication [30] and human surgical specimens for tumor marker profiling [31].

Although much effort has been devoted to method development for MSI, most of the successful examples have used sectioned animal tissue or tissues with flat surfaces. Examples of MSI of tissues having irregular shapes and spatially discontinuous cells are scarce. Herein, we present a carbon-substrate-based printing method for selective MSI of tomato trichome metabolites at high spatial resolution without the need for tedious microsampling. This sensitive scheme is capable of profiling specialized metabolites of thousands of individual trichomes on a single tomato leaf. The high spatial resolution offers the potential to explore chemical heterogeneity across a population of individual trichomes within a plant tissue.

2.2 Materials and methods

2.2.1 Chemicals

Acetonitrile, 2-propanol, methanol, dichloromethane, and formic acid (88 % aqueous solution) were purchased from VWR Scientific. α-cyano-4-hydroxycinnamic acid (CHCA), 2,5-dihydroxybenzoic acid (DHB), and tomatine were obtained from Sigma-Aldrich (St. Louis, MO, USA). Glassy carbon plates were purchased from SPI Supplies (West Chester, PA, USA).

2.2.2 Plants

Seeds for plants were obtained from the Tomato Genetics Resource Center at the University of California, Davis. The plants used for this study were grown in a greenhouse at Michigan State University, and were propagated by cuttings. The plant tissues were harvested about 4 weeks after cuttings had been taken, and the leaflets were collected from the second set of leaves from the apex of the plant.

2.2.3 Sample preparation

A dissecting glass microscope slide was mechanically ground with rotating grinding by the Glass Shop of the Michigan State University Department of Chemistry. A 2B pencil (Spartan Bookstore, Michigan State University) was used to draw a layer of graphite on one surface of the glass slide. The coverage of the surface by graphite was determined by examining the glass slide using transmitted light microscopy to ensure no large graphite-free spot (larger than 0.1 mm) was present. The glass slide was placed in a drying oven at 80 °C overnight, as removal of moisture strengthened adhesion of graphite to the glass surface. The slide was then immersed sequentially for 1 h in each of Milli-Q water, dichloromethane, and methanol, and was dried under a gentle stream of nitrogen. The slide was placed on a block of dry ice to chill the surface as a prelude to transfer of trichomes. Such cooling also helps quench enzyme activity in the trichome and preserves the chemical composition during sample processing.

A fresh leaflet from *S. habrochaites* LA1777 was cut by a razor blade from the base of the leaflet (petiolule). Since the analysis time for an imaging experiment increases with the square of the linear dimension of the sample, leaflets smaller than 3 cm x 3 cm were chosen to

limit the time needed for analysis. The symmetric leaflet on the side of the petiole that was not used for imaging was also collected, and was used to estimate the leaflet thickness for construction of a Parafilm mask that was designed to minimize the crushing of tissue during contact printing. A mask was constructed by either stretching or folding a sheet of Parafilm until the film thickness matched the thickness of the second leaflet as determined by visual inspection. A rectangular region was removed from the middle of the Parafilm mask, and the leaflet was positioned in the center of this recessed area. A graphite-coated glass slide was gently placed above the leaflet, and a 500-ml Pyrex beaker containing 200 ml water was placed on top of the slide for 60 s to provide a reproducible amount of pressure for contact transfer of trichomes from the tissue to the slide. The beaker, slide, and leaflet were removed to reveal trichomes printed on the substrate (see Figure 2.2). Mass calibrant reference solutions were spotted onto the corners of the slides for calibrating the time-of-flight mass axis before each analysis. The glass slides, containing trichomes transferred by the contact printing process, were attached to the MALDI sample stage using adhesive tape. Conductive material (e.g., aluminum foil) was attached to ensure electrical contact between the coated slide surface and the metallic sample stage. For imaging of single trichomes, the trichomes were collected by contact printing onto the surface of a glassy carbon plate or a bare glass slide. Use of an uncoated glass slide aids visualization of trichomes under optical microscopes using transmitted or reflected light or fluorescent imaging. A target imaging area was marked with liquid paper beforehand to provide position references, and a CCD camera mounted on the microscope collected reflected light optical images. Before laser desorption/ionization (LDI) imaging of trichomes transferred to uncoated glass slides was performed, the slide was

subjected to carbon coating under a vacuum at the Michigan State University Center for Advanced Microscopy.

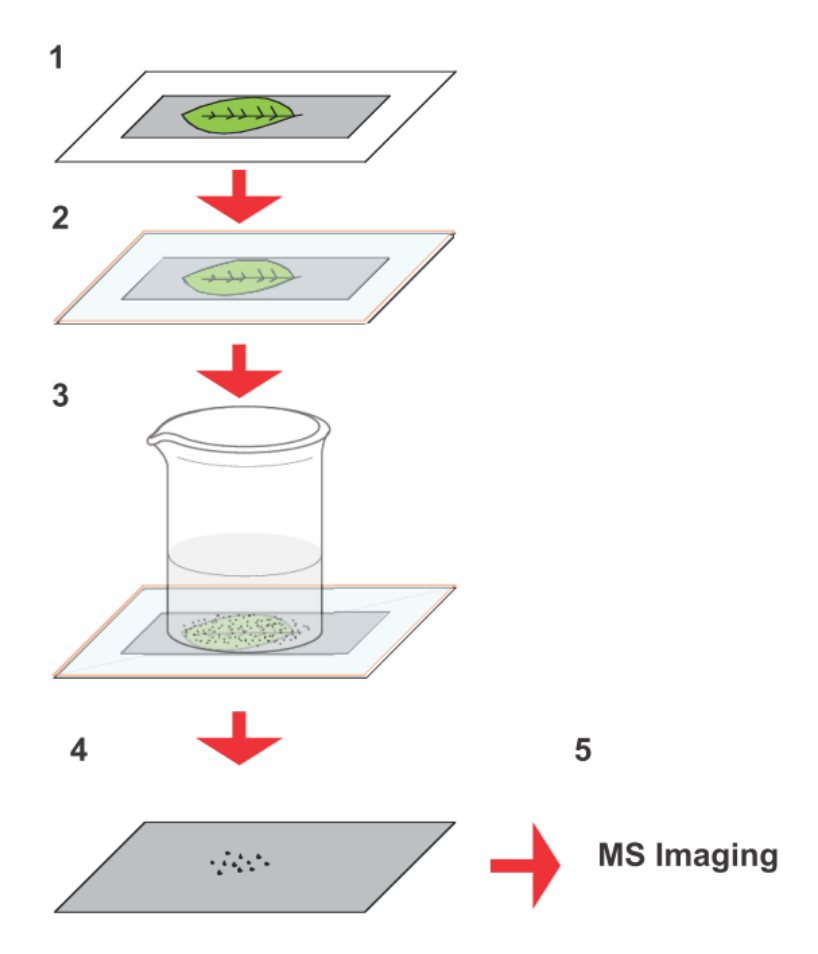


Figure 2.2. Schematic of the process used for contact printing of glandular trichomes from *S. habrochaites* LA1777 leaflets for laser desorption/ionization mass spectrometry imaging. Steps in the printing process were: (1) placement of the leaflet on a chilled carbon substrate using a Parafilm mask constructed to match the leaflet thickness, (2) the leaflet is covered using a carbon-coated slide, (3) a 500-mL beaker containing 200 mL of water is placed on top of the slide and allowed to stay in place for 60 seconds, (4) the beaker, slide, and leaflet are removed to reveal trichomes printed on the carbon substrate, and (5) the substrate is transferred onto the mass spectrometer MALDI stage and analyzed.

2.2.3 LDI imaging

MSI data were generated using a MALDI time-of-flight mass spectrometer (AXIMA cfr-plus, Shimadzu, Columbia, MD, USA) equipped with a 337-nm N₂ laser delivering 3-ns

pulses at a frequency of 10 Hz. In the MSI experiment, data were acquired in either positive ionization mode or negative ionization mode using the linear time-of-flight detector. In some cases, the same printed slide was analyzed twice using different polarity of ion detection without further sample preparation. The slide surface was first interrogated using 20 laser shots per pixel. For whole leaflet imaging, the stage step size was set to 125 µm. For singletrichome analyses, the stage step size was set to 25 µm, and signals from 200 laser shots per pixel were combined and stored for each pixel. Ion signals between m/z 50 and m/z 1,500 were collected. Major metabolites were previously annotated through leaf dip extracts using liquid chromatography (LC)-mass spectrometry (MS) [32]. Metabolites detected in LDI were identified by first matching LDI spectra for single deposited trichomes with the LC/MS spectra of leaf dip extracts. Post-source decay (PSD) LDI mass spectra were acquired for further confirmation of metabolite structures using fragment ion masses. All LDI imaging data acquisition and processing was performed using Launchpad software (version 2.8.1, Kratos Analytical). The raw MSI data were exported to Biomap software (Novartis) for further processing.

2.2.4 LC/MS analysis

Metabolites in leaflet glandular trichomes were selectively extracted by dipping the leaflets in 2 ml 2-propanol-acetonitrile-water (3:3:2 v/v/v) for 1 min. Extracts were centrifuged at 10,000 g for 10 min at 4 °C, and the supernatants were analyzed without further processing. Separations were performed on a prototype Supelco Discovery Bio-C18 column (1 mm \times 150 mm, 3 μ m particles) held at 30 °C that was interfaced with an LCT Premier mass spectrometer (Waters, Milford, MA, USA). A solvent gradient was executed based on 0.15 %

aqueous formic acid (solvent A) and methanol (solvent B) as follows: initial condition 5 % solvent B; linear gradient to 50 % solvent B (5 min); 95 % solvent B (33 min); 100 % solvent B (35 min); hold at 100 % solvent B until 38 min; return to 5 % solvent B (43 min). The flow rate was 0.1 ml/min, and the injection volume was 10 μ l. The LCT Premier mass spectrometer was operated using electrospray ionization and under the control of MassLynx version 4.1. The electrospray ionization conditions were as follows: capillary voltage, 3,200 V; cone voltage, 10 V; source temperature, 90 °C; desolvation gas flow rate, 300 l/h; desolvation gas temperature, 200 °C; cone gas flow rate, 20 l/h. Detection was performed in both positive ion mode and negative ion mode over m/z 50-1,500 using centroided peak acquisition and dynamic range enhancement. Aperture 1 voltages were 10, 45, and 75 V for three functions to generate molecular ions and fragment ions in a single analysis. The fragment ions were aligned to the pseudomolecular ions by matching of their retention times.

2.3 Results and discussion

2.3.1 Contact printing transfer of trichome metabolites

Selective contact transfer of trichomes from a leaflet of *S. habrochaites* onto a solid substrate, e.g., glass microscope slide, is demonstrated in Figure 2.3 The optical image documents that the type VI trichome gland structure was retained after the transfer with minimal physical damage, as evident from the bundle of four cells in the larger printed structures, and the absence of stalk cells. Examination of glands transferred from near the midvein confirmed that type VI glands were largely transferred intact. Type I/IV trichomes lack external cell walls, yet the transfer retained the visible outline of the boundaries of the gland, perhaps owing to the viscosity of the gland contents.

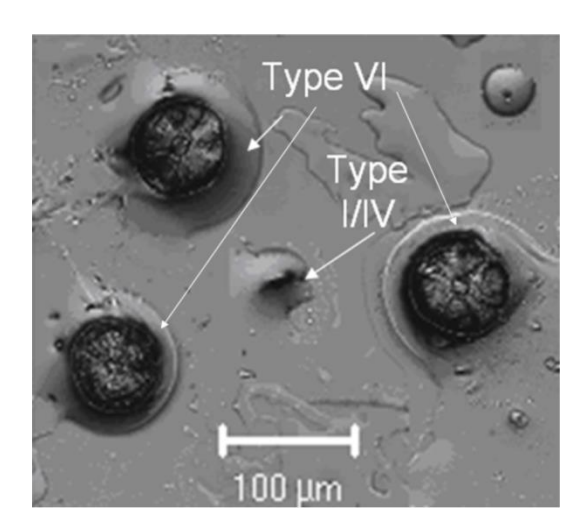


Figure 2.3. Transmitted light optical image of trichomes from the adaxial leaf surface of *S. habrochaites* LA1777 transferred to a glass microscope slide by contact printing.

To achieve greater reproducibility of gland transfer, it was judged desirable to standardize the pressure applied during contact printing. For optimization, a 500-ml glass beaker containing various amounts of water was placed on top of the glass slide during the contact printing process. Visual inspection of the transferred trichomes was performed under the dissecting microscope, and the optimal result (maximum transfer without evidence of trichome physical deformation) was obtained using 200 ml water in the beaker (a constant force of approximately 500 N/m²).

On the basis of our earlier microsampling and LC/MS results, different trichome types exhibit distinct chemical profiles, with acyl sugars selectively accumulating in type I/IV glands, and flavonol glycosides selectively accumulating in type VI glands [32]. We used detection of cell-specific metabolite markers to determine whether the transferred trichomes were contaminated by metabolites that leaked from epidermal pavement cells. On the basis of the LC/MS profiling of metabolites from pooled trichomes of a single gland type, the glycoalkaloid dehydrotomatine was not detected in type I, type IV, or type VI trichomes, but

was abundant in extracts of the entire leaf. This metabolite serves as a marker of epidermal pavement cell constituents, and its detection indicates nonselective transfer of material from cells other than Solanum trichomes. No glycoalkaloid dehydrotomatine was detected from the extraction of the contents of the trichome-printed glass slide using LC/MS, which indicates that the transferred trichomes were not significantly contaminated by metabolites from epidermal cells.

2.3.2 Whole-leaf imaging using LDI from pencil lead surfaces

The selection of graphitic carbon for the substrate surface was made on the basis of its ease of manipulation, efficient absorption of laser light, inertness and ease of cleaning, and availability in numerous forms, including pencil lead, graphite paint, and graphite plates [33-36]. These materials often contain impurities that contribute background peaks in LDI mass spectra. To minimize these, the pencil-lead-coated slide was rinsed with methanol, 2-propanol, and water before trichome transfer. After the substrate had been cleaned, the background ions between m/z 100 and m/z 1500 were fewer in number and lower in abundance than in spectra obtained using the traditional MALDI matrix compounds CHCA and DHB (Figure 2.4). However, surface rinsing of the pencil-lead-coated slide did not remove all contaminants, perhaps owing to the affinity of some compounds for graphitic carbon. For comparisons across these matrices, different laser powers were used for the various matrices to achieve approximately the same base peak ion current for each matrix. These laser power settings (arbitrary units) were 105 for DHB, 85 for CHCA, and 90 for pencil lead (approximately 3 mW). When spectra were generated using negative ion mode, the pencil lead background showed carbon cluster peaks with m/z = 12n (n is an integer, up to m/z 180). Most of the

abundant specialized metabolites in tomato trichomes have molecular masses greater than 200 Da, and few known metabolites have exact masses that overlap with carbon clusters. The low-mass carbon cluster peaks in negative ion mode can also be used to calibrate the instrument mass axis at low masses.

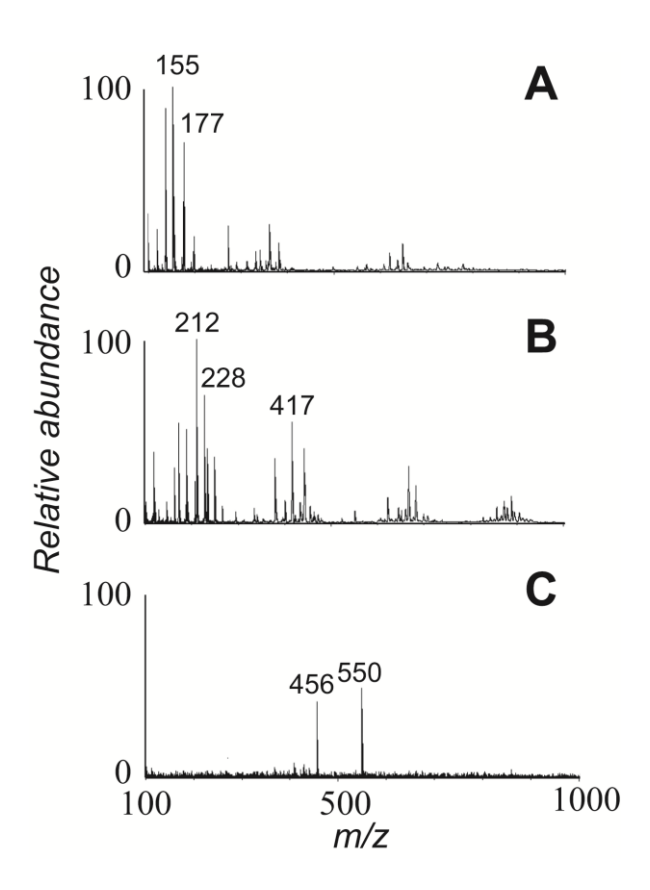


Figure 2.4. The background matrix-assisted laser desorption/ionization (MALDI) and LDI mass spectra of 2,5-dihydroxybenzoic acid, α -cyano-4-hydroxycinnamic acid, and methanol-rinsed pencil lead in positive ion. The mass spectra over m/z 50-1,000 in positive ion mode of 2,5-dihydroxybenzoic acid (A), α -cyano-4-hydroxycinnamic acid (B), and methanol-rinsed pencil lead (C) were shown. The spectra have been scaled to the same absolute signal abundance (100 % is equivalent to 800 mV), and the laser power was selected to obtain similar base peak ion abundances during acquisition of the spectra.

Before imaging experiments were performed, leaf dip extracts containing trichome metabolites were spotted onto pencil-lead-coated surfaces, and mass spectra were obtained in

both positive ion mode and negative ion mode (Figure 2.5). Four classes of major metabolites (acyl sugars, flavonoids, alkaloids, and sesquiterpene acids) were detected in both LC/MS of S. habrochaites LA1777 leaf dip extracts and LDI analyses of the same extracts. All four classes of metabolites listed in Table 2.1 were also detected using tissue printing with imaging. Single-gland extracts spotted on the graphite substrate yielded enough signal to profile all four classes of metabolites. In some cases, product ion MS/MS spectra were generated using PSD to confirm assignment to structural classes. PSD spectra were generated for all metabolite ions listed in Table 2.1, and the fragment ion masses supported all metabolite annotations in Table 2.1 Definitive elucidation of acyl sugar metabolite structures has more recently been achieved through isolation and characterization using ultra-high-pressure LC, 2D NMR spectroscopy, and high-resolution MS, as described elsewhere [37]. Among these metabolites, sesquiterpene acid did not yield fragment ions of adequate abundance for structure confirmation, whether in PSD spectra or in LC/MS/MS analyses. This compound was annotated on the basis of accurate pseudomolecular mass measurement and an earlier report of sesquiterpene acid structures in this plant species [38].

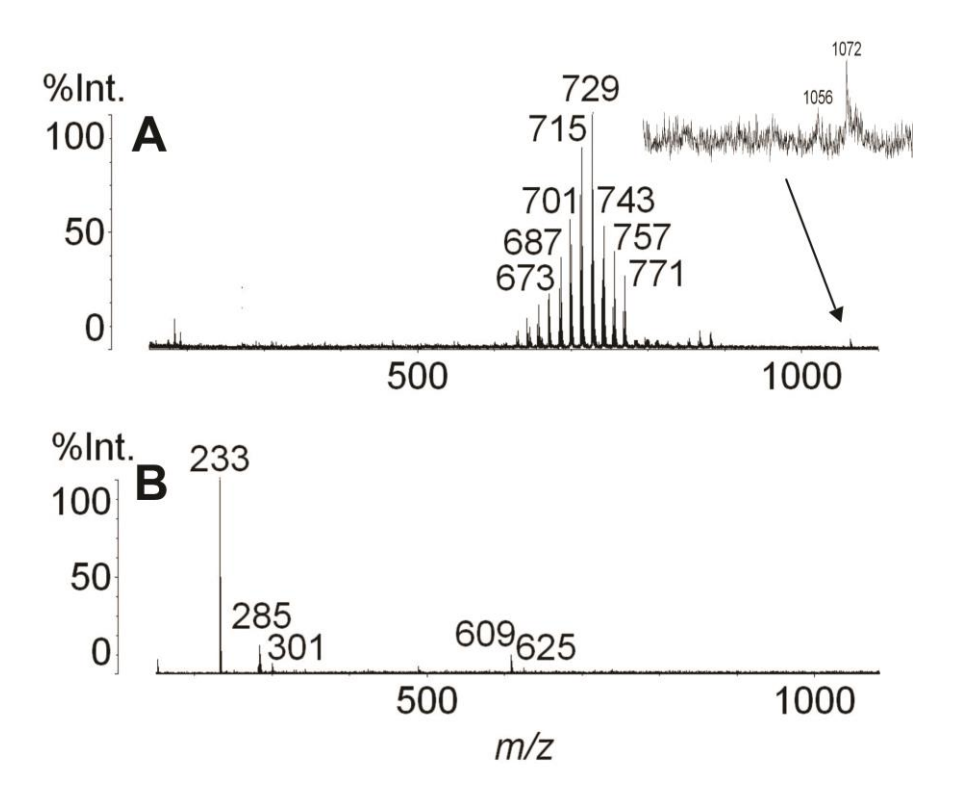


Figure 2.5. LDI mass spectra of trichome extracts from S. habrochaites LA1777 spotted on pencil-lead-coated glass slides using (A) positive ion mode and (B) negative ion mode.

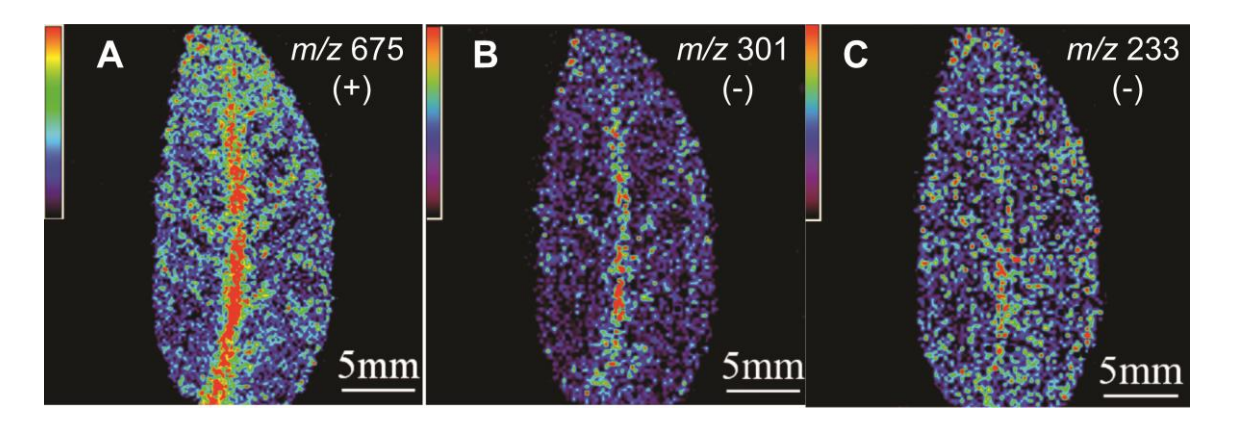


Figure 2.6. LDI mass spectrometry images of selected ions for contact-printed trichomes from an S. habrochaites LA1777 leaflet on pencil-lead-coated glass slides. (A) ion abundances of m/z 731 (acyl sugar S4:21 [M+K]⁺) using positive ion mode and a laser power setting of 95, a 125-µm stage step, and 20 laser shots per pixel, (B) m/z 301 in negative ion mode (aglycone fragment of quercetin glycosides), and (C) m/z 233 ([M - H]⁻ of various sesquiterpene acids) for the same leaf sample under negative ion mode with a laser power setting of 105, 20 laser shots per pixel. The key for color coding (0-100 % of highest abundance) is presented at the left in (A)-(C).

Table 2.1. Major ions observed in laser desorption/ionization spectra of *Solanum habrochaites* LA1777 trichome metabolites on pencil-lead-coated glass slides.

Metabolite annotation	Polarity	Major ion(s)	Nominal m/z
Acyl sugar S4:14	Positive	$[M + Na]^{+}/[M + K]^{+}$	617/633
Acyl sugar S4:15	Positive	$[M + Na]^{+}/[M + K]^{+}$	631/647
Acyl sugar S4:16	Positive	$[M + Na]^{+}/[M + K]^{+}$	645/661
Acyl sugar S4:17	Positive	$[M + Na]^{+}/[M + K]^{+}$	659/675
Acyl sugar S4:18	Positive	$[M + Na]^{+}/[M + K]^{+}$	673/689
Acyl sugar S4:19	Positive	$[M + Na]^{+}/[M + K]^{+}$	687/703
Acyl sugar S4:20	Positive	$[M + Na]^{+}/[M + K]^{+}$	701/717
Acyl sugar S4:21	Positive	$[M + Na]^{+}/[M + K]^{+}$	715/731
Acyl sugar S4:22	Positive	$[M + Na]^{+}/[M + K]^{+}$	729/745
Acyl sugar S4:23	Positive	$[M + Na]^{+}/[M + K]^{+}$	743/759
Acyl sugar S4:24	Positive	$[M + Na]^{+}/[M + K]^{+}$	757/773
Acyl sugar S4:25	Positive	$[M + Na]^{+}/[M + K]^{+}$	771/787
Tomatine	Positive	$[M+Na]^+/[M+K]^+$	1056/1072
Sesquiterpene acids	Negative	[M - H] ⁻	233
Kaempferol- <i>O</i> -diglucoside and quercetin- <i>O</i> -rhamnosylglucoside (rutin)	Negative	[M - H] ⁻	609
Quercetin-O-diglucoside	Negative	[M - H] ⁻	625

The acyl sugar nomenclature is as follows [45]: a single letter corresponding to the base sugar (S represents sucrose) followed by the total number of acyl carbon atoms. For example, a sucrose tetraester acylated with 14 carbon fatty acids would be designated as S4:14.

Imaging of printed trichomes from the upper surface of a leaflet from *S. habrochaites* LA1777 revealed distributions of major metabolites across the tissue. Figure 2.6 shows the color-coded intensity map of $[M+K]^+$ for an acylsucrose with 17 acyl group carbon atoms

(m/z 675, Figure 2.6 A) found in type I/IV glands, the aglycone fragment of quercetin glycosides (m/z 301, Figure 2.6 B) in type VI glands, and a deprotonated sesquiterpene acid (m/z 233, Figure 2.6 C) also in type VI glands. For all three m/z images, the midvein area in the center of the leaflet generates a stronger signal than the rest of the tissue, but this is less pronounced for the sesquiterpene acid. Since flavonoid glycosides and sesquiterpene acids selectively accumulate in type VI glands, these images suggest that the relative amounts of these in individual type VI glands are not uniform across the tissue. Light microscope inspection of the leaflet before printing showed higher trichome density around the midvein, particularly for type I/IV glands. Whether the strong ion abundances near the midvein largely reflect trichome densities or systematic differences in the composition of individual trichomes has yet to be established since microsampling of individual trichomes of a single type near the midvein is impractical owing to high trichome density. At present, we cannot conclusively establish whether transfer of trichomes from the thicker parts of the leaflet is more efficient than transfer from other regions of the leaflet, but the MSI data and microscopic examination of leaflets after printing suggest efficient (at least 70-90 %) transfer across all gland types and leaflet areas. For the taller type I/IV glands that are particularly abundant near the midvein, a significant fraction of the trichome mass consists of material already exuded from the glands, which makes them sticky and facilitates adhesion to the substrate. As a result, there is reason to believe that transfer of type I/IV glands is nearly 100 % efficient regardless of the location of the gland on the tissue. The densities of these glands near the midvein are so great that it is anticipated that many MS image pixels near the midvein contain material from more than one gland.

Despite the growing number of published reports of the use of MSI for protein and metabolite localization [39-42], validations of the quantitative performance of MSI analyses have been scarce. Numerous LDI images generated for this investigation suggested that relative abundances of certain metabolites within individual glands of a single trichome type (e.g., type I/IV, now considered a single type [32]) showed systematic differences dependent on the distance from the leaflet midvein. To determine how well the LDI imaging results agreed with microsampling and LC/MS analysis, an experiment was conducted to assess whether matrix effects influence the quantitative measure of metabolite abundances observed in LDI imaging data. The experimental design aimed to establish metabolite abundances per unit area, sampled from near the midvein and to the same area near the leaflet edge. Two leaflets of similar size from the same S. habrochaites LA1777 plant were harvested. Glass Pasteur pipettes were used to sample a core (diameter 0.5 mm) in the leaflet tissue from near the midvein and from near the leaflet edge, with the removed tissue being contained within the pipette tip. Four spots near the midvein and four spots near the leaflet edge were sampled for each leaflet, using a separate Pasteur pipette for each sampling. After removal of the plant tissue cores, pipette tips were broken off and inserted into extraction solvent (acetonitrilewater-2-propanol 3:3:2) to extract metabolites using ultrasonication for each cored sample. One set of extracts was analyzed using LC/MS in negative ion mode, and the m/z 233 extracted ion chromatogram peak areas were integrated and combined. This signal corresponds to combined contributions of several isomeric sesquiterpene acids (e.g., santalenoic and bergamotenoic acids) [38] that are specific to type VI trichomes [32]. The choice of this signal avoids contributions from cells other than trichomes that are removed during the coring process. Corresponding cores from similar positions on the second leaflet

were extracted, and the extracts were analyzed using LDI with pencil lead as the substrate. Aliquots (1.0 μ l) were spotted on the carbon substrate into a 2-mm-diameter well that was made by coring a Parafilm mask using the tip of a Pasteur pipette. The mass spectra for each spot were combined using 200 laser shots per well, and the signal for m/z 233 was tabulated. A comparison of the ratio of the m/z 233 signal near the midvein relative to the signal near the leaf edge using the two analytical methods is presented in Figure 2.7 B. Both methods confirm the greater abundance of sesquiterpene acids per unit tissue area near the midvein, and this finding is consistent with the observation in the LDI imaging (Figure 2.6 C).

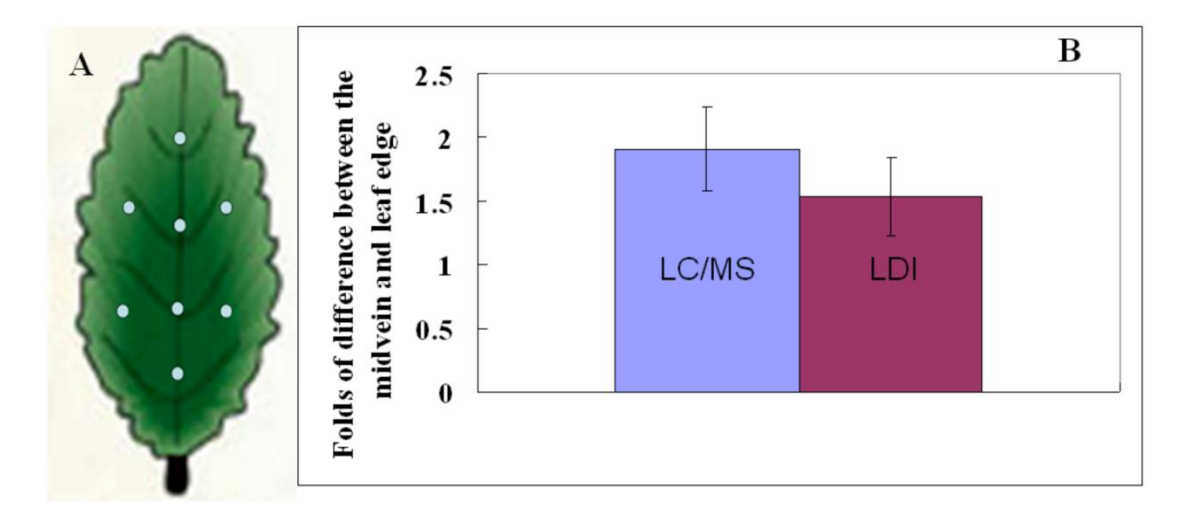


Figure 2.7. The hole-drilling on the leaf surface for validation of LDI metabolite profiling LC/MS and the ratio of the signal from sesquiterpene acid detected. (A) The hole-drilling experiment on the leaf surface for validation of LDI metabolite profiling using liquid chromatography—mass spectrometry (LC/MS). Four areas were collected around the leaf midvein and four areas were collected on the leaf edge. (B) The ratio of the signal from sesquiterpene acid detected in the midvein (m/z 233) cut to the leaf edge was measured using two different analytical methods: LC/MS and LDI. The experiment was conducted on two different leaves. P = 0.18 (n = 4). This statistically insignificant P value indicates that the LC/MS and LDI data are in agreement.

For profiling of metabolites in individual trichomes, the spatial resolution of imaging should resolve objects smaller than 50 µm (the approximate diameter of the type VI trichome

and the approximate average distance between two trichomes). For the AXIMA cfr-plus instrument, the laser spot size was estimated to be approximately 100 µm. To assess the spatial resolution of this instrument, trichomes were printed into copper transmission electron microscope grids with different spacings between grid elements. The grids were mounted on the top of the pencil-lead-coated substrate. Plant leaves were pressed against each grid several times, positioning trichomes into the space between the grid lines. LDI imaging was conducted after the grid had been removed from the substrate because of concerns that the thickness of the transmission electron microscope grid might interfere with illumination of the trichomes by the laser and with ion transmission from the surface to the mass analyzer. The diameter of the laser spot was larger than the smallest grid spacing tested (50 µm). To analyze objects smaller than the size of the laser spot, oversampling was performed [43] using a step size of 25 µm and 200 laser shots per pixel. The resulting 100-µm grid can be clearly resolved, but the smaller spacing of the 50-µm grid hindered trichome transfer to the substrate surface (Figure 2.8). Nevertheless, the resulting image suggests that spatial resolution approaching 50 μm was achieved using this approach, allowing single-trichome profiling.

Pencil lead coating of substrate surfaces is a fast and simple sample preparation method for chemical imaging of leaf metabolites over a wide tissue area. However, when higher spatial resolution is needed for imaging of individual trichomes, small defects in the carbon coverage can compromise the analysis. A closer examination of the pencil-lead-coated slide under the optical transmission microscope showed occasional spots of diameter less than 30 µm where no carbon had been deposited.

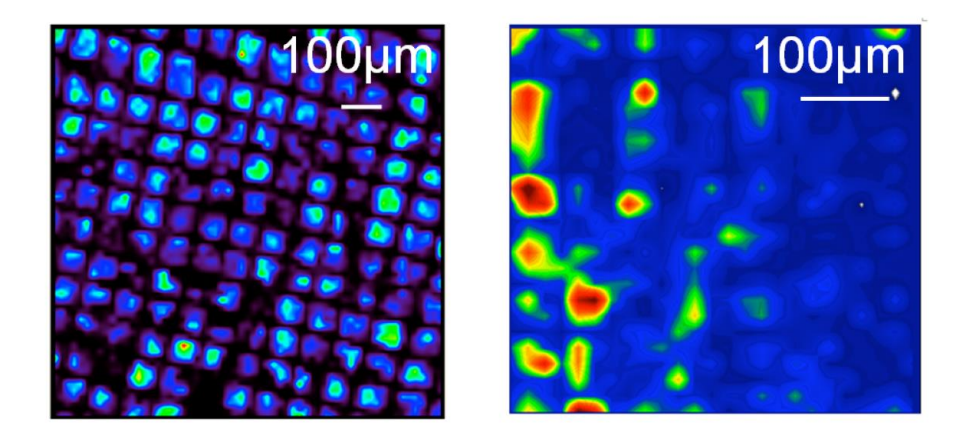


Figure 2.8. Imaging of metabolites from *S. habrochaites* LA1777 leaf trichomes transferred into the (left) 100 μ m and (right) 50 μ m TEM grids. Ion abundances are displayed for m/z 731 (acylsugar S4:21 [M+K]⁺), using positive mode with laser power setting = 95, 25 μ m stage step size, and 200 laser shots per pixel.

2.3.3 Single-trichome imaging

To circumvent the influence of carbon surface defects on ion yields, a glassy carbon plate was judged to be a promising alternative. Glassy carbon has structural features resembling fullerenes [44] and has been used for small-molecule analysis by LDI [45]. Figure 2.9 shows LDI images obtained in both positive ion mode and negative ion mode of trichomes transferred from a small (5 mm \times 10 mm) leaflet of *S. habrochaites* LA1777 to a glassy carbon surface by contact printing. The images document metabolite profiles with spatial resolution of individual trichomes. Further examination of the mass spectra generated at different locations across the leaflet suggested a heterogeneous spatial distribution of metabolites in spectra attributed to specific trichome types. In the positive ion mode spectra, an example spectrum selected from a bright spot on the m/z 731 image near the midvein shows a series of ions separated by 14 Da that correspond to a homologous series of potassium cationized acyl sugars that selectively accumulate in type I/IV glands [32]. The ion at m/z 731 corresponds to $[M+K]^+$ of acylsucrose S4:21 (acyl sugar nomenclature based on

[46]). The spectrum of a pixel remote from the midvein also displays a strong m/z 731 signal, but shows relative abundances of S4:21 ions (m/z 715 and 731; [M+Na]⁺ and [M+K]⁺, respectively) greater than those for other acyl sugar homologs. Since the acyl groups are anticipated to derive from specific amino acids or related elongation products, the differences in the relative abundances across glands of a common type suggest that metabolic fluxes into specialized metabolites have a significant dependence on the location of the trichome within leaf tissue. Similar heterogeneity was observed in the negative ion mode image, which revealed a dominance of flavonoids, detected as m/z 301 (quercetin aglycone anion), near the midvein, but greater prominence of sesquiterpene acids (m/z 233) in regions closer to the edge of the leaflet. Since both classes of metabolites accumulate primarily in type VI glands [32], the results suggest substantial chemical heterogeneity among these glands. Whether this reflects different access of trichomes to metabolite precursors in phloem near the midvein remains to be determined and further investigation into the factors that control accumulation of metabolites in individual trichomes is under way.

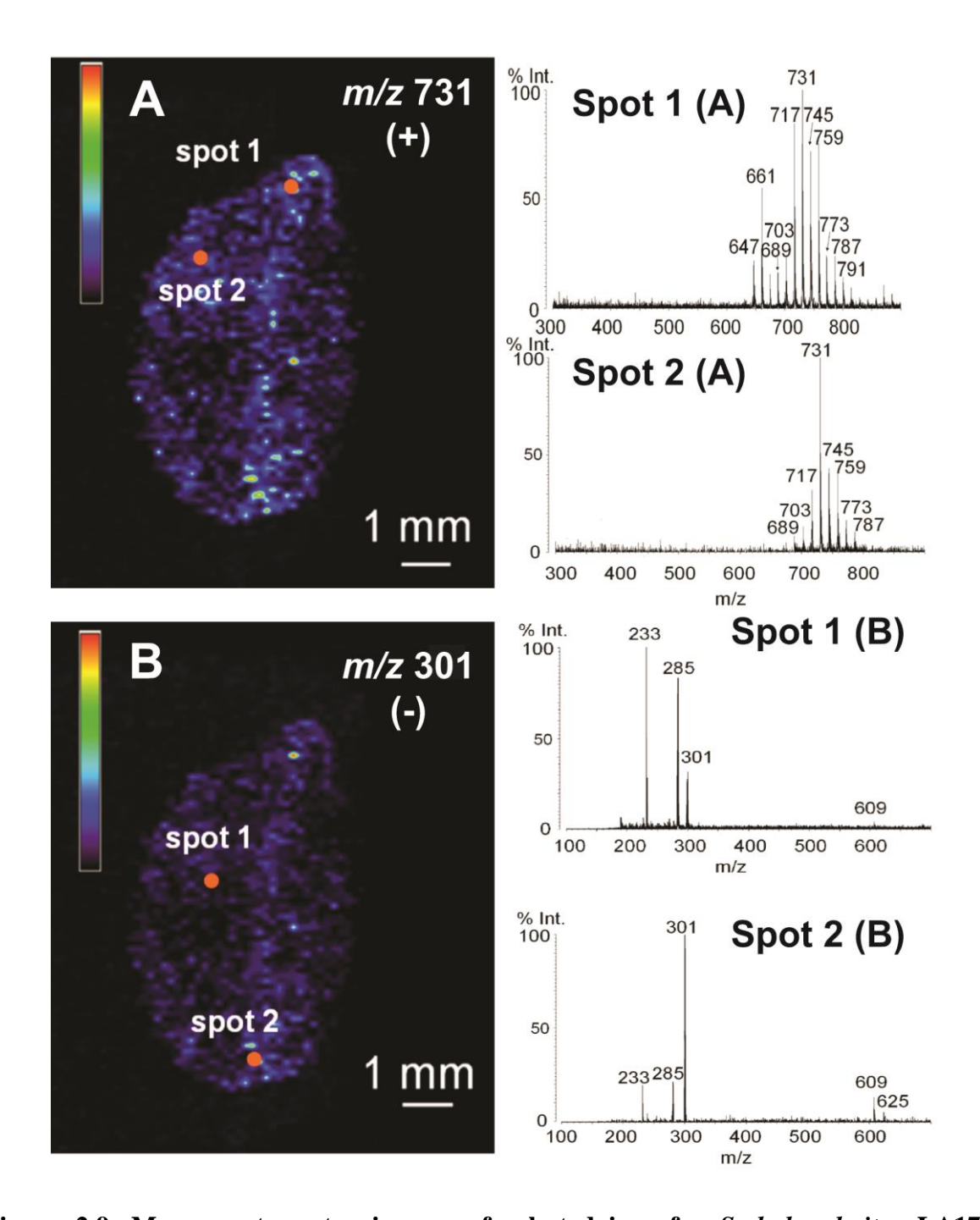


Figure 2.9. Mass spectrometry images of selected ions for *S. habrochaites* LA1777 trichomes transferred to glassy carbon. (A) Image for m/z 731 in positive ion mode, corresponding to acyl sugar S4:21 ($[M+K]^+$), using a laser power setting of 105, a 125- μ m stage step, and 20 laser shots per pixel. Mass spectra are displayed for individual pixels labeled spot 1 and spot 2 on the image. (B) Image for m/z 301 in negative ion mode (fragment ion of quercetin glycosides) for the same leaf sample using a laser power setting of 115, a 125- μ m step size, and 20 laser shots per pixel. Mass spectra are displayed for individual pixels labeled spot 1 and spot 2 on the image.

The differences in metabolic phenotypes between individual type VI trichomes within a small leaflet region are more pronounced in the images shown in Figure 2.10, which shows a reflected light microscope image of the transferred trichomes on a glassy carbon surface (Figure 2.10) and the corresponding LDI image of m/z 233 and m/z 301 in negative ion mode. To address the challenges of aligning optical and MS images, four position indicators were applied to the substrate using liquid paper, which is easily visualized using the camera in the MALDI instrument. These reference points lie outside the area shown in the images in Figure 2.10. These images demonstrate that metabolite signals are obtained with spatial resolution of individual trichomes. To further confirm the physical integrity of trichomes after the transfer printing process, a fluorescence microscope image was obtained (Figure 2.10 D), which shows fluorescence is confined to the interior of the type VI trichomes. To obtain this image, it was not feasible to use a carbon substrate; however, a thin film of carbon was deposited afterward using vacuum evaporation and deposition, in the same manner as is common in sample preparation for scanning electron microscopy. The LDI image (Figure 2.10 E, F) was obtained by transferring the carbon-coated slide into the MALDI instrument. To obtain higher spatial resolution, oversampling was performed [43] using a laser power setting of 145. Owing to the small stage step size and the relatively slow laser repetition rate (10 Hz), the imaging of an entire leaflet at single-gland resolution would take about 15 days to complete, so the imaging was conducted over only a small area. As was the case with the glassy carbon substrate, substantial differences in the intensities of the sesquiterpene acid signal at m/z 233 and the signal of the aglycone fragment of quercetin glycosides at m/z 301 were observed in negative ion mode for trichomes adjacent to one another on the leaf surface. For example, trichome 7 in Figure 2.10 E showed a weak signal for sesquiterpene acid at m/z 233 but

showed the strongest signal for the aglycone fragment of quercetin glycosides at m/z 301 (Figure 2.10 F). This striking heterogeneity of trichome chemistry provides a compelling reason for performing chemical imaging of trichomes. If all trichomes on a leaf surface were chemically identical, the rationale for imaging might fade.

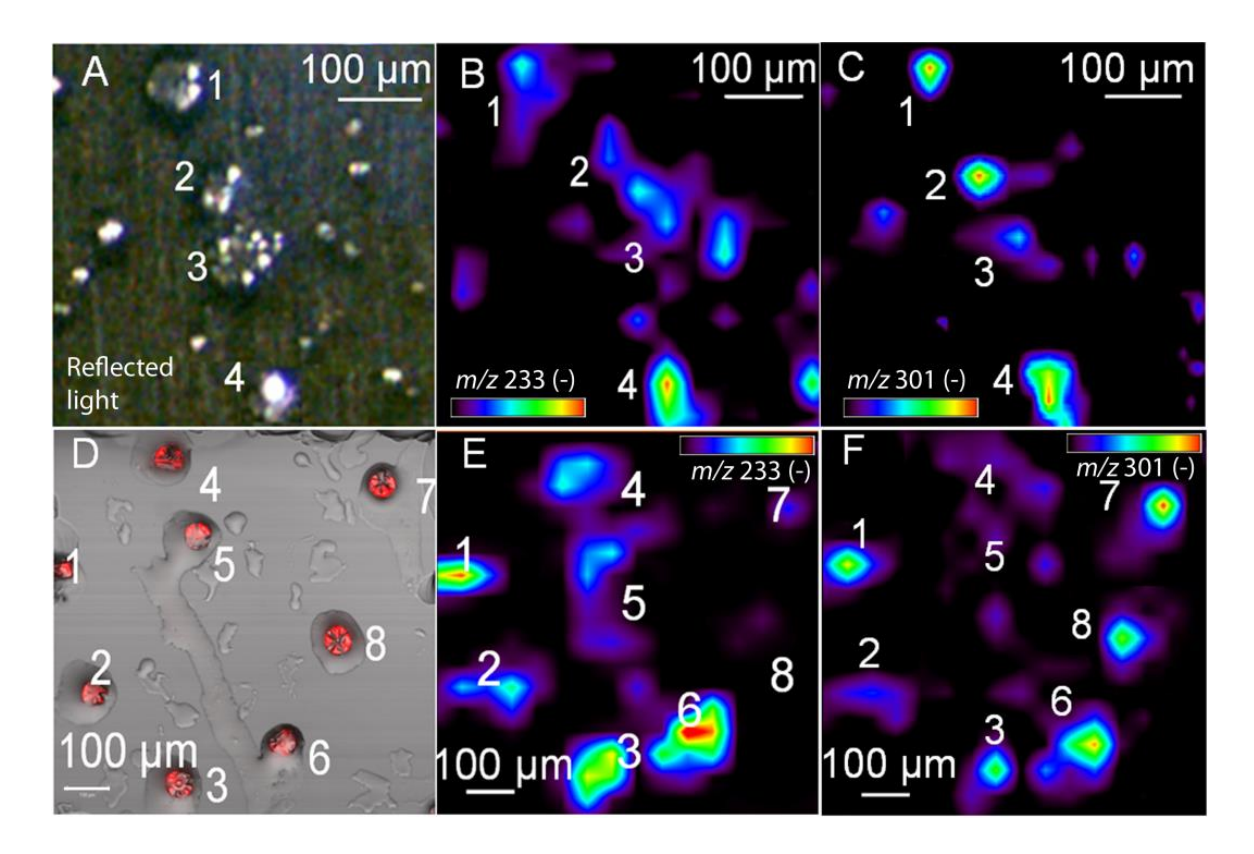


Figure 2.10. Reflected light LDI image and fluorescent image of a contact printing of *S. habrochaites* LA1777 trichomes on a glass. (A) Image of LA1777 trichomes printed on a glassy carbon surface and (B) reflected light LDI image of the m/z 233 ion (sesquiterpene acids) in negative ion mode on the same glassy carbon area. The step size was 25 μm, with 200 laser shots per pixel. (C) LDI image of the m/z 301 ion (aglycone fragment of quercetin glycosides) in negative ion mode on the same glassy carbon area. The step size was 25 μm, with 200 laser shots per pixel. (D) Fluorescent image of a separate contact printing of LA1777 trichomes on a glass slide using 543-nm excitation and 560-nm band-pass emission showing fluorescent type VI glands. The slide was subjected to carbon coating afterward. (E) Mass spectrometry image of the same glass slide as in d after carbon coating, showing the ion abundance map for m/z 233 in negative ion mode using 200 laser shots per pixel with a 25-μm step size. (F) Mass spectrometry image of the same glass slide as in (D) after carbon coating, showing the ion abundance map for m/z 301 in negative ion mode using 200 laser shots per pixel with a 25-μm step size. Color scales reflect 0-100 % of highest abundance.

2.3.4 Heterogeneity in localization and quantity of acylsugars in M82 leaf trichomes

The LDI imaging approach was employed to explore the quantity and heterogeneity of acylsugar special metabolites in M82 leaf trichomes. Figure 2.11 displays LDI images from adaxial leaf trichomes of commercial tomato (S. lycopersicum M82). These images are singleion abundance maps for acylsucroses containing only short-chain (≤ 6 carbon) aliphatic esters, which are among the most abundant forms. Two specific metabolites, the tri-acylsucrose S3:15 and the tetra-acylsucrose S4:17, were detected in positive-ion mode images as [M+Na]⁺ or [M+K]⁺ forms. In Figure 2.11 B, the red color shows higher ion abundance and blue codes for lower abundance. From the colors of the left two images we can see that the [M+K]+ ion (m/z 675) corresponding to tetra-acyl sugar S4:17(2,5,5,5) is more abundant at most pixels across the leaf than the corresponding ion (m/z) 633) of the tri-acyl sugar S3:15(5,5,5), which lacks the acetate ester group at position 2 These profiles are consistent with the profiles of acylsugar metabolites using UHPLC/TOF MS and NMR [37, 46]. The images indicate that S4:17 are distributed somewhat evenly across the leaflet tissue, but S3:15 is particularly concentrated around the midvein near the base of the leaflet. The reasons for the different relative abundances are not yet clear, but would be consistent with either reduced expression of the acyltransferase that adds the acetyl group (now called SIASAT4 [47]), lower pools of acetyl CoA in these trichomes, or more efficient hydrolytic removal of the acetyl group by hydrolases. The heterogeneity of metabolite composition across a single leaflet suggests that chemical imaging of this kind might be a valuable tool that can guide micro-collection of mRNA such that transcript abundances that correlate with localized trichome chemistry might be more effectively exploited for assessment of gene functions.

Concurrent with these imaging experiments, the laboratory of Professor Robert Last at Michigan State University identified a BAHD acyltransferase gene (Soly01g105580, initially named SIAT2, but more recently assigned the designation of SIASAT4) that catalyzes acetylation of tri-acylsucroses at the 2-position, using acetyl CoA as co-substrate, to yield tetra-acylsucroses [46]. To assess the effectiveness of SIAT2 silencing (Figure 2.11 A) using RNAi across the leaflet tissue, leaflets of the SIAT2 silenced line and wild type M82 were harvested and trichomes were transferred to a carbon substrate by contact printing as described above. The transgenic M82 was kindly provided by Dr. Anthony Schilmiller from Last lab. LDI images presented in Figure 2.11 B1 and B2 show evidence of S3:15 and S4:17 in the wild type M82 trichomes, with the former being particularly abundant near the base of the leaflet near the midvein. In contrast, LDI images of the silenced M82 plant showed that the tetra-acylsucrose S4:17 was almost completely absent from the leaflet, but tri-acylsucrose S3:15 was abundant and widespread in its distribution across the tissue. This imaging result is consistent with RT-PCR sequence analysis and LC/MS metabolite profiling that documented RNAi-mediated suppression of AT2 expression in S. lycopersicum M82 plants, reduced acylsugar acetylation, and an increase in the ratio of S3:15 to S4:17 (unacetylated vs. acetylated; [46]). Meanwhile, these images deliver some interesting hints that the distribution of trichome acylsugars across the leaflet is far from uniform, as type 1/4 glands are distributed more widely than the acylsugar abundances observed in the LDI images. This application demonstrates that LDI imaging results can indicate chemical heterogeneity among cells of a common type and this information can be used to guide metabolic engineering of specialized metabolism in plants.

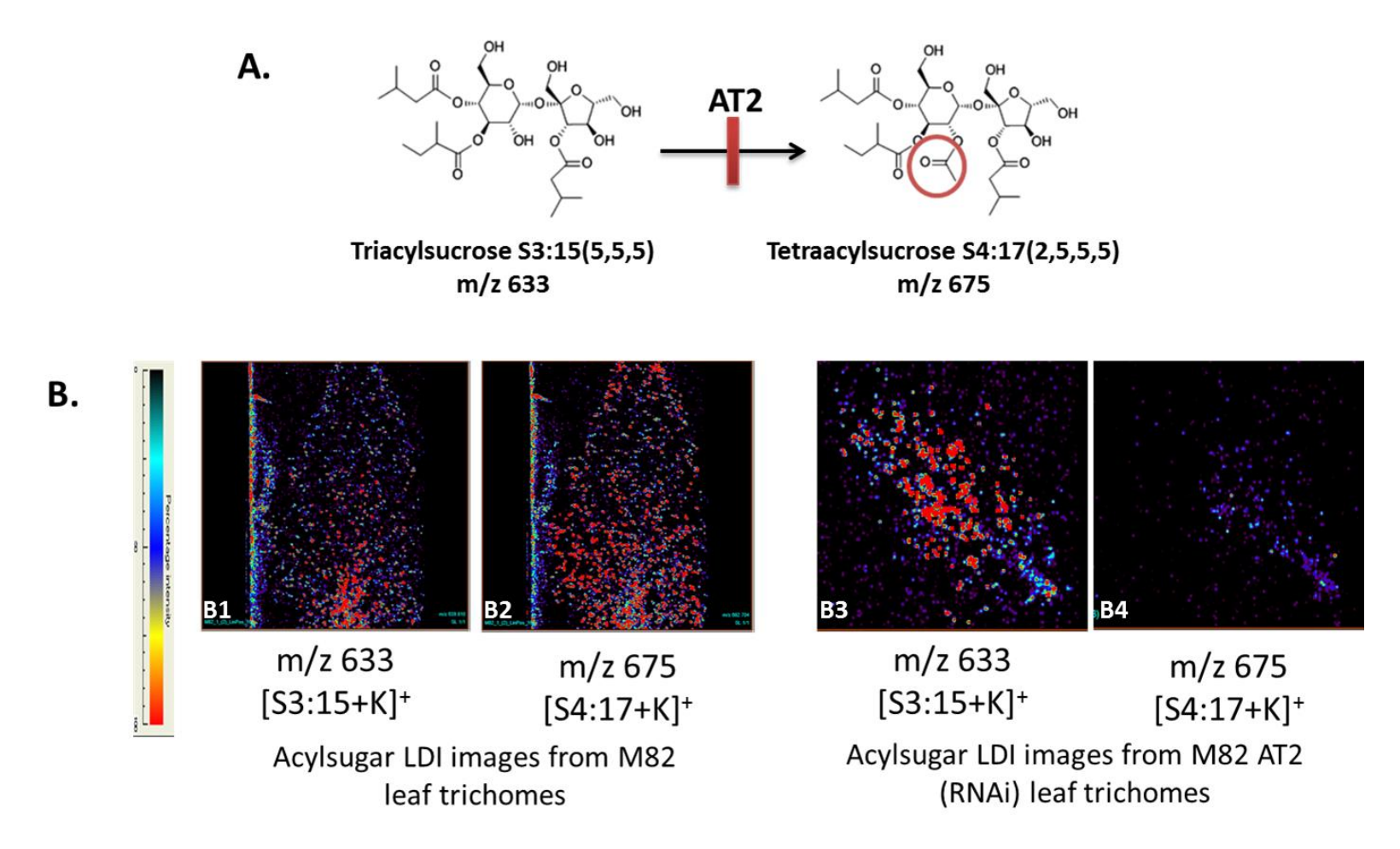


Figure 2.11. Localization of acylsugars in *S. lycopersicum* M82 leaf trichomes using contact printing and LDI imaging from carbon-coated slides. (A) The RNAi lines are M82 plants transformed with a T-DNA that was designed to suppress the expression of only AT2, a BAHD acyltransferase that acetylates tri-acylsucroses to make tetra-acylsucroses. (B) Images showing spatial distribution of abundances for: (B1: m/z 633 corresponding to [M+K]⁺ of S3:15 and B2: m/z 675 corresponding to [M+K]⁺ of S4:17 in in *S. lycopersicum* M82 leaflet trichomes; B3: m/z 633 corresponding to [M+K]⁺ of S3:15 and B4: m/z 675 corresponding to [M+K]⁺ of S4:17. in RNAi line leaf trichomes.

2.4 Conclusions

Combining contact printing with matrix-free ionization from a carbon-based substrate yielded chemical profiles of individual trichomes with minimal disruption of position that is often the result of matrix deposition. The contact printing scheme has several merits: (1) tedious sample preparation steps are avoided; (2) metabolite analysis does not suffer from interference from the matrix or the solvent, which can compromise spatial integrity of the sample; (3) contact printing to a cold substrate provides a mechanism for quenching metabolism during sample preparation; and (4) the technique allows selective imaging of fragile but prolific epidermal cells without interference from other cell types. The simplicity of sample preparation makes such experiments accessible to a broad range of researchers with limited technical expertise in sample preparation.

This printed transfer scheme offers other novel applications. By use of the printed transfer method, trichomes from both upper and lower leaf surfaces can be transferred to separate substrate surfaces in a single step. This makes possible more complete analysis of a single leaf or other plant tissues. Furthermore, this carbon-based substrate imaging scheme has potential use for field sampling in agricultural or ecological studies. Since the carbon substrate can be easily frozen, stored, and shipped, this approach can be used to collect epidermal cells from plant tissues at locations remote from the laboratory, maintaining spatially preserved chemical information.

REFERENCES

REFERENCES

- 1. Hall, R.D. Plant metabolomics in a nutshell: Potential and future challenges, in *Annual Plant Reviews Volume 43* 1-24 (Wiley-Blackwell, 2011).
- 2. Kehr, J. High resolution spatial analysis of plant systems. *Current opinion in plant biology* **4**, 197-201 (2001).
- 3. Martin, C., Bhatt, K. & Baumann, K. Shaping in plant cells. *Current opinion in plant biology* **4**, 540-549 (2001).
- 4. WAGNER, G.J., WANG, E. & SHEPHERD, R.W. New Approaches for Studying and Exploiting an Old Protuberance, the Plant Trichome. *Annals of Botany* **93**, 3-11 (2004).
- 5. McCaskill, D. & Croteau, R. Strategies for bioengineering the development and metabolism of glandular tissues in plants. *Nat Biotech* **17**, 31-36 (1999).
- 6. Schilmiller, A.L., Last, R.L. & Pichersky, E. Harnessing plant trichome biochemistry for the production of useful compounds. *The Plant Journal* **54**, 702-711 (2008).
- 7. Luckwill, L.C. *The genus lycopersicon : an historical, biological, and taxonomic survey of the wild and cultivated tomatoes.* (University Press, Aberdeen; 1943).
- 8. Brandt, S., Kloska, S., Altmann, T. & Kehr, J. Using array hybridization to monitor gene expression at the single cell level. *Journal of experimental botany* **53**, 2315-2323 (2002).
- 9. Brandt, S.P. Microgenomics: gene expression analysis at the tissue-specific and single-cell levels. *Journal of experimental botany* **56**, 495-505 (2005).
- 10. Chao, T.-C. & Ros, A. Microfluidic single-cell analysis of intracellular compounds. *Journal of The Royal Society Interface* **5**, S139-S150 (2008).
- 11. Emmert-Buck, M.R. et al. Laser Capture Microdissection. Science (New York, N.Y.) 274, 998-1001 (1996).
- 12. Karrer, E.E. *et al.* In situ isolation of mRNA from individual plant cells: creation of cell-specific cDNA libraries. *Proceedings of the National Academy of Sciences* **92**, 3814-3818 (1995).
- 13. Katsuragi, T. & Tani, Y. Single-Cell Sorting of Microorganisms by Flow or Slide-Based (Including Laser Scanning) Cytometry. *Acta Biotechnologica* **21**, 99-115 (2001).

- 14. Nelson, A.R., Allbritton, N.L. & Sims, C.E. Rapid Sampling for Single-Cell Analysis by Capillary Electrophoresis, in *Methods in Cell Biology*, Vol. Volume 82 709-722 (Academic Press, 2007).
- 15. Schulte, A. & Schuhmann, W. Single-Cell Microelectrochemistry. *Angewandte Chemie International Edition* **46**, 8760-8777 (2007).
- 16. Yang, Q. *et al.* Single cell determination of nitric oxide release using capillary electrophoresis with laser-induced fluorescence detection. *Journal of Chromatography* A **1201**, 120-127 (2008).
- 17. Murphy, R.C., Hankin, J.A. & Barkley, R.M. Imaging of lipid species by MALDI mass spectrometry. *Journal of Lipid Research* **50**, S317-S322 (2009).
- 18. Seeley, E.H. & Caprioli, R.M. Molecular imaging of proteins in tissues by mass spectrometry. *Proceedings of the National Academy of Sciences* **105**, 18126-18131 (2008).
- 19. Shroff, R., Vergara, F., Muck, A., Svatoš, A. & Gershenzon, J. Nonuniform distribution of glucosinolates in Arabidopsis thaliana leaves has important consequences for plant defense. *Proceedings of the National Academy of Sciences* **105**, 6196-6201 (2008).
- 20. Simmons, T.L. *et al.* Biosynthetic origin of natural products isolated from marine microorganism–invertebrate assemblages. *Proceedings of the National Academy of Sciences* **105**, 4587-4594 (2008).
- 21. Yang, Y.-L., Xu, Y., Straight, P. & Dorrestein, P.C. Translating metabolic exchange with imaging mass spectrometry. *Nat Chem Biol* **5**, 885-887 (2009).
- 22. Gholipour, Y., Nonami, H. & Erra-Balsells, R. Application of pressure probe and UV-MALDI-TOF MS for direct analysis of plant underivatized carbohydrates in subpicoliter single-cell cytoplasm extract. *J Am Soc Mass Spectrom* **19**, 1841-1848 (2008).
- 23. Nemes, P. & Vertes, A. Atmospheric-pressure Molecular Imaging of Biological Tissues and Biofilms by LAESI Mass Spectrometry. e2097 (2010).
- 24. Shrestha, B. & Vertes, A. Direct Analysis of Single Cells by Mass Spectrometry at Atmospheric Pressure. e2144 (2010).
- 25. Shrestha, B. & Vertes, A. In Situ Metabolic Profiling of Single Cells by Laser Ablation Electrospray Ionization Mass Spectrometry. *Analytical Chemistry* **81**, 8265-8271 (2009).

- 26. Tak áts, Z., Wiseman, J.M., Gologan, B. & Cooks, R.G. Mass Spectrometry Sampling Under Ambient Conditions with Desorption Electrospray Ionization. *Science (New York, N.Y.)* **306**, 471-473 (2004).
- 27. Laskin, J., Heath, B.S., Roach, P.J., Cazares, L. & Semmes, O.J. Tissue Imaging Using Nanospray Desorption Electrospray Ionization Mass Spectrometry. *Analytical Chemistry* **84**, 141-148 (2012).
- 28. Varner, J.E. & Ye, Z. Tissue printing. *The FASEB Journal* **8**, 378-384 (1994).
- 29. Jacobsen, J.V. & Knox, R.B. Cytochemical localization and antigenicity of α-amylase in barley aleurone tissue. *Planta* **112**, 213-224 (1973).
- 30. Kotecha, S.A., Eley, D.W. & Turner, R.W. Tissue printed cells from teleost electrosensory and cerebellar structures. *The Journal of Comparative Neurology* **386**, 277-292 (1997).
- 31. Gaston, S.M. *et al.* Tissue-print and print-phoresis as platform technologies for the molecular analysis of human surgical specimens: mapping tumor invasion of the prostate capsule. *Nat Med* **11**, 95-101 (2005).
- 32. McDowell, E.T. *et al.* Comparative functional genomic analysis of Solanum glandular trichome types. *Plant physiology* (2010).
- 33. Black, C., Poile, C., Langley, J. & Herniman, J. The use of pencil lead as a matrix and calibrant for matrix-assisted laser desorption/ionisation. *Rapid Communications in Mass Spectrometry* **20**, 1053-1060 (2006).
- 34. Cha, S. & Yeung, E.S. Colloidal Graphite-Assisted Laser Desorption/Ionization Mass Spectrometry and MSn of Small Molecules. 1. Imaging of Cerebrosides Directly from Rat Brain Tissue. *Analytical Chemistry* **79**, 2373-2385 (2007).
- 35. Cha, S. *et al.* Direct profiling and imaging of plant metabolites in intact tissues by using colloidal graphite-assisted laser desorption ionization mass spectrometry. *The Plant Journal* **55**, 348-360 (2008).
- 36. Zhang, H., Cha, S. & Yeung, E.S. Colloidal Graphite-Assisted Laser Desorption/Ionization MS and MSn of Small Molecules. 2. Direct Profiling and MS Imaging of Small Metabolites from Fruits. *Analytical Chemistry* **79**, 6575-6584 (2007).
- 37. Ghosh, B., Westbrook, T.C. & Jones, A.D. Comparative structural profiling of trichome specialized metabolites in tomato (Solanum lycopersicum) and S. habrochaites: acylsugar profiles revealed by UHPLC/MS and NMR. *Metabolomics* 10, 496-507 (2014).

- 38. Coates, R.M., Denissen, J.F., Juvik, J.A. & Babka, B.A. Identification of .alpha.-santalenoic and endo-.beta.-bergamotenoic acids as moth oviposition stimulants from wild tomato leaves. *The Journal of Organic Chemistry* **53**, 2186-2192 (1988).
- 39. Fernández, J.A., Ochoa, B., Fresnedo, O., Giralt, M.T. & Rodr guez-Puertas, R. Matrix-assisted laser desorption ionization imaging mass spectrometry in lipidomics. *Anal Bioanal Chem* **401**, 29-51 (2011).
- 40. Rauser, S., Deininger, S.O., Suckau, D., Hofler, H. & Walch, A. Approaching MALDI molecular imaging for clinical proteomic research: current state and fields of application. *Expert Rev Proteomics* **7**, 927-941 (2010).
- 41. Seeley, E.H. & Caprioli, R.M. MALDI imaging mass spectrometry of human tissue: method challenges and clinical perspectives. *Trends in Biotechnology* **29**, 136-143 (2011).
- 42. Shanta, S.R.K., Young-Jun; Kim, Young-Hwan; Kim, Kwang-Pyo; Application of MALDI Tissue Imaging of Drugs and Metabolites: A New Frontier for Molecular Histology. *Biomolecules and Therapeutics* **19**, 149-154 (2011).
- 43. Jurchen, J., Rubakhin, S. & Sweedler, J. MALDI-MS imaging of features smaller than the size of the laser beam. *J Am Soc Mass Spectrom* **16**, 1654-1659 (2005).
- 44. Harris, P.J.F. Fullerene-related structure of commercial glassy carbons. *Philosophical Magazine* **84**, 3159-3167 (2004).
- 45. Huang, J.-P., Yuan, C.-H., Shiea, J. & Chen, Y.-C. Rapid Screening for Diuretic Doping Agents in Urine by C60-Assisted Laser-Desorption-Ionization-Time-of-Flight Mass Spectrometry. *Journal of Analytical Toxicology* **23**, 337-342 (1999).
- 46. Schilmiller, A. *et al.* Mass spectrometry screening reveals widespread diversity in trichome specialized metabolites of tomato chromosomal substitution lines. *The Plant journal: for cell and molecular biology* **62**, 391-403 (2010).
- 47. Schilmiller, A.L. & Moghe, G.D. Functionally divergent alleles and duplicated Loci encoding an acyltransferase contribute to acylsugar metabolite diversity in Solanum trichomes. **27**, 1002-1017 (2015).

Chapter 3. Profiling of Stable Isotope Enrichment in Solanum Trichome Specialized Metabolites of Using Liquid Chromatography and Multiplexed Nonselective Collision-Induced Dissociation

The research discoveries described in this chapter have been published in part in the following journal article: Z. Wang and A. D. Jones, Profiling of Stable Isotope Enrichment in Specialized Metabolites Using Liquid Chromatography and Multiplexed Nonselective Collision-Induced Dissociation. *Analytical Chemistry*. 2014, 86, 10600 – 10607

3.1 Introduction

Plants are remarkable in both the number and the complexity of metabolites they produce through divergent specialized metabolism [1]. Given this diversity, understanding and engineering of plant metabolic networks is challenged by limited knowledge regarding the identities of specialized metabolites, biosynthetic pathways that are responsible for their formation and processes that regulate their accumulation. Advances in metabolomics and analytical chemistry hold promise for discovering novel solutions to explore and engineer green "chemical factories" [2, 3] and plants with improved resistance to pests.

Metabolite profiling of plant specialized metabolites has been accelerated with improvements in hyphenated technologies that marry gas chromatographic (GC) and liquid chromatographic (LC) separation strategies with mass spectrometry (MS) and nuclear magnetic resonance (NMR) detection [4]. LC/MS and GC/MS offer distinct advantages in the wide range of detectable metabolites, the expansive coverage of metabolite classes, and also high sensitivity and accuracy of quantification [5-7]. The integration of NMR with LC/MS and LC/diode array analyses has shown special capacity in determination of structures of unknown metabolites [8] and NMR strategies for investigating plant metabolism, including the use of stable isotopes, have been the subject of two particularly useful reviews [9, 10]. Compared to NMR, MS offers lower detection limits but often fails to provide positional label incorporation information [11]. However, fragmentation in MS offers an approach to assess positional labeling in the substructures of a metabolite. All these techniques advance the application of metabolite profiling in addressing questions of functional genomics and system biology.

Though successful and inspiring, most investigations of plant specialized metabolism have focused on a snapshot of metabolome, transcriptome, and proteome pro files, and it has been common for metabolite levels to be assessed at a single time point or stage of development [3, 12]. However, plant specialized metabolites are usually not end products of metabolism, and accumulation of specialized metabolites reflects a dynamic balance involving synthesis, storage/transport, and degradation at specific growth conditions. Assessments of rates of synthesis and turnover of specialized metabolites are not directly obtained from metabolite levels but can be probed using isotopic tracers, providing information vital for plant metabolic engineering [11, 13].

Unraveling of metabolic dynamics has often relied on isotopic labeling as a convincing way to dictate and track specific metabolites in plant tissues [14-16]. A variety of isotopic labeling approaches have been demonstrated, including steady-state labeling or dynamic labeling strategies, based upon feeding plant cells or tissues with specific isotopic tracer(s) and measuring the changes of isotope incorporation into a variety of substances. ¹³C labeling has found extensive use in measuring carbon fluxes into target proteins, lipids, and other central plant metabolites [17, 18]. Although much effort has been devoted to isotopic tracer studies, most research has focused on either central metabolic flux analysis to enhance biomass yields or to aid annotation and chemical formula assignment for endogenous metabolites. Application of stable isotope labeling to investigations of specialized metabolism has been slower to develop owing to limited knowledge about pathways, intermediates and their pool sizes, and metabolic fluxes, particularly in nonmodel plants. Mass spectrometry has emerged as an essential tool for measuring enrichments of stable isotope tracers, but the depth

and reliability of quantitative information that MS analyses provide in measurements of labeling of specialized metabolites have not been adequately explored.

Though ¹³C NMR techniques have great utility for establishing isotopic enrichments at specific carbons in a metabolite, the large quantities of material needed for such experiments often limit such analyses to more abundant metabolites, particularly when sample size is limited. As a consequence, mass spectrometry is often the first-pass analytical technique of choice for measuring ¹³C incorporation [2]. Mass spectrometry tactics capable of comprehensive quantification of ¹³C incorporation at specific carbons of central metabolites (e.g., small organic acids and amino acids) have been rare but have found success by first screening a comprehensive set of multiple reaction monitoring (MRM) transitions and selecting those that provide information about label position to establish label incorporation in specific locations within a metabolite as has been demonstrated through GC/MS/MS analyses of derivatized aspartic acid [19]. Such an approach is valuable for metabolic flux analysis, but its extension to larger specialized metabolites (e.g., the tomato glycoalkaloid tomatine has 50 carbon atoms) would require a huge number of MRM transitions for each metabolite, making this approach impractical. In addition, mathematical deconvolution of the label rises in complexity with the number of carbon atoms and with structural redundancy common in specialized metabolism, since comprehensive cleavage of all carbon-carbon bonds, needed for simple assessment of labeling at each position, rarely occurs upon collision-induced dissociation (CID).

To our knowledge, mass spectrometric measurements of carbon fluxes into and out of specialized metabolites have been limited, often focusing on elemental formula assignments. The Saito laboratory used ¹³C labeling to establish of the number of carbon atoms in sulfur-

containing metabolites in onion bulbs [20], and a similar report employed ¹³C labeling for annotation of plant metabolites [21]. Another investigation produced ¹³C-labeled artemisinin from Artemisia annua grown under ¹³CO₂. Since mass spectrometry techniques often fail to give essential information about positions of label incorporation, this report used ¹³C NMR to establish that artemisinin was predominantly biosynthesized from (E,E)-farnesyldiphosphate (FPP) and that the central isoprenoid unit had been obtained via the nonmevalonate pathway [22]. A recent report quantified the incorporation of ¹³C-label from [¹³C₃]pyruvate in primary metabolites using GC/MS and in one specialized metabolite (loganic acid) in methyl jasmonate-elicited Catharanthus roseus cell cultures using ultraperformance liquid chromatography/Fourier transform mass spectrometry (UPLC/FTMS) [23]. Their findings serve as a foundation for future investigations by documenting the extent of carbon flow from primary to specialized metabolic pathways. However, a large proportion of specialized metabolites are not amenable to GC separations, and LC/MS analyses usually employ soft ionization methods that are useful for measurements of total label incorporation but yield limited information about labeling in specific substructures. In some cases, labeling in substructures may be assessed through generation of fragment ions, for example, using collision-induced dissociation. Such analyses are usually performed using MS/MS, in which ions that fall within a narrow range of m/z values are isolated and subjected to activation. In some instruments, both selection and precursor activation may introduce mass bias, as observed in certain analyses of ¹³C-labeled peptides [24], and this subject has been recently addressed in more detail [25]. MS^E offers an option to generate spectra with both fragmenting and nonfragmenting collision conditions in a single acquisition for nontargeted analysis but

does not necessarily provide sufficient information about energy-dependence of fragment ion formation and may not yield desired fragmentation for all metabolites [26].

To address this issue, this report presents a nontargeted metabolomics approach to perform nonbiased quantitative assessments of labeling using nonselective multiplexed CID in the collision cell of a quadrupole time-of-flight (QTOF) mass spectrometer [27, 28]. To demonstrate proof of concept, tomato plants were grown under a ¹³CO₂-enriched atmosphere, and ¹³C enrichments in whole specialized metabolites and substructures of these metabolites were quantified. The workflow of this approach is illustrated in Figure 3.1.

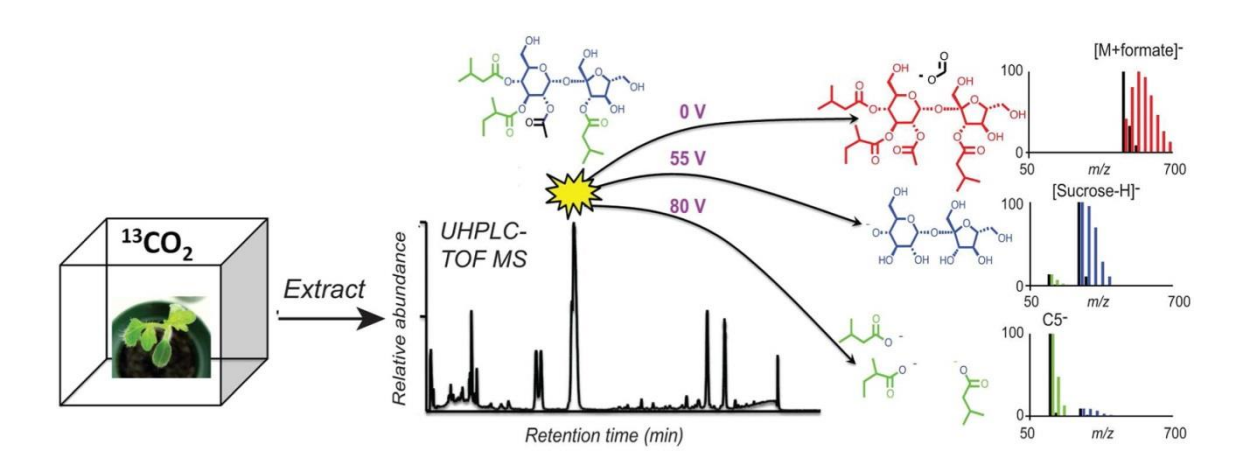


Figure 3.1. The workflow of nontargeted metabolomic approach for nonbiased quantitative assessments of labeling using nonselective multiplexed CID. Tomato plants were grown under the ¹³CO₂-enriched atmosphere, and ¹³C enrichments in specialized metabolite intact molecules and substructures were quantified on a QTOF mass spectrometer.

3.2 Materials and methods

3.2.1 Chemicals

HPLC grade acetonitrile, 2-propanol, methanol, formic acid (88% aqueous solution), and ACS grade sulfuric acid (95%-98%, J.T. Baker) were purchased from VWR Scientific. Sodium [13 C] bicarbonate (98 atom % 13 C) was obtained from Sigma-Aldrich (St. Louis, MO).

3.2.2 ¹³C labeling of plants

Tomato (*Solanum lycopersicum* M82; LA3475) seeds for plants were obtained from the UC Davis/C. M. Rick Tomato Genetics Resource Center. Tomato seeds were germinated at ambient conditions, and seedlings were then transferred and maintained in a 61 cm \times 64 cm \times 64 cm custom plexiglass box under an atmosphere pulsed with 13 CO₂ to reach about 400 ppm. The custom box was placed in a growth chamber at Michigan State University. Pulsed addition of 13 CO₂ was accomplished by mixing 20 mg of sodium [13 C] bicarbonate and 800 μ L of 1 M sulfuric acid in a glass test tube every 24 h, beginning at the sixth day post germination. Unlabeled control tomato plants were grown in the same growth chamber under ambient atmosphere.

3.2.3 Sample preparation

Within 2 weeks post germination, the first terminal leaflet was removed at 10 days post-germination in the chamber box, after 5 days of labeling. In parallel, control group unlabeled tomato plants were sampled at the same date. The terminal leaflet tissues were collected from the first node of leaves from the base of the plant. Leaflets were harvested using a razor blade by cutting from the base of the leaflet (petiolule) and were quickly dipped into 1mL of isopropanol/MeOH/H₂O (3:3:2 v/v/v) for 1 min. Extracts were then evaporated to dryness under vacuum using SpeedVac and then redissolved in 100 μ L of 4:1 (v/v) MeOH/H₂O. Redissolved extracts were centrifuged at 10 000g for 10min at 4 °C, and 100 μ L of the supernatants were transferred to an autosampler vial for ultrahigh performance liquid chromatography/mass spectrometry (UHPLC/MS) analysis.

3.2.4 UHPLC/MS analysis with Multiplexed collision-induced dissociation (CID)

Separations were performed using UHPLC with a Supelco Ascentis Express C18 column (2.1 × 50 mm, 2.7 µm particles) held at 40 °C that was interfaced to a Xevo G2-S QTOF mass spectrometer (Waters, Milford, MA). A solvent gradient was executed based on 10 mM aqueous ammonium formate (A) and methanol (B) as follows: initial conditions 5% B; linear gradient to 50% B (3 min); 60% B (15 min); 70% B (16 min); 80% B (24 min); 100% B (26 min); hold at 100% B until 28 min; return to 5% B at 28.01 min and hold until 32 min. The flow rate was 0.4 mL min⁻¹, and the injection volume was 10 µL. The mass spectrometer was operated using electrospray ionization (ESI) in negative-ion mode under the control of MassLynx version 4.1 software. The ESI conditions were as follows: capillary voltage, 2.14 kV; sample cone voltage, 35 V; source temperature, 90 °C; desolvation gas flow, 800 L/h; desolvation gas temperature, 280 °C; cone gas flow, 0 L/h. Mass spectra were acquired over m/z 50-1500 using centroid peak acquisition and extended dynamic range in resolution mode $(M/\Delta M \sim 23~000, \text{ fwhm})$. Collision voltages were switched among 0, 20, 35, 55, and 80 V for five parallel data acquisition functions to generate molecular and fragment mass information in a single analysis using acquisition time of 0.1 s per function. The fast ($\sim 50 \,\mu s/t$ ransient) acquisition times offered by time-of-flight mass analysis allow averaging of about 2000 transients during the 100 ms duration of each data acquisition function. The hybrid time-todigital (TDC)/analog-to-digital (ADC) detector yields extended dynamic range relative to earlier TDC detectors. In the current investigation, five CID functions were employed to achieve a minimum of fragmentation at the lowest potential and successive amounts of fragmentation at higher potentials. Previous studies that generated CID breakdown curves for metabolites have shown that varying CID potentials over 0-100 V frequently yields 3 to 4

energy ranges where different ions dominate MS/MS spectra [29], and the results of our recent work on acylsugar and terpenoid metabolites were consistent with these earlier findings [30, 31]. For this reason, five collision energy functions were judged beneficial for minimizing the overlap of broad isotopologue distributions, while limiting the reduction of signal in multiple acquisition functions.

3.2.5 Data processing

Spectra were processed using MassLynx v.4.1 software (Waters Corp.). Annotations of metabolites were based on accurate mass information, retention times (RT), and characteristic fragment ion masses. Isotopologue abundances were integrated without smoothing for both pseudomolecular and fragment ions using QuanLynx software (Waters Corp.), and ¹³C mol% of each isotopologue was calculated as were weighted average masses reflecting total ¹³C incorporation.

3.3 Results and discussion

3.3.1 Profiling and characterization of trichome metabolite diversity

UHPLC/MS profiling of leaf dip extracts revealed dozens of known specialized metabolites in extracts of both labeled and unlabeled tomato trichomes (Figure 3.2), indicating that growth conditions in the closed chamber led to minimal alterations to trichome chemistry. Abundant metabolites included the steroidal glycoalkaloid tomatine ([M + formate]⁻; monoisotopic m/z 1078.5), the flavonoid glycoside rutin ([M – H]⁻; m/z 609) and acylsucroses S4:17, S3:22, and S4:24 ([M + formate]⁻ at m/z 681, 737, and 779). Acylsugar nomenclature uses "S" to describe a sucrose derivative, the first number (e.g., 4) indicates the

number of acyl groups attached to the sugar core, and the second number (e.g., 24) indicates the total number of carbon atoms in all acyl groups [28]. The labeling experiment was judged successful because all of the above metabolites showed increased levels of heavier isotopologues after plants were grown under ¹³C-enriched atmosphere. Substances not showing increases in heavy isotopologues were judged to be substances not synthesized during the labeling period, including background contaminants.

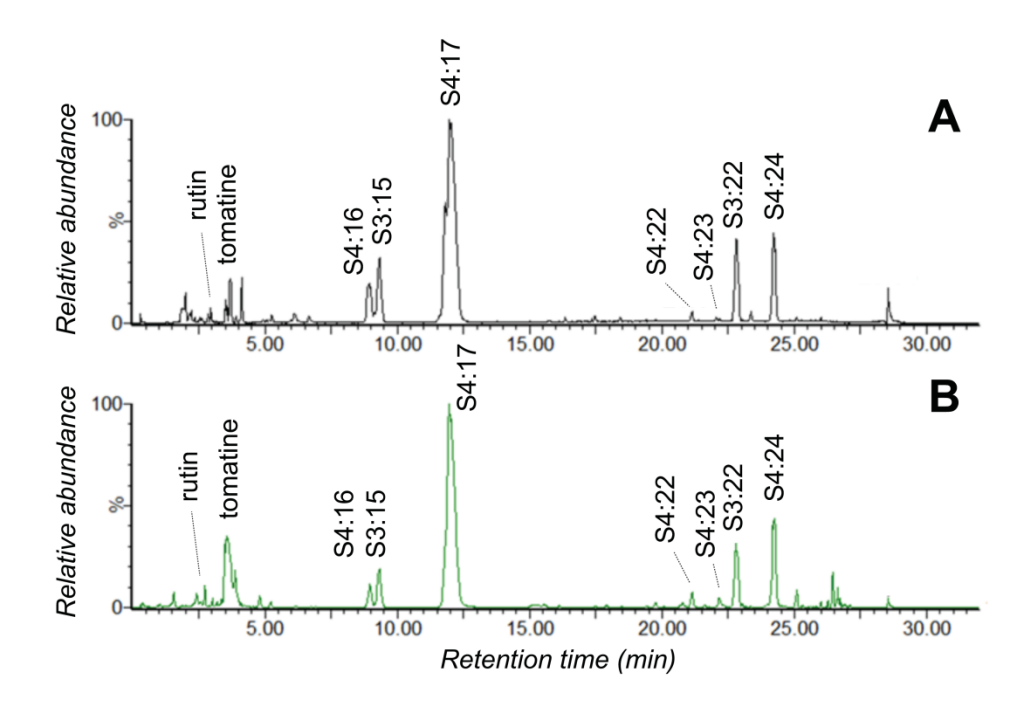


Figure 3.2. UHPLC-TOF-MS based peak base peak intensity (BPI) chromatograms of (¹³C labeled and unlabeled control tomato leaf dip. (A) ¹³C labeled and (B) unlabeled control tomato leaf dip extracts, generated using the lowest (0 V) collision potential and negative-ion mode electrospray ionization. Annotations of major acylsugar metabolites, rutin, and tomatine are included on the chromatograms.

Six abundant acylsucroses, abbreviated as S3:15, S4:16, S4:17, S3:22, S4:22 and S4:24 (Figure 3.3) were selected to evaluate the measurement of ¹³C labeling in specialized tomato metabolites. Negative mode ESI mass spectra of acylsugars showed formate adduct

ions ([M + formate]] in lower CID potential functions (collision functions 1 and 2) that contain all elements of the intact acylsugar. Earlier LC/MS profiling from our laboratory documented that different *Solanum* glandular trichome types accumulate distinct specialized metabolites, including terpenoids and flavonoids that selectively accumulated in type VI glands and acylsugars that predominate in type I/IV glands [30]. All structures presented in Figure 3.3 except S3:15 match those whose structures were determined by NMR in previous reports from our laboratories [28, 31]. For this one exception, exact substitution positions and branching of acyl groups were predicted based on known selectivity in positions of acyl group substitutions as reported in tomato.

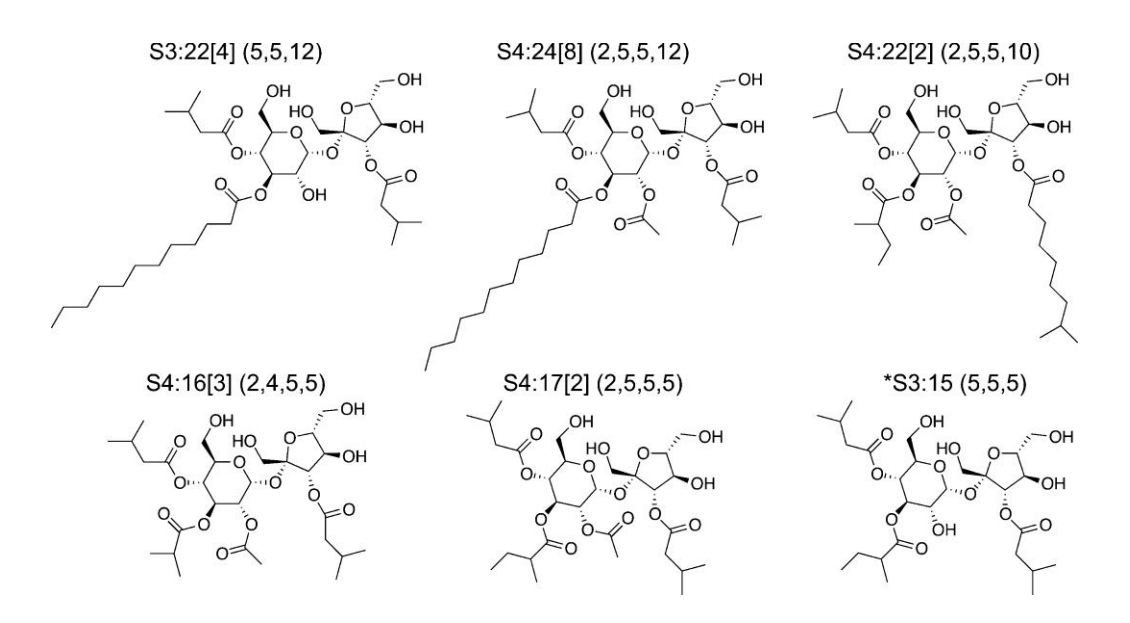


Figure 3.3. Chemical structures of the six most abundant acylsugars in extracts of tomato leaflet. Acylsugar nomenclature is as follows: a single letter corresponding to the base sugar (S = sucrose) followed by total number of acyl carbon atoms. For example, a sucrose tetraester acylated with total 17 carbon atoms in the acyl groups would be designated as S4:17. *All the acyl chain substitution patterns, except S3:15, have been analyzed by NMR spectroscopy and described in a recent publication [31].

Deep profiling and relative quantification of acylsugars in M82 and two relative introgression lines (IL) at different developmental stages illustrate the diversity and dynamics of acylsugar biosynthesis in S. lycopersicum M82 trichomes. For instance, more than thirty acylsugar metabolites including many low abundance isomer peaks were detected in extracts of a younger leaflet from S. lycopersicum M82 harvested at 9 days post germination (Figure 3.4). Some observed metabolites were novel acylsugars that had not been characterized before, including C6 esterified acylsugars S4:18(2,5,5,6) and S4:25(2,5,6,12). The detection of low abundance C6 containing acylsugars demonstrated that M82 plant has the genetic capacity to produce a C6 acyl chain substitution, even though these metabolites had not been observed previously [28, 31] and detailed pathways remain mysterious. Fragmentation using higher energy functions (40, 55 and 80 V) showed clear evidence of the C6 containing substructures (m/z 251, 373, 387 at 40 V function) and C6 fatty acid cation (m/z99 at 80 V function) (Figure 3.5 A). Besides, under positive ESI mode, acylsugars usually fragment between two rings of the sucrose by cleavage of the glycosidic bond [32], with the more abundant fragment ion corresponding to the fructose ring plus its substituents. The fragment ions at m/z 261 and 387 in the CID spectra of S4:18 suggest a mixture of coeluting isomers, with C6 substitution on either fructose (Fru) or glucose (Glu) rings of the acylsucrose. The ratio of Fru-C5 isomer and Fru-C6 isomer ranged from 2:1 to 5:1 for three different C6 acylsugars, S4:18(2,5,5,6), S3:23(5,6,12) and S4:25(2,5,6,12) (Figure 3.5 A and B).

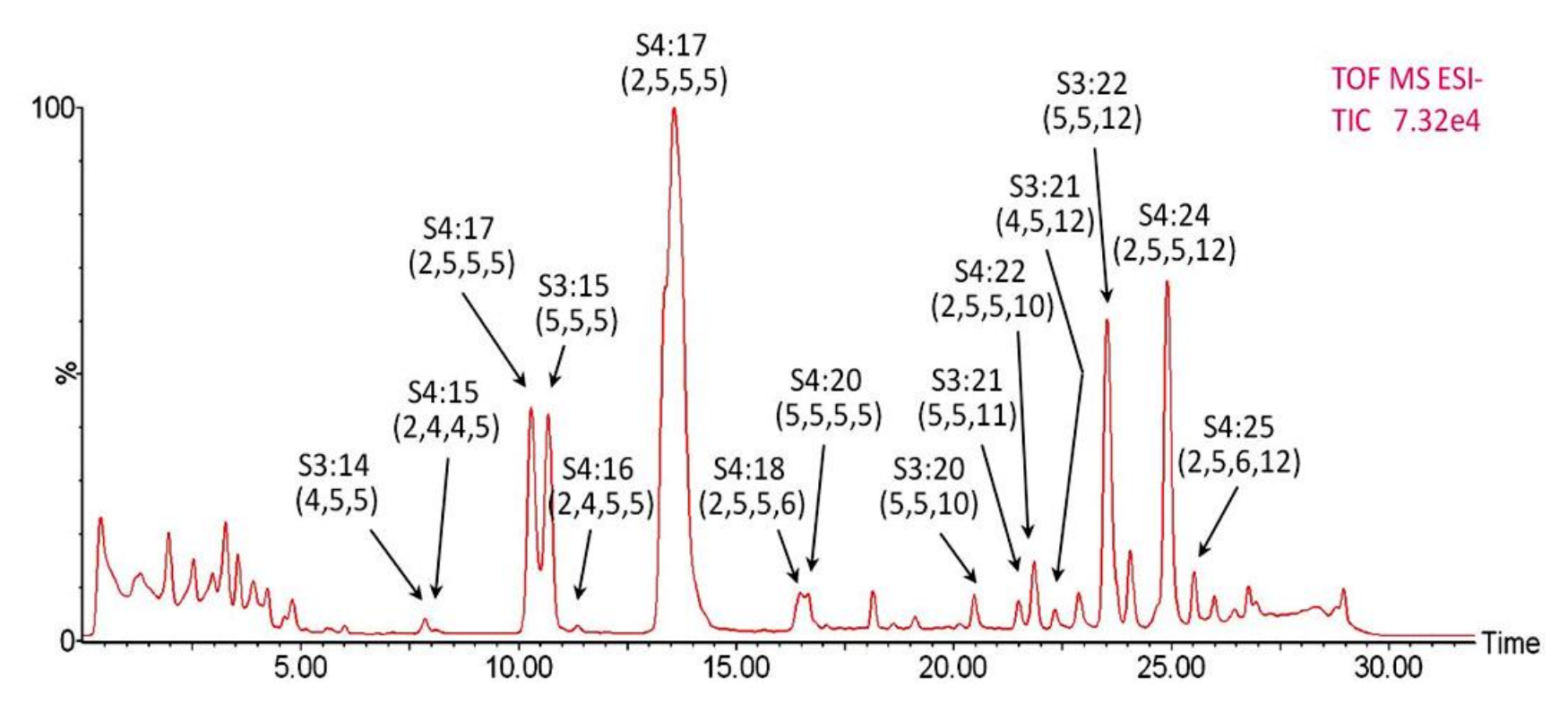
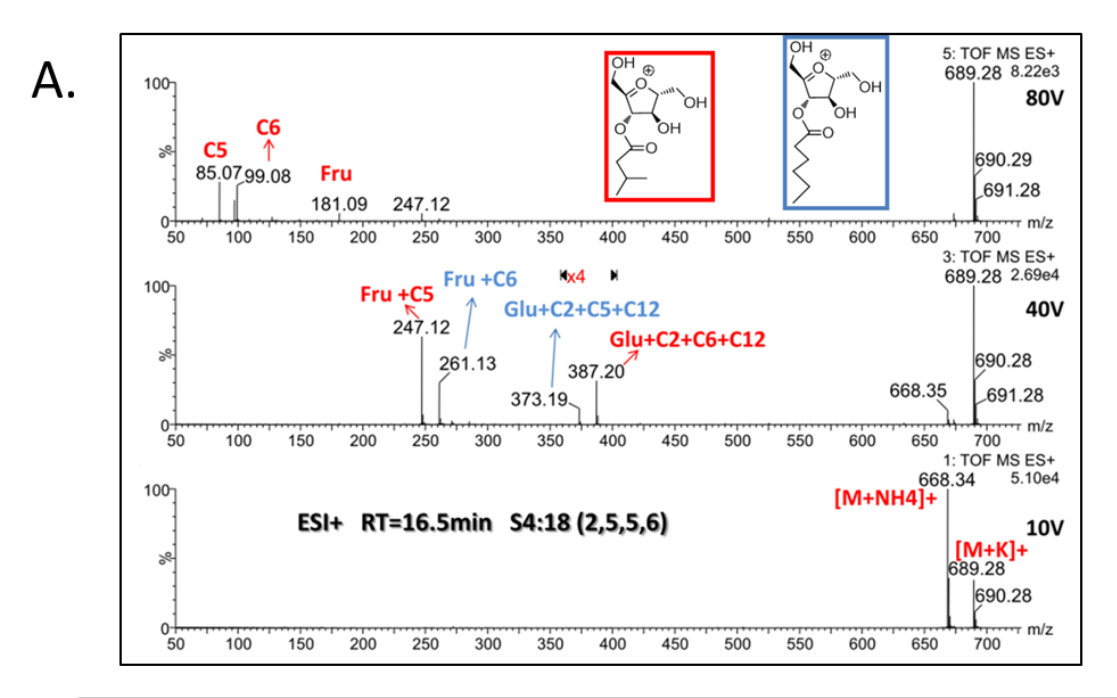


Figure 3.4. UHPLC/MS Total ion chromatogram (TIC) of leaflet dip extract sampled from *S. lycopersicum* M82 plant sampled 9 days post germination. Peaks are annotated as acylsugar metabolites. UHPLC separation of this sample was on a fused core C18 column (2.1×50 mm; 2.7 μm). Gradient is based upon a 32-min LC method using ammonium formate and methanol as mobile phase.



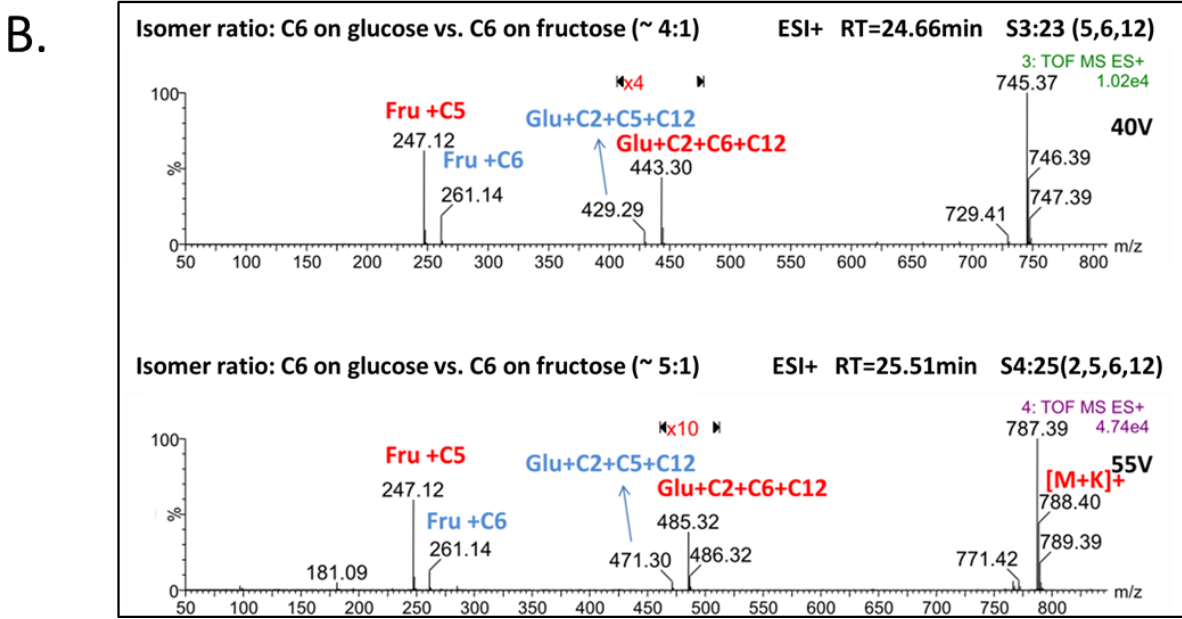


Figure 3.5. Positive-ion mode electrospray ionization mass spectra of C6 containing acylsugars showing fragments generated using non-mass selective collision induced dissociation (CID). Under higher energy functions (40 and 80 V), fragment showed detailed C6 containing substructures (A). C6 can be on ring of fructose (Fru, blue annotation) or glucose (Glu, red annotation). Isomer ratios are different in three C6 containing acylsugars, ranging from 2:1 (S4:18, A) to 5:1 (S4:25, B).

New acylsugars were also identified in IL11-3 trichome extracts through extracted ion chromatogram (XIC) and detailed analysis of mass spectra. In particular, a low abundance diacylsugar with one C5 and one long chain (C10 or C12) was discovered in IL11-3 (Figure 3.6). Correspondingly, tri-acylsugars with one more C2 attached to the sucrose core for these three di-acylsugars were also detected. Di-acylsugars, which were considered as key precursors of tri- and tetra- acylsugars, had never been detected in M82 plants before. Substitution of 11-3 region DNA into the M82 background was thus predicted to interrupt acylsugar biosynthesis genes and resulted not only in lower levels of total acylsugar accumulations, but accumulation of different acylsugar of new structures as well.

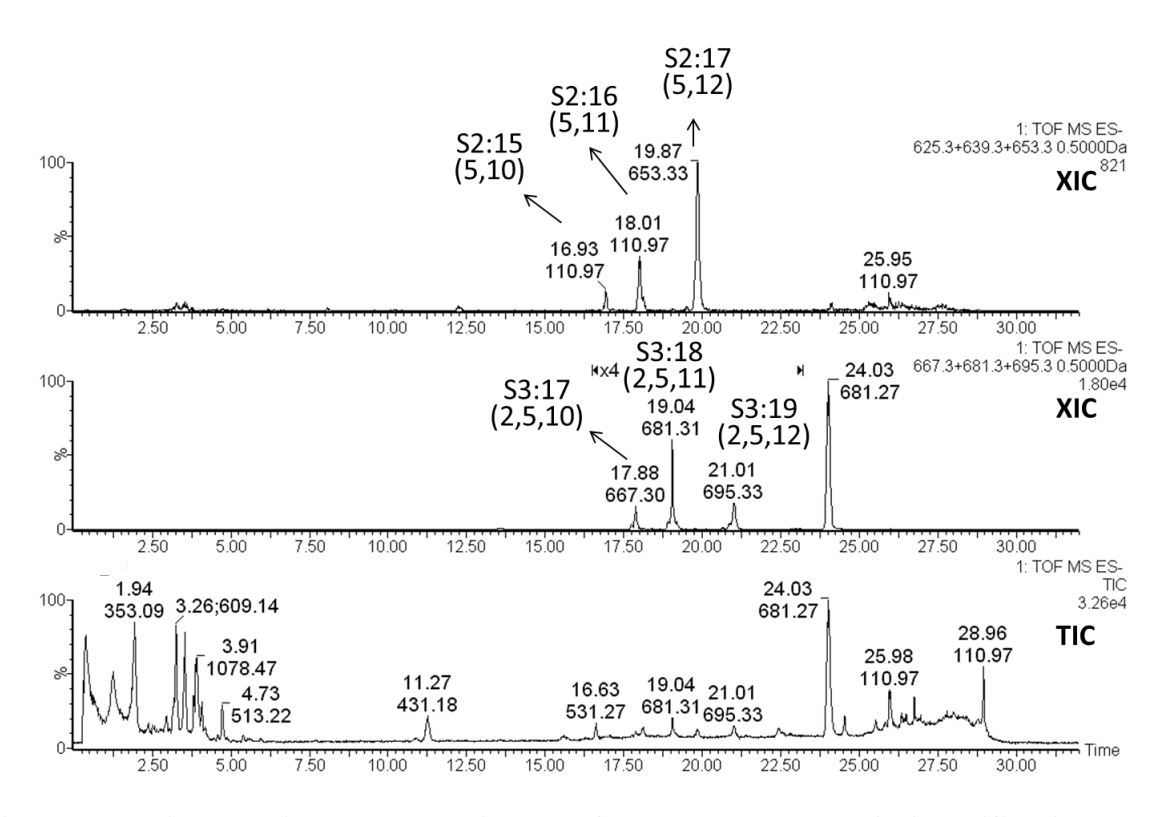


Figure 3.6. Di- and tri-acylsugars with one C5 and one long chain identified in IL11-3. Extracted ion chromatogram (XIC) of positive ESI spectra showed three di-acylsugars S2:15 (5,10), S2:16 (5,11) and S2:17 (5,12). TIC displayed total acylsugars accumulation in IL11-3 was very low compare to M82.

3.3.2 Labeled acylsugar metabolites

Unlabeled acylsugar S4:17 from control group tomato yielded spectra with isotopologue abundances matching those predicted from natural isotopic abundances. Specifically, the abundance of the isotopologue containing one heavy isotope is about 33% of the monoisotopic ion m/z 681, consistent with natural isotope abundances given the 30 carbon atoms in the formate adduct. After 5 days of labeling using ¹³CO₂, all specialized metabolites in tomato plants contained enriched levels of ¹³C as evident from the increased abundances of heavy isotopologues. Enrichments in acylsugars are clear (Figure 3.7) from the demonstrated isotopologue distributions of labeled S4:17 (C₂₉H₄₉O₁₆), the most abundant acylsugar in tomato leaflet dip extract profiles. In control plants where no ¹³CO₂ was used, the most abundant $[M + formate]^-$ isotopologue in function 1 (0 V) was the monoisotopic ion at m/z681. Measurable but smaller amounts of heavy isotopologues m/z 682 and m/z 683 in the unlabeled plant extract derive from natural abundances of heavy isotopes (Figure 3.7 A). After labeling, not only did the most abundant isotopologue shift to a greater m/z value, but the absolute abundance of the monoisotopic acylsugar formate adduct ion for the whole leaflet extract also decreased (Figure 3.7 B). The range of S4:17 isotopologues spread wider as the period of labeling was extended, consistent with a mixture of labeled and unlabeled precursors of S4:17. Isotopologues heavier than m/z 684.30, which were barely detected in unlabeled S4:17, emerged after 5 days of labeling.

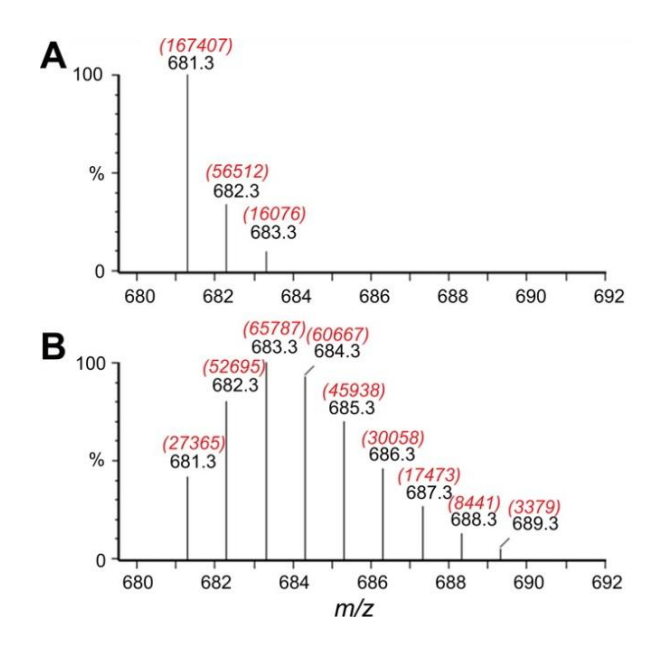


Figure 3.7. [M+formate] isotopologue ions of acylsugar S4:17 from (A) control and (B) 5-day ¹³CO₂-labeled group in tomato leaflet trichome extract. Black (lower) annotations are m/z values of individual isotopologue ions, and red annotations (in the color version; upper values in parentheses) are integrated extracted ion chromatogram peak area values of each corresponding isotopologue.

3.3.3 Enrichment calculation in metabolite Ions

To investigate the efficiency of 13 C enrichment in specialized metabolites, isotopologue profiles from mass spectra of metabolites were analyzed as followed. The absolute abundance of each isotopologue was determined by integrating [M + formate]⁻ extracted ion chromatograms (XICs). Abundance of each isotopologue was used to calculate the weighted average m/z value. For each isotopologue, the measurement of labeling enrichment was based on the difference between the abundance-weighted mean m/z of enriched and natural abundance ions. Atom % of 13 C enrichment of each ion was then calculated using the following equation:

13
C% enrichment = $\frac{\overline{M}_L - \overline{M}_U}{13.00335 - 12}$

where \overline{M}_L is the weighted average isotopologue mass of the labeled ion and \overline{M}_U is the weighted average isotopologue mass of the unlabeled ion, and the denominator is the difference between 13 C and 12 C atomic masses.

This calculation provides a simple representation of stable isotope labeling, but results are susceptible to error propagation that results from variance in measurement of low-abundance isotopologues for which measurements are less precise. While we recognize that fitting of predicted isotopologue distributions to measured values as described by MacCoss *et al.* decreases propagation of error in measurement of low abundance isotopologues [33], such calculations are yet more complex in pulse-chase experiments when multiple labeling populations of enriched metabolites may form.

To demonstrate the calculation using S4:17 formate adduction as an example (Table 3.1), the integrated peak areas of acylsugar S4:17 ($C_{29}H_{48}O_{15}$) isotopologues are annotated as red numbers above corresponding m/z values (Figure 3.7 B). The weighted average m/z of [M + formate]⁻ of S4:17 after 5-day growth under $^{13}CO_2$ was m/z 684.21. The empirical weighted average m/z of unlabeled (natural abundance) S4:17 was calculated to be m/z 681.70. The difference in average masses (684.21-681.70) divided by the mass difference between ^{13}C and ^{12}C (1.00335 Da) gives 2.50 ^{13}C atoms in labeled S4:17 molecules. The $^{13}C\%$ enrichment is calculated to be 8.62% (2.50 out of 29 carbons in S4:17). Acylsugar S4:17 extracted from control group tomato plants gave a weighted average mass within 0.15% of the value calculated from average natural isotope abundances.

After 5 days of labeling, all six acylsugars contained 8.5 - 8.9 mol% enrichment of ¹³C in the intact metabolites (Table 3.2). Acylsugars S4:17, S3:22, S4:22, and S4:24 each yielded mass spectra consistent with 8.9 mol% of ¹³C enrichment, S4:16 had 8.7 mol%, and S3:15

had 8.5 mol% of 13 C. The average mass of acylsugar S4:17 continued to increase with increased labeling time: ~ 5 Da after 7 days of labeling and 7 Da after 9 days of labeling. The distribution of isotopologues reflects biosynthesis of acylsugars from a mixture of 13 C-labeled and unlabeled precursor pools, the latter attributed to formation of unlabeled CO_2 from respiration or soil microbial activity. Weighted averages of isotopologues for metabolites from control unlabeled plants were consistent with a natural abundance of about 1.1% 13 C as long as abundances were sufficient to yield reasonable ion statistics (Table 3.2).

Table 3.1 ¹³C enrichments in tomato acylsugar S4:17 and substructure fragments after 5 days of labeling using ¹³CO₂^a

ions	collision energy function	labeled weighted avg m/z	area of labeled base isotopologue ^c	unlabeled weighted avg m/z^d	theoretical weighted avg m/z	no.	no. of C^f	¹³ C mol %
[M + formate]	1	684.205	67184	681.7012	681.7004	2.50	29	$8.62 \pm 0.01\%$
$[M - H - C2]^{-}$	2	595.967	2701	593.6169	593.6383	2.35	27	$8.70~\pm~0.04\%$
$[M - H - C2 - 2C5]^{-}$	3	426.890	1115	425.3900	425.4055	1.50	17	$8.82\pm0.04\%$
C5 ⁻	5	101.557	2053	101.1306	101.1243	0.43	5	$8.53 \pm 0.10\%$
sucrose core ^g	N/A^i	N/A^i	N/A^i	N/A^i	N/A^i	1.07	12	8.95%
$C2^h$	N/A^i	N/A^i	N/A^i	N/A^i	N/A^i	0.15	2	7.69%

 $^{^{}a13}$ C mol% is expressed as mean \pm standard error based on four biological replicates. b Collision cell voltages for individual acquisition functions were function 1: 0 V; 2: 20 V; 3: 35 V; 4: 50 V; 5: 80 V. c Extracted ion chromatogram peak area for the most abundant isotopologue ion. d Experimental abundance-weighted average m/z for unlabeled acylsugar. e Number of additional 13 C atoms added by enrichment, calculated as described in the text. f Total number of carbon atoms contained in this portion of the acylsugar. g Values calculated for the 12 carbons of the sucrose core from the difference in labeling of C5 $^{-}$ and $[M - H - C2 - 2C5]^{-}$. Low abundances of $[sucrose - H]^{-}$ prevented reliable direct measurements of the sucrose core labeling. h Values calculated for the acetyl group from differences in labeling of $[M - H]^{-}$ measured in collision function 2 and $[M - H - C2]^{-}$. i Not applicable, these values were calculated from differences in labeling of other ions.

Table 3.2 ¹³C enrichments in various ions generated using UHPLC-TOF MS with non-selective multiplexed collision-induced dissociation of additional acylsugar metabolites extracted from a tomato leaflet after 5 days of labeling with ¹³CO₂. Highlighted entries in the table are those for which the integrated peak areas were less than 100 counts-min, a level below which the peak area RSDs increased sharply with decreasing signal. ¹³C enrichments in control unlabeled plants were calculated from weighted isotopologue abundances of [M+formate]⁻ and fragment ions.

Metabolite ID	Ion annotation	Collision Function	Labeled weighted Ave. <i>m/z</i>	# ¹³ C enrichment after labeling	¹³ C mol% enrichment after labeling	Mono. Ave. Peak Area (counts/mi nute)	Weighted Ave. m/z of Unlabeled Control	Theoretica l Ave. m/z for unlabeled metabolite	Дт (ррт)
	DA formatal	1	684.204±0.00	2.907±0.00	8.91% ±0.01%	27820	681.702	681.706	-5.06
	[M-formate]	2	684.143±0.00	2.846±0.00	$8.70\% \pm 0.02\%$	6062	681.678	681.706	-40.71
	[M-H]-	2	638.225±0.03	2.934±0.03	9.01% ±0.10%	185	635.726	635.681	72.11
	[M-C2]-	2	595.968±0.01	2.687 ± 0.01	$8.84\% \pm 0.04\%$	1054	593.617	593.644	-44.89
Acylsucrose S4:17 (2,5,5,5)	[M-C2-2C5]-	3	426.890±0.01	1.724±0.01	9.03% ±0.04%	790	425.390	425.408	-41.26
	Sucrose	3	342.386±0.02	1.277 ± 0.02	9.53% ±0.19%	212	342.156	341.290	2530.88
	C5 acyl group	3	101.603±0.01	0.543 ± 0.01	9.75% ±0.18%	2594	101.193	101.126	668.93
		4	101.557±0.01	0.496 ± 0.01	8.81% ±0.13%	2971	101.142	101.126	163.62
		5	101.553±0.01	0.493 ± 0.01	$8.74\% \pm 0.10\%$	2053	101.131	101.126	49.94
	[M-formate]-	1	641.889±0.01	2.603±0.01	8.53% ±0.03%	1741	639.616	639.664	-74.97
		2	641.885 ± 0.01	2.599 ± 0.01	8.51% ±0.04%	230	639.586	639.664	-122.09
	[M-H]-	2	595.907±0.02	2.626 ± 0.02	$8.61\% \pm 0.06\%$	292	593.542	593.628	-144.55
Acylsucrose S3:15 (5,5,5)	[1V1-11]-	3	595.455±0.02	2.175 ± 0.02	7.94% ±0.07%	99	593.583	593.628	-76.12
	[M-2C5]-	3	426.894±0.03	1.729 ± 0.03	9.06% ±0.20%	148	425.389	425.408	-44.11
		4	427.071±0.03	1.905 ± 0.03	10.01% ±0.18%	77	425.724	425.408	744.32
	Sucrose	3	342.316±0.04	1.208 ± 0.04	9.96% ±0.29%	147	341.292	341.290	5.80
		4	342.746±0.04	1.638 ± 0.04	12.54% ±0.31%	17	341.978	341.290	2011.79

Table 3.2 (cont'd)

	· · · ·								
		3	101.545±0.01	0.485 ± 0.01	8.59% ±0.25%	1105	101.119	101.126	-64.71
	C5 acyl group	4	101.536±0.01	0.475 ± 0.01	8.40% ±0.19%	1194	101.127	101.126	11.76
		5	101.554 ± 0.02	0.494 ± 0.02	8.77% ±0.34%	683	101.118	101.126	-74.35
	[M-formate]-	1	740.804±0.01	3.408±0.01	8.91% ±0.02%	3576	737.847	737.850	-4.07
	[M-10rmate]-	2	740.750±0.00	3.354 ± 0.00	$8.76\% \pm 0.01\%$	517	737.787	737.850	-85.62
	D. (1.005)	2	525.668±0.04	2.392±0.04	$8.86\% \pm 0.17\%$	81	523.593	523.592	3.53
	[M-2C5]-	3	525.738±0.04	2.463±0.04	9.15% ±0.19%	78	523.603	523.592	21.11
	DM C121	2	511.407±0.01	2.184 ± 0.01	$8.81\% \pm 0.05\%$	1520	509.470	509.522	-102.79
	[M-C12]-	3	511.403±0.05	2.180 ± 0.05	$8.80\% \pm 0.24\%$	214	509.471	509.522	-99.63
Acylsucrose	Sugraga	3	342.370±0.01	1.262 ± 0.01	9.41% ±0.07%	1159	341.250	341.290	-116.55
S3:22 (5,5,12)	Sucrose	4	342.396±0.03	1.287 ± 0.03	$9.62\% \pm 0.24\%$	273	341.275	341.290	-43.21
	C12 acyl group	3	200.403±0.01	1.233±0.01	9.17% ±0.08%	1052	199.292	199.315	-114.21
		4	200.355±0.01	1.185 ± 0.01	$8.77\% \pm 0.11\%$	1266	199.281	199.315	-169.24
		5	200.385 ± 0.03	1.215 ± 0.03	$9.01\% \pm 0.24\%$	653	199.281	199.315	-168.33
	C5 acyl group	3	101.628±0.01	0.567 ± 0.01	10.24% ±0.12%	1422	101.226	101.126	994.37
		4	101.576±0.00	0.516 ± 0.00	$9.20\% \pm 0.09\%$	1979	101.159	101.126	335.52
		5	101.572±0.01	0.511 ± 0.01	9.11% ±0.12%	1746	101.150	101.126	240.12
		1	783.001±0.01	3.594±0.01	8.87% ±0.02%	3246	779.883	779.886	-4.53
	[M-formate]-	2	782.971 ± 0.00	3.564 ± 0.00	8.79% ±0.01%	1274	779.866	779.886	-26.35
	[M-C2]-	2	694.810±0.02	3.419 ± 0.02	8.95% ±0.06%	112	691.795	691.824	-42.92
	[M-C5]-	2	652.440±0.04	3.096 ± 0.04	8.88% ±0.13%	166	649.682	649.745	-96.70
Acylsucrose S4:24 (2,5,5,12)	Sucrose	3	342.513±0.08	1.404±0.08	10.59% ±0.68%	62	341.227	341.290	-182.57
		4	342.460±0.02	1.352±0.02	10.16% ±0.21%	55	341.341	341.290	150.32
		3	200.433±0.02	1.263±0.02	9.41% ±0.21%	179	199.297	199.315	-87.89
	C12 acyl	4	200.428±0.05	1.258 ± 0.05	9.37% ±0.44%	212	199.314	199.315	-3.82
	group	5	200.358±0.04	1.188 ± 0.04	8.79% ±0.36%	115	199.289	199.315	-127.88
	C5 acyl group	3	101.840±0.03	0.779 ± 0.03	14.48% ±0.66%	238	101.617	101.126	4836.23

Table 3.2 (cont'd)

10010 2.2 (• • • • • • • • • • • • • • • • • • • •								
		4	101.702±0.04	0.642 ± 0.04	$11.72\% \pm 0.75\%$	316	101.331	101.126	2030.61
		5	101.679±0.04	0.619 ± 0.04	11.26% ±0.85%	261	101.215	101.126	886.18
	[M-formate]-	1	670.020±0.01	2.739 ± 0.01	8.67% ±0.04%	4069	667.638	667.674	-53.13
		2	670.031±0.02	2.750 ± 0.02	$8.71\% \pm 0.07\%$	456	667.581	667.674	-138.42
	[M-C2]-	2	581.853±0.02	2.589 ± 0.02	$8.84\% \pm 0.06\%$	141	579.605	579.612	-11.71
	[M-C5]-	2	539.477±0.03	2.259 ± 0.03	$8.71\% \pm 0.14\%$	229	537.501	537.532	-57.52
	[M-C2-C5]-	2	497.321±0.04	2.113 ± 0.04	$9.95\% \pm 0.20\%$	172	495.472	495.495	-46.44
Acylsucrose S4:16 (2,4,5,5)		3	101.550±0.03	$0.490\pm\!0.03$	$8.68\% \pm 0.58\%$	194	101.178	101.126	514.28
51110 (2,1,6,6)	C5 acyl group	4	101.585±0.04	0.525 ± 0.04	9.38% ±0.73%	174	101.130	101.126	46.27
		5	101.558±0.02	0.498 ± 0.02	$8.85\% \pm 0.38\%$	130	101.090	101.126	-350.54
	C4 acyl group	3	87.652 ± 0.07	0.607 ± 0.07	$14.07\% \pm 1.80\%$	125	87.395	87.099	3393.17
		4	87.740 ± 0.05	0.696 ± 0.05	$16.28\% \pm 1.23\%$	152	87.292	87.099	2216.47
		5	87.593 ± 0.02	0.548 ± 0.02	12.59% ±0.56%	116	87.409	87.099	3554.28
	[M-formate]-	1	754.723±0.03	3.348±0.03	8.91% ±0.09%	286	751.784	751.833	-65.36
		2	754.741±0.07	3.366 ± 0.07	8.76% ±0.19%	72	751.763	751.833	-93.44
	[M-C2]-	2	666.555±0.11	3.195±0.11	8.88% ±0.33%	14	663.757	663.771	-21.07
	[M-C5]-	2	624.207±0.07	2.895 ± 0.07	8.87% ±0.24%	19	621.660	621.692	-50.99
Acylsucrose	[M-C2-C5- C10]-	2	426.671±0.05	1.505 ±0.05	7.75% ±0.31%	31	425.401	425.406	-10.61
S4:22 (2,5,5,10)	C10 acyl group	3	171.975±0.13	0.837 ± 0.13	$7.26\% \pm 1.30\%$	24	171.150	171.261	-643.43
		4	172.067±0.07	0.928 ± 0.07	$8.17\% \pm 0.66\%$	25	171.219	171.261	-245.02
		5	171.963±0.06	0.824 ± 0.06	7.13% ±0.62%	12	171.201	171.261	-349.13
		3	101.885±0.06	0.824 ± 0.06	$15.38\% \pm 1.24\%$	12	101.090	101.126	-349.68
	C5 acyl group	4	101.558±0.09	0.498±0.09	8.84% ±1.91%	28	101.096	101.126	-292.53
		5	101.547±0.09	0.487 ± 0.09	8.63% ±1.76%	30	101.090	101.126	-349.88

3.3.4 Assessment of isotope enrichments using Multiplexed CID

To measure labeling in various metabolite substructures, multiplexed CID conditions were applied with rapid switching between acquisition functions and parallel separate data acquisition for each function. The potential of the QTOF collision cell was switched from 0 to 80 V across five functions, with no ion activation in the first function, 20, 35, and 55 V in functions 2, 3 and 4, and 80 V in function 5. Labeling information was generated for substructures of a wide range of metabolites through measurement of labeling in fragment ions. In function 1 (0 V), all acylsugar mass spectra gave high yields of formate adduct ([M + formate]), since acylsugars lack groups with sufficient acidity to yield substantial amounts of [M – H] (Figure 3.8). Formate-bound dimer ions [2M + formate] were also observed but in low abundance (<10%) relative to [M + formate] . Raising the collision voltage to 20 V yielded [M – H] in function 2 but with lower ion abundance compared with [M + formate] in function 1. The higher ion abundances of [M + formate] provide improved quantitative precision than obtained for [M - H] in function 2, so abundances of formate adduct isotopologues measured in function 1 were used to calculate ¹³C enrichments in the intact metabolite. Since formate was present in HPLC solvent, the formate carbon was not included when the ¹³C mol% enrichments of each molecule were calculated.

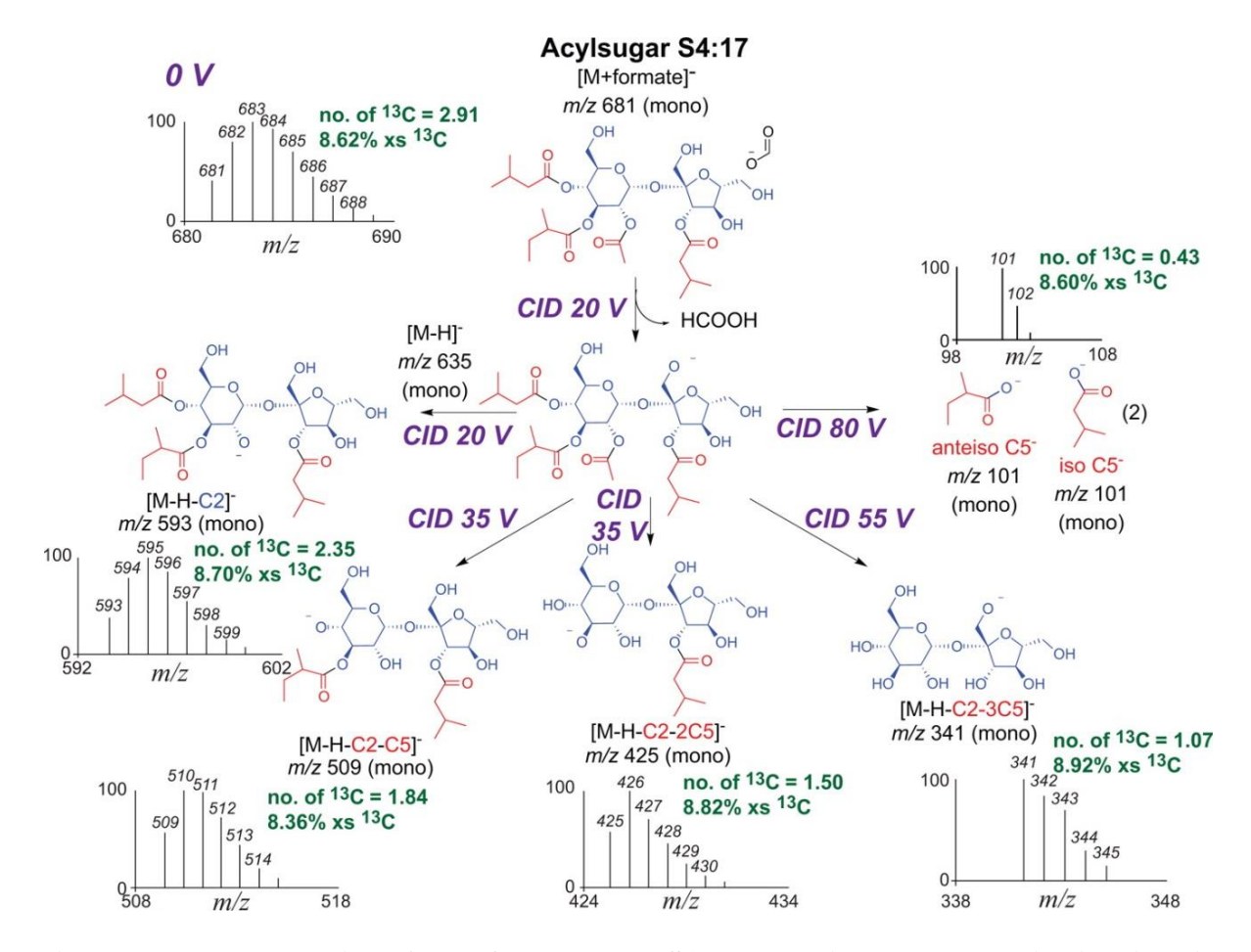


Figure 3.8. Nonselective CID of acylsugar S4:17 and isotopologue distribution in molecular adduct ions and fragment ions. The zoom-in spectra were generated using UHPLC/TOF MS analysis of a tomato leaflet extract sampled after 5 days of labeling with $^{13}CO_2$. For the structures, red color indicates the acyl chain substitutions and blue color indicates the sucrose core. Increasing collision voltage leads to more extensive fragmentation and increases in abundances of lower mass fragments. The spectra under each fragment ion structure show the isotopologue abundances due to ^{13}C incorporation. The term "no. of ^{13}C " shows the mean number of ^{13}C atoms enriched in each ion, calculated as described in the text and as reported in Table 3.1.

As the collision cell potential increased in functions 2-5, a number of characteristic fragment ions were generated though successive losses of neutral ketenes derived from the various acyl groups. In negative mode CID spectra, typical fragments include three types: (i) pseudomolecular ions including formate adducts ($[M + formate]^-$); (ii) fragment ions from successive neutral losses of the ester group ketenes that are annotated as $[M-H-C2]^-$, $[M-H-C2]^-$, $[M-H-H-H]^-$);

 $H - C5]^-$; and (iii) acyl group carboxylates including $C4^-$ (m/z 87), $C5^-$ (m/z 101), $C10^-$ (m/z 171), and $C12^-$ (m/z 199). As shown in Figure 3.8, more extensive fragmentation, yielding lower mass fragment ions, was observed in the higher energy functions for acylsugar S4:17. The most abundant ion in the first function (0 V) of the spectrum was formate adduct [M + $HCOO]^-$ with monoisotopic m/z of 681.30 as the base peak in extracts of unlabeled plants. In the higher collision energy functions, fragments formed from neutral losses of C5 and/or C2 ketenes. Peak m/z 593.27 in function 2 (20 V) corresponds to loss of neutral ketene derived from an acetyl group [M – H – $C2]^-$; peak m/z 425.17 in function 3 (35 V) corresponds to the fragment ion generated by losses of a C2 and two C5 groups [M – H – C2 – $2C5]^-$; peak m/z 341.10 in function 4 (55 V) corresponds to deprotonated sucrose core without any acylgroups and arises from loss of all three C5 and one C2 groups [M – H – C2 – $3C5]^-$. In the highest collision energy function (function 5, 80 V), acid carboxylate anion $C5^-$ (m/z 101) dominates the spectrum of S4:17.

¹³C enrichment levels of fragment ions were calculated using the same method described above for pseudomolecular ions, but using the empirical unlabeled isotopologue abundances as the reference point. Integrated peak areas of fragment isotopologues were used as weights for average mass and ¹³C atom incorporation calculation. As demonstrated in Table 3.1, fragments of S4:17 were evenly enriched in ¹³C in [M – H –C2]⁻, [M – H – C2 – 2C5]⁻, and the C5 acid chains.

Acylsugars are hypothesized to be synthesized by acyltransferase-catalyzed esterification of hydroxyl groups of glucose and/or sucrose with branched acyl groups derived from branched-chain amino acid pathways and elongation by fatty acid synthase (FAS)-mediated transformations [28,34]. Measurements of ¹³C enrichment in differential

substructures yield information about the dynamics of specialized metabolite accumulation and turnover, and measurements at multiple time points aid estimation of precursor pool sizes and fluxes of carbon through biosynthetic pathways.

3.3.5 Advantages of Multiplexed CID for measuring stable isotope enrichments

Extracts of tomato trichomes were analyzed using UHPLC coupled with multiplexed CID on a QTOF instrument, and this approach generated nonselective breakdown of all isotopologues of each metabolite while avoiding mass bias introduced by precursor isolation in MS/MS spectra. For acylsugars, fragment ions were distributed among the four acquisition functions that employed elevated collision energies. Application of multiplexed CID on a TOF or QTOF mass spectrometer avoids quantitative biases that are introduced when isotopologues within a narrow m/z range are selected for ion activation (Figure 3.9). For a highly labeled metabolite, a fraction of molecules may have all carbon atoms enriched with ¹³C, and since labeling of specialized metabolites may often yield a range of molecular masses spanning 50 Da or more to encompass all isotopologues, selection of a range of m/z values to be subjected to CID will either introduce mass biases or provide minimal selectivity. When nonselective multiplexed CID is performed, by cycling the collision energy across five sequential functions (0, 20, 35, 55, and 80 V) a single profiling analysis generates varied levels of fragments without predefining precursor ions in advance. This nonselective CID fragmentation method provides a powerful and nontargeted approach for deciphering complex metabolomes, particularly when metabolites exhibit heterogeneity in stable isotope enrichments. In the current investigation, abundances of the most and least abundant isotopologue ions span at least 3 orders of magnitude.

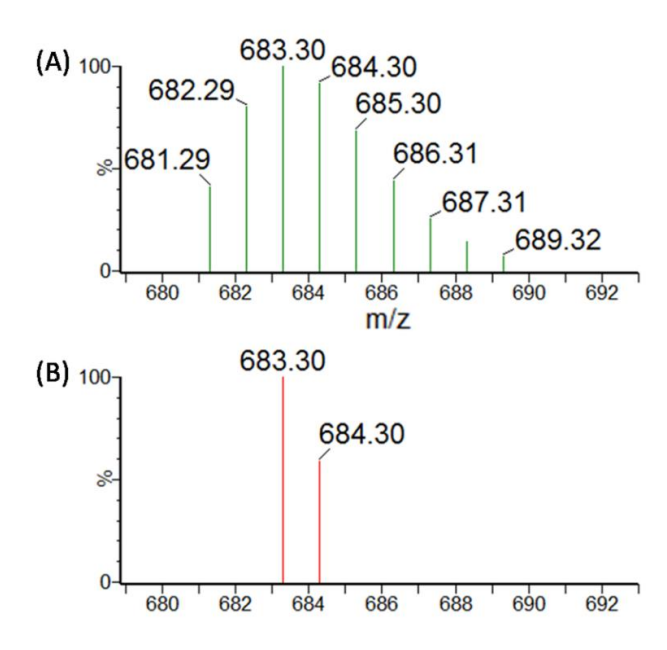


Figure 3.9. Precursor mass selection of labeled S4:17 [M+formate] by data-dependent mass-selective CID. The zoom-in spectra were generated using UHPLC-TOF MS analysis of a tomato leaflet extract sampled after 5 days of labeling with ¹³CO₂. Spectrum (A) is a survey scan showing all isotopologues that were detected without mass-selective precursor ion isolation. Spectrum (B) is the precursor ions that were transmitted by the quadrupole to the collision cell for product ion MS/MS analysis using a window of approximately 2 *m/z* controlled through the quadrupole resolution tune settings (a setting commonly used for generation of MS/MS spectra).

3.3.6 Performance evaluation of LC/MS measurements

The technical error of peak area measurement in UHPLC/MS profiling was determined by subjecting the same labeled sample to five replicate UHPLC/QTOF-MS analyses. For each replicate, average peak area values were generated for all isotopologues of intact molecule and fragments, and relative standard deviations (RSDs) were calculated. As demonstrated in Figure 3.10 using acylsugar S4:17 as an example, $[M + formate]^-$ represented the intact metabolite, with isotopologues ranging from m/z 681 to m/z 694. Each point indicates the average peak area value for an isotopologue of the formate adduct ion required from five replicate profiles. The curves show hyperbolic shapes of the dependence of RSD

upon peak area, which indicates that the technical relative standard deviation (y-axis) has a strong dependence on the magnitude of the ion signal, or peak areas in this profiling, as expected based on ion statistics. For formate adduct ion ($[M + formate]^-$), when the isotopologue peak area decreased to 100 counts-min, the RSD rose above 10%. For three fragment ions $[M - H - C2]^-$, $[M - H - C2 - 2C5]^-$, and $C5^-$, when the peak area values decreased below 50 counts-min, the RSD increased to greater than 10%. RSD values were greater for pseudomolecular ions (e.g., $[M + formate]^-$) relative to fragment ions generated at higher collision voltages because interference from chemical noise is more prevalent in collision function 1. The reasons for the smaller RSD values for fragments relative to $[M + formate]^-$ are not entirely clear but can be attributed in part to the narrower range of isotopologue masses for the lower m/z fragments and greater likelihood of isobaric interferences with low-abundance isotopologues of the formate adduct at the lowest collision energy.

To achieve a reliable measurement of labeling patterns in the profile, the quantification limit in this study was then set as 100 peak area units (counts-min). Ions with peak areas less than 100 counts-min yielded RSD errors with the RSD increasing sharply with decreasing peak area. Owing to the limitations of ion statistics these were judged insufficient for direct calculation of weighted average mass and ¹³C enrichment levels as needed to construct reliable metabolic flux analysis models.

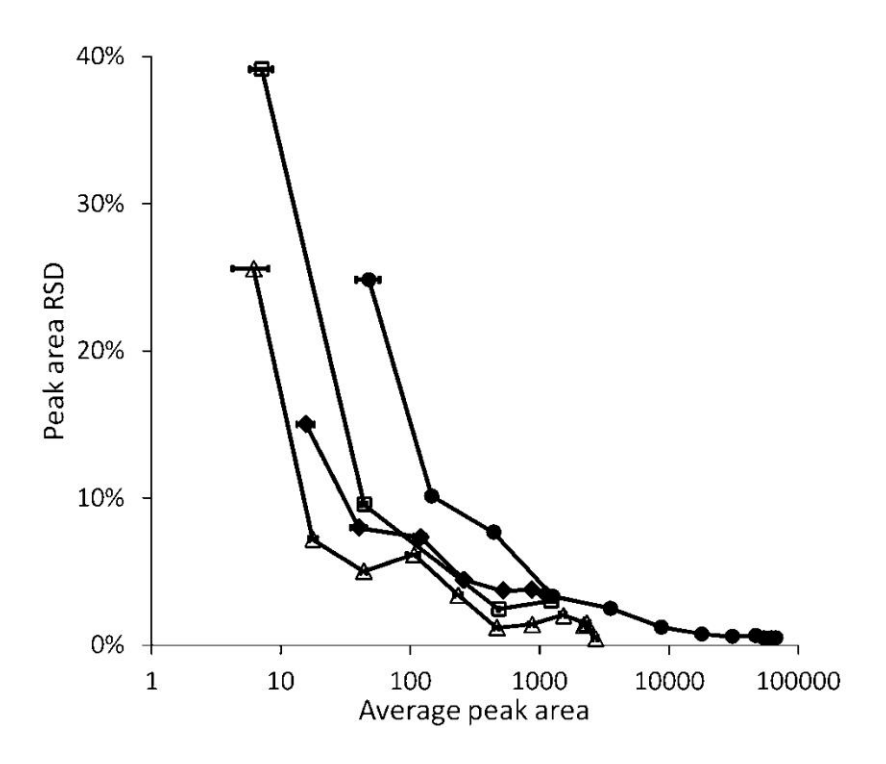


Figure 3.10. Peak area relative standard deviations as a function of average extracted ion chromatogram (XIC) peak area values for all individual isotopologue ions of acylsugar S4:17 generated from 5 days of $^{13}CO_2$ labeling. [M + formate] $^{-}$ (\bullet) is from collision function 1, and fragment ions [M - H - C2] $^{-}$ (Δ) are from function 2, [M - H - C2 - 2C5] $^{-}$ (\bullet) are from function 3, and C5 $^{-}$ (\Box) are from function 5. The error bars represent the relative standard deviations of isotopologue peak area values of five technical replicates. Error bars for all areas greater than 100 are too small to be observed.

3.3.7 Comparisons of total metabolite and substructure enrichments

CID of acylsugars yielded a variety of fragment ions useful for assessing 13 C enrichments. For example, the ion abundances of the sucrose core were always below the 100 counts-min threshold (Table 3.2). For acylsugar S4:17, 13 C enrichment in the sucrose core was calculated through subtraction of enrichments in two fragments $[M - H - C2 - 2C5]^-$ (monoisotopic m/z 425) and C5 acyl group (Table 3.1), which differ in content by only the sucrose core. For this acylsugar, both fragments yielded integrated peak areas above the 100 counts-min threshold. 13 C atom incorporation numbers (No. of 13 C) were calculated to be 1.50 in $[M - H - C2 - 2C5]^-$ and 0.43 in C5 acyl group (Table 3.1). The difference (1.50 – 0.43)

gives 1.07^{-13} C atoms enriched in the sucrose core, which corresponds to 8.95% of total carbons in the sucrose core. Similar calculations can be applied to substructures that do not give sufficient ion currents, such as the C2 acetyl group in acylsugar S4:17. As presented in Table 3.1, calculated numbers of 13 C atoms in [M + formate] minus the 13 C atoms in [M – H – C2] gives 0.15^{-13} C atoms in the acetyl (C2) group, corresponding to 7.69% of total carbons in the C2 group being 13 C.

As shown in Table 3.1, the numbers of 13 C atoms enriched in formate adduct and fragment ions were calculated as the weighted average m/z value minus average m/z value generated from natural isotope abundances. In acylsugar S4:17, the accuracy of enrichment levels is assessed by adding the no. of 13 C enrichments for the individual acyl groups and the sucrose core that comprise S4:17 (one C2, three C5, and one sucrose), which add up to give 2.51 13 C. This number is in close agreement with the direct calculation of 2.50 13 C atom from $[M + formate]^-$ or a difference of only 0.4%. This provides validation of the measurement of the 13 C enrichment level in fragment ions, that is accurate and unbiased and, in this case, subject to only minimal effect from coelution by interfering substances. All calculation strategies mentioned above extend additional measurement of isotope enrichment in fragments that reflect the various precursors of metabolite biosynthesis. Multiplexed CID facilitates this approach in a data-independent manner by extending the dynamic range of LC/TOF MS analysis and is compatible with the UHPLC chromatographic time scale.

3.3.8 Comparison of ¹³C enrichment in six acylsugars and their fragments

The ¹³C enrichment levels in pseudomolecular and fragment ions from five additional acylsugars from tomato (Table 3.2) reflect ¹³C incorporation into these related metabolites and

their substructures. In S4:17, sucrose moieties (8.95% ¹³C enrichment) had similar enrichments as C5 acyl chains (8.53% ¹³C), but enrichment in the acetyl group was lower (7.69%). These results indicated that the ¹³C was incorporated into acyl chains and sucrose in similar proportions when S4:17 were synthesized or that the precursor pool sizes for acyl chain biosynthesis and sucrose biosynthesis were at similar levels with similar ¹³C fluxes. For long chain acylsugar S4:24 which contains a linear C12 acyl group presumed to be synthesized in the fatty acid biosynthetic pathway, the C12 carboxylate was slightly more enriched (9.2 mol%; mean of functions 3, 4, and 5) in the molecule than the C5 acyl groups (8.6 mol%, mean of functions 3, 4, and 5).

3.3.9 Labeling of other trichome metabolites species

Apart from acylsugars, the flavonoid glycoside rutin and steroidal glycoalkaloid tomatine are two abundant metabolites detected in profiling of metabolites in tomato trichome extracts (Figure 3.2). Rutin (quercetin-3-O-rutinoside) was found to accumulate in type VI secreting trichomes [35], while tomatine has been reported in stem and leaf tissues of tomato plants [36]. These two metabolites represent enzymatic activities of cell or tissue type other than type I/IV trichomes of tomato leaf. Labeling patterns were anticipated to be different from acylsugar metabolites which are produced in type I trichomes of *Solanum* leaflet. Figure 3.11 shows mass spectra for tomatine (A-D) and rutin (E-H) from labeled and unlabeled control M82 plants. [M + formate] of steroidal glycoalkaloid tomatine has the monoisotopic mass of m/z 1078.5; [M – H] of the flavonoid glycoside rutin has the monoisotopic mass of m/z 609. The isotopologue pattern was complex when the plants were labeled under $^{13}CO_2$ conditions for different lengths of time. Calculation for mol% of ^{13}C in tomatine and rutin

molecules followed the same method described in 3.3.3 Enrichment Calculation in Metabolite Ions. Table 3.3 shows the average of mol% of ¹³C enrichment (3 biological replicates) and standard deviation (SD) values for tomatine and rutin during five days of labeling and then five days of growth in ambient atmosphere. This dataset was collected using the optimized hydroponic growth condition for M82 plants in the sealed growth chamber described in Chapter 4. Compare to acylsugars which usually achieved up to 45% of ¹³C enrichment after five days of labeling, tomatine (35%) and rutin (36%) have lower level of ¹³C incorporation during the same labeling periods.

Table 3.3 13 C enrichments in M82 tomatine and rutin during five days of labeling using 13 CO₂ and then five days growing in ambient atmosphere.

Labeling Days	Rutin	C ₂₇ H ₂₉ O ₁₆ [M-H]	m/z 1032 C ₅₀ H ₈₂ NO ₂₁ *Tomatine [M-H] ⁻			
	Ave. ¹³ C%	SD. ¹³ C%	Ave. ¹³ C%	SD. ¹³ C%		
1d_ ¹³ C	15.7%	2.7%	11.1%	1.4%		
2d_ ¹³ C	28.4%	4.5%	19.7%	2.6%		
3d_ ¹³ C	23.4%	1.8%	22.2%	5.1%		
4d_ ¹³ C	28.8%	3.9%	28.1%	3.6%		
5d_ ¹³ C	36.3%	4.2%	34.6%	1.5%		
back 1d_12C	25.3%	7.8%	26.2%	3.5%		
back 2d_12C	21.2%	8.0%	26.9%	4.6%		
back 3d_12C	17.4%	2.9%	23.4%	2.5%		
back 4d_12C	21.2%	2.0%	26.1%	2.5%		
back 5d_12C	19.1%	4.2%	22.1%	2.3%		

^{*} Tomatine [M-H] was detected and quantified using ion isotopologues in fragmentation function with collision voltage of 20 V.

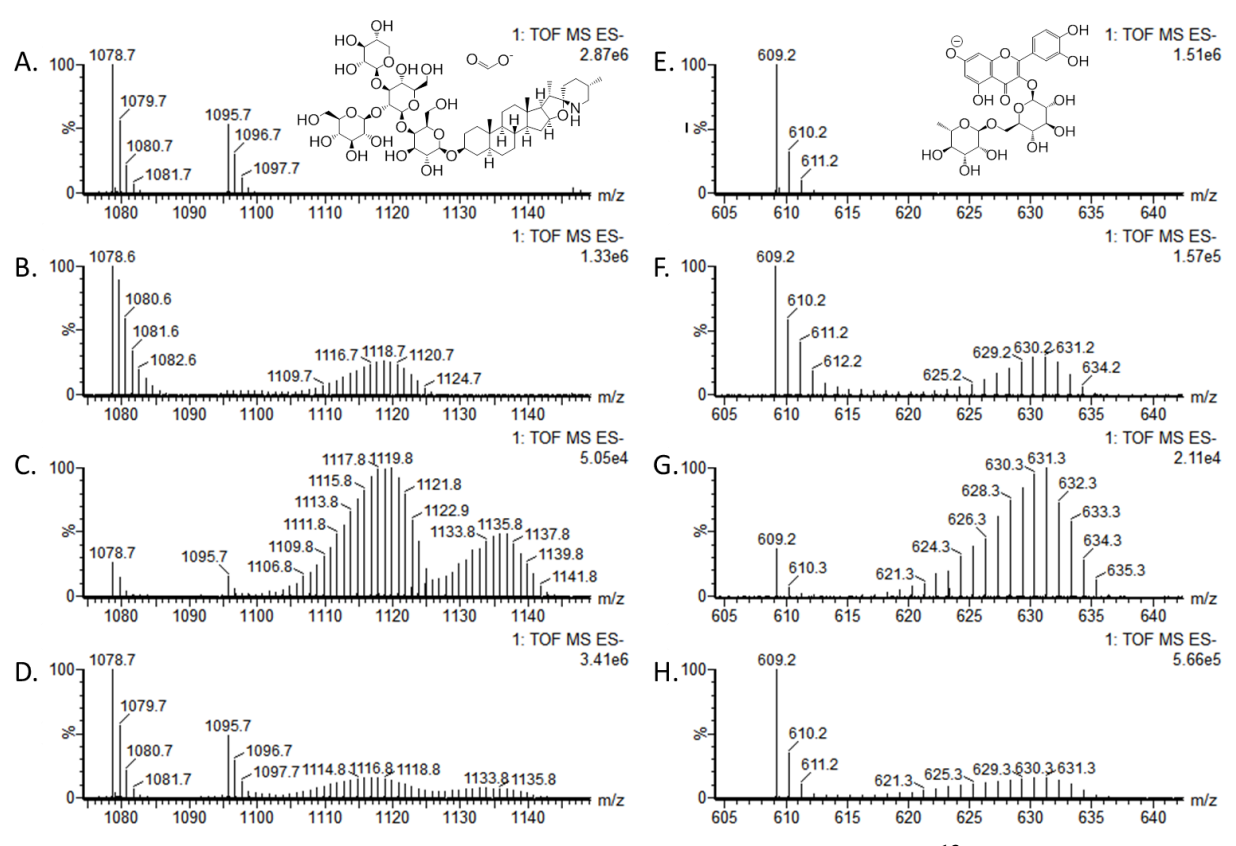


Figure 3.11. Negative-ion mode mass spectra for tomatine (A-D) and rutin (E-H) from 13 C-labeled and unlabeled control M82 plants. [M + formate] of steroidal glycoalkaloid tomatine has a monoisotopic mass of m/z 1078.5; [M - H] of the flavonoid glycoside rutin has a monoisotopic mass of m/z 609. A and E showed the spectra of tomatine and rutin from unlabeled control M82 leaflet A1. B and F showed the spectra of tomatine and rutin from M82 leaflet C1 which has been labeled for 5 days and then moved back to ambient air for 2days. C and G showed the spectra of tomatine and rutin from M82 leaflet C1 which has been labeled for 4 days. D and H showed the spectra of tomatine and rutin from M82 leaflet A1 which has been labeled for 5 days. The structure of tomatine formate adduct [M + formate] and rutin deprotonated ion [M - H] are presented in A and E.

3.4 Conclusions

One might ask whether the complexity of generating mass spectra separately using multiple collision energy functions provides tangible advantages relative to employing rolling collision energy profiles or employing a smaller number of separate collision functions (e.g., MS^E), particularly since the data processing for multiplexed analysis is more complex. Of course, the advantages that accrue from collision energy multiplexing will depend on the chemical complexity of the sample. In order to avoid the potential mass biases of mass window isolation of precursor ions, application of different collision energies in separate acquisition functions provides a means to resolve overlapping ions. When labeling experiments are performed in a manner that minimizes contributions from unlabeled precursors, one may obtain broad and complex distributions of isotopologues ranging from completely labeled (all C are ^{13}C) to completely unlabeled ions. In such cases, the probability of isobar overlap from different ion types (e.g., $[M + formate]^-$ and $[M + Cl]^-$) becomes substantial, and collision energy-based resolution offers potential solutions that can improve measurements of isotope enrichments.

Though this report has focused on acylsucrose metabolites, the analytical strategy described herein is applicable to a wide range of specialized metabolites as well as alternative techniques for ion activation. Since ¹³CO₂ is a universal tracer incorporated through photosynthetic carbon fixation, whole plant metabolomes can be labeled using this approach. Multiplexing of collision conditions allows labeling to be measured in metabolite substructures detected in the form of fragment ions, avoiding biases introduced by precursor mass selection and activation. Such detailed comparison of metabolic dynamics of metabolites not amenable to GC/MS offers potential to improve

our understanding of dynamic biosynthetic and catabolic contributions to metabolite fluxes. We anticipate that information of this kind will contribute to improve metabolic engineering of plants and microbes for production of valuable chemicals.

REFERENCES

REFERENCES

- 1. Weng, J.K., Philippe, R.N. & Noel, J.P. The rise of chemodiversity in plants. *Science (New York, N.Y.)* **336**, 1667-1670 (2012).
- 2. Last, R.L., Jones, A.D. & Shachar-Hill, Y. Towards the plant metabolome and beyond. *Nature reviews. Molecular cell biology* **8**, 167-174 (2007).
- 3. Dunn, W.B. & Ellis, D.I. Metabolomics: Current analytical platforms and methodologies. *TrAC Trends in Analytical Chemistry* **24**, 285-294 (2005).
- 4. Glinski, M. & Weckwerth, W. The role of mass spectrometry in plant systems biology. *Mass Spectrom Rev* **25**, 173-214 (2006).
- 5. Lisec, J., Schauer, N., Kopka, J., Willmitzer, L. & Fernie, A.R. Gas chromatography mass spectrometry-based metabolite profiling in plants. *Nature protocols* **1**, 387-396 (2006).
- 6. De Vos, R.C. *et al.* Untargeted large-scale plant metabolomics using liquid chromatography coupled to mass spectrometry. *Nature protocols* **2**, 778-791 (2007).
- 7. Braunberger, C. *et al.* LC-NMR, NMR, and LC-MS identification and LC-DAD quantification of flavonoids and ellagic acid derivatives in Drosera peltata. *Journal of chromatography. B, Analytical technologies in the biomedical and life sciences* **932**, 111-116 (2013).
- 8. Ward, J.L., Baker, J.M. & Beale, M.H. Recent applications of NMR spectroscopy in plant metabolomics. *The FEBS journal* **274**, 1126-1131 (2007).
- 9. Ratcliffe, R.G. & Shachar-Hill, Y. PROBING PLANT METABOLISM WITH NMR. *Annual review of plant physiology and plant molecular biology* **52**, 499-526 (2001).
- 10. Fernie, A.R. & Morgan, J.A. Analysis of metabolic flux using dynamic labelling and metabolic modelling. *Plant, cell & environment* **36**, 1738-1750 (2013).
- 11. Klie, S. *et al.* Conserved changes in the dynamics of metabolic processes during fruit development and ripening across species. *Plant physiology* **164**, 55-68 (2014).
- 12. Fernie, A.R., Geigenberger, P. & Stitt, M. Flux an important, but neglected, component of functional genomics. *Current opinion in plant biology* **8**, 174-182 (2005).

- 13. Birkemeyer, C., Luedemann, A., Wagner, C., Erban, A. & Kopka, J. Metabolome analysis: the potential of in vivo labeling with stable isotopes for metabolite profiling. *Trends Biotechnol* **23**, 28-33 (2005).
- 14. Bueschl, C., Krska, R., Kluger, B. & Schuhmacher, R. Isotopic labeling-assisted metabolomics using LC-MS. *Anal Bioanal Chem* **405**, 27-33 (2013).
- 15. Klein, S. & Heinzle, E. Isotope labeling experiments in metabolomics and fluxomics. *Wiley Interdisciplinary Reviews: Systems Biology and Medicine* **4**, 261-272 (2012).
- 16. Chen, W.P. *et al.* An automated growth enclosure for metabolic labeling of Arabidopsis thaliana with 13C-carbon dioxide an in vivo labeling system for proteomics and metabolomics research. *Proteome science* **9**, 9 (2011).
- 17. Romisch-Margl, W. *et al.* 13CO2 as a universal metabolic tracer in isotopologue perturbation experiments. *Phytochemistry* **68**, 2273-2289 (2007).
- 18. Choi, J., Grossbach, M.T. & Antoniewicz, M.R. Measuring complete isotopomer distribution of aspartate using gas chromatography/tandem mass spectrometry. *Anal Chem* **84**, 4628-4632 (2012).
- 19. Nakabayashi, R. *et al.* Combination of Liquid Chromatography–Fourier Transform Ion Cyclotron Resonance-Mass Spectrometry with 13C-Labeling for Chemical Assignment of Sulfur-Containing Metabolites in Onion Bulbs. *Analytical Chemistry* **85**, 1310-1315 (2013).
- 20. Giavalisco, P. *et al.* High-resolution direct infusion-based mass spectrometry in combination with whole 13C metabolome isotope labeling allows unambiguous assignment of chemical sum formulas. *Anal Chem* **80**, 9417-9425 (2008).
- 21. Schramek, N. *et al.* Artemisinin biosynthesis in growing plants of Artemisia annua. A 13CO2 study. *Phytochemistry* **71**, 179-187 (2010).
- 22. Antonio, C. *et al.* Analysis of the interface between primary and secondary metabolism in catharanthus roseus cell cultures using (13)C-stable isotope feeding and coupled mass spectrometry. *Molecular plant* **6**, 581-584 (2013).
- 23. Allen, D.K. *et al.* Quantification of peptide m/z distributions from 13C-labeled cultures with high-resolution mass spectrometry. *Anal Chem* **86**, 1894-1901 (2014).
- 24. Allen, D.K., Evans, B.S. & Libourel, I.G.L. Analysis of Isotopic Labeling in Peptide Fragments by Tandem Mass Spectrometry. *PloS one* **9**, e91537 (2014).

- 25. Wrona, M., Mauriala, T., Bateman, K.P., Mortishire-Smith, R.J. & O'Connor, D. 'All-in-one' analysis for metabolite identification using liquid chromatography/hybrid quadrupole time-of-flight mass spectrometry with collision energy switching. *Rapid communications in mass spectrometry: RCM* 19, 2597-2602 (2005).
- 26. Gu, L., Jones, A.D. & Last, R.L. Broad connections in the Arabidopsis seed metabolic network revealed by metabolite profiling of an amino acid catabolism mutant. *The Plant journal: for cell and molecular biology* **61**, 579-590 (2010).
- 27. Schilmiller, A. *et al.* Mass spectrometry screening reveals widespread diversity in trichome specialized metabolites of tomato chromosomal substitution lines. *The Plant journal: for cell and molecular biology* **62**, 391-403 (2010).
- 28. Weinmann, W., Wiedemann, A., Eppinger, B., Renz, M. & Svoboda, M. Screening for drugs in serum by electrospray ionization/collision-induced dissociation and library searching. *J Am Soc Mass Spectrom* **10**, 1028-1037 (1999).
- 29. McDowell, E.T. *et al.* Comparative functional genomic analysis of Solanum glandular trichome types. *Plant physiology* (2010).
- 30. Ghosh, B., Westbrook, T.C. & Jones, A.D. Comparative structural profiling of trichome specialized metabolites in tomato (Solanum lycopersicum) and S. habrochaites: acylsugar profiles revealed by UHPLC/MS and NMR. *Metabolomics* **10**, 496-507 (2014).
- 31. MacCoss, M.J., Wu, C.C., Matthews, D.E. & Yates, J.R., 3rd Measurement of the isotope enrichment of stable isotope-labeled proteins using high-resolution mass spectra of peptides. *Anal Chem* **77**, 7646-7653 (2005).
- 32. Feng. S., Profiling of specialized metabolites in glandular trichomes of the genus Solanum using liquid chromatography and mass spectrometry, PhD Dissertation, Michigan State University (2009).
- 33. Schilmiller, A.L., Charbonneau, A.L. & Last, R.L. Identification of a BAHD acetyltransferase that produces protective acyl sugars in tomato trichomes. *Proceedings of the National Academy of Sciences of the United States of America* **109**, 16377-16382 (2012).
- 34. Schilmiller, A.L., Last, R.L. & Pichersky, E. Harnessing plant trichome biochemistry for the production of useful compounds. *The Plant Journal* **54**, 702-711 (2008).
- 35. Friedman, M. Anticarcinogenic, Cardioprotective, and Other Health Benefits of Tomato Compounds Lycopene, α-Tomatine, and Tomatidine in Pure Form and in

Fresh and Processed Tomatoes. *Journal of agricultural and food chemistry* **61**, 9534-9550 (2013).

Chapter 4. Dynamics and Stable Isotope Labeling of Tomato Specialized Metabolite	S

4.1 Introduction

Glandular trichomes in the family Solanaceae accumulate large quantities of specialized metabolites, including terpenes, flavonoids and acylsugars [1-3]. Because of this, glandular trichomes have potential to serve as important and renewable "chemical factories" [2]. These specialized metabolites have been reported to convey direct and indirect plant resistance against certain pests [4, 5], and engineering their accumulation offers commercial values in development of pest-resistant crops and in the form of valuable chemicals [5].

Beyond the direct commercial values of trichome board compounds, the glandular trichome has been regarded a prototype tissue to explore the diversity of plant biochemistry and plant specialized metabolism [2, 3, 6, 7]. Among trichome metabolites, acylsugars have attracted attention in recent years because of their proven insect resistance properties [8, 9] and commercial value as surfactants [10, 11], antimicrobials [12, 13] and pharmaceutical excipients [14]. The quantities and chemotypes of acylsugar metabolites have been regarded as targets for tomato breeding so as to obtain stronger and eco-friendly insect control [15-17]. In some cultivated and wild tomato accessions, structurally diverse acylsugar metabolites form complex chemotypes that vary in content of straight and/or branched aliphatic acid esters of different chain lengths attached to different hydroxyl group positions of sucrose or glucose [7, 18]. Given this diversity, a variety of synthetic and regulatory enzymes is expected to participate in complex metabolic networks that regulate abundance and chemical diversity of this class of specialized metabolites.

Recently, by virtue of cross-referencing genomic and genetic resources and advanced analytical tools for fast metabolomics screening and metabolite identification, several trichome specific genes and enzymes were identified to involved in acylsugar biosynthesis and contribute to chemical diversity of acylsucroses that accumulate in cultivated and wild tomato species. Four acylsugar acyltransferase (ASAT) enzymes that sequentially add specific acyl chains onto sucrose cores to assemble a variety of Solanum acylsugars were characterized (Figure 4.1). In particular, two trichome-specific S. lycopersicum BAHD acyltransferases [19] were identified to produce the di-acylsucrose intermediates from sucrose and acyl-CoA [37]. Part of the acylsucrose diversity in S. habrochaites arises from genetic variation in these two ASATs which prefer different acyl chain length substrates and positions for substitution [7, 20]. Beyond di-acylsucroses, S. lycopersicum ASAT3 (SI-ASAT3) adds a third acyl chain to the five-membered (furanose) ring to form tri-acylsucroses [20]. Variant forms of ASAT3 were found in wild tomato accessions that use acyl-CoA esters of different chain lengths or acylate the sixmembered (pyranose) ring of mono-acylated sucrose. On top of that, an ASAT4 enzyme (formerly AT2) was discovered that catalyzes acetylation of tri-acylsucroses using acetyl-CoA to make tetra-acylsucroses in S. lycopersicum and S. habrochaites trichomes [21]. Recent evolutionary changes (e.g. loss of function alleles) of ASAT genes are found in populations of S. habrochaites from northern Peru and Ecuador [7] and demonstrate that ASAT diversification plays an important role in shaping the phenotypic diversity in trichomes of wild tomato.

ASAT1
$$\stackrel{\text{iC5}}{\longrightarrow}$$
 $\stackrel{\text{R}_4}{\longrightarrow}$ $\stackrel{\text{OII}}{\longrightarrow}$ $\stackrel{\text{OH}}{\longrightarrow}$ $\stackrel{\text{O$

S. lycopersicum Acylsucrose.

Figure 4.1. Acylsucrose structure in *S. lycopersicum* and acyl chain substitution patterns. The carbon position is named 1 to 6 for pyranose ring, and 1 to 6 for furanose ring. R2, R3 and R4 indicate acyl chains substituted at 2, 3, and 4 positions of pyranose ring hydroxyl groups, and R3 indicates acyl chains substituted at the 3 position of furanose ring. ASAT1, ASAT2, ASAT3 and ASAT4 are four AcylSugar AcylTransferase (ASAT) enzymes that sequentially add acyl chains to the sucrose core. Grey characters indicate different acyl-CoA preference for different ASAT enzymes in *S. lycopersicum* trichomes.

However, acyl chain substitution by ASATs explained part, but not all, of acylsugar chemical diversification. The complexity of the acylsugar metabolic network has also been attributed to variations in the source of precursor molecules. For instance, an isopropylmalate synthase 3 (IPMS3) recently discovered in cultivated tomato affects the proportions of 2-methylpropanoic acid (iC4) and 3-methylbutanoic acid (iC5) acyl chain in acylsugars from accessions of the wild tomato *Solanum pennellii* [22].

Apart from biosynthesis, the genetic mechanisms underlying this phenotypic diversity were recently revealed to be associated with disassembly and catabolism as well. AcylSugar acylHydrolase1 and 2 (ASH1 and ASH2) were identified to remove acyl chains from specific positions of certain types of acylsugars *in vitro* [38]. Schilmiller *et al.* reported that introgression of a dominant locus containing these two

ASH genes from the wild tomato *Solanum pennellii* LA0716 into the cultivated tomato (*S. lycopersicum* M82) genetic background resulted in reduced levels of acylsugars in an introgression line IL5-3 derived from *S. lycopersicum* x *S. pennellii*. This discovery of acylsugars catabolism reinforces the importance that a rational engineering of biosynthetic pathway for desired amount of metabolites should take into account of multiple possibilities for inflow and outflow of relevant metabolic processes [38].

Before we can certify the feasibility of metabolic engineering of these insecticidal metabolites in plants and microbes, one of the greatest gaps in fundamental knowledge about accumulation of most plant specialized metabolites lies in limited assessment and understanding of the quantitative fluxes and kinetics of metabolic pathways [23, 24]. An intricate design of control and regulation of the metabolic activities of at the levels of genes, enzymes and metabolites is required for successful plant breeding and engineering of accumulation of bioactive specialized metabolites. To manipulate glandular trichomes and enhance acylsugar accumulation, we need to understand the processes that control flux through metabolic pathways, recognize steps that limit metabolite accumulation, and learn how to control metabolite accumulation by manipulating the on/off or up/down switches.

Even though important and promising, few publications have been reported for flux analysis of specialized metabolism in plants, though important advances have been made for assessing fluxes in central metabolism [24]. Adapting these approaches to specialized metabolism has been challenging because we have limited knowledge of complete metabolic pathways and intermediates, activities of biosynthetic enzymes, the pool sizes of precursors and intermediates, and information regarding cellular

compartmentation and transport of substrates and end products [25]. Unlike microbial systems that are well suited for existing flux analysis methods and stimulating models, plant systems are more complex, and subcellular compartmentation and inter-organelle transport processes are more divergent [26, 27]. On the other hand, the well-established steady-state labeling approaches for quantitative flux analysis of plant central metabolic pathways are not readily suited for most plant specialized metabolism [24, 28]. This is partially because specialized metabolites take several cell cycles and cell organelles to reach steady-state labeling, especially for highly branched or poorly elucidated pathways, while labeling of central carbon metabolites may take place within seconds [24]. When clear biosynthetic pathways and in vitro enzyme preliminary kinetics are available, dynamic labeling approaches provide a way forward for flux analysis of certain specialized metabolic networks. For instance, Boatright et al. performed quantitative analysis of isotopic abundances and pool sizes of benzenoid/phenylpropanoid-related compounds and revealed that two alternative pathways operate in the benzenoid branched pathway in petunia flowers [29]. Matsuda et al. applied the dynamic labeling approach to seven phenylpropanoid metabolites in potato tuber using L-phenylalanine- d_5 and determined the flux partitioning at the p-coumaroyl CoA branch point [30, 31]. Derived from this, Elmar et al. proposed a method to estimate the phenylpropanoid pathway metabolic flux by fitting pulse-chase labeling experiment data into simplified first order and power-law kinetics, and calculated flux-control coefficients [32]. These publications demonstrated that dynamic tracing experiments permit the estimation of metabolic flux rates and distribution of network activities for some well-studied specialized metabolic pathways. However, this type of flux analysis is still rare for most plant specialized metabolism, given that inadequate knowledge of pathways, intermediates, and technologies for assessing labeling and tracing experiments in plants are available.

Monitoring the time-dependent incorporation of stable isotope labels from a precursor or substrate allows for uncovering of the existence or absence of a particular pathway, even when the biosynthetic pathways are not completely defined [24]. To demonstrate this, this manuscript reports the flux analysis of acylsugar metabolites harvested in the introgression line IL5-3 derived from conventional and wild tomato which accumulated lower levels of acylsugars than either parent [3]. Dynamic labeling of acylsugars through ¹³CO₂ offers a non-invasive in vivo approach for investigating the genetic basis of acylsugar accumulation and complements modern genetics approaches. Our recent development of analytical methods for nonbiased quantitative assessments of labeling in specialized plant metabolites facilitates such investigations into metabolic dynamics of specialized metabolism [33]. This current report extends our understanding on catabolic activities of acylsugar metabolites within *Solanum* trichomes and underscores the importance of metabolite turnover, degradation and reassembly on regulation of specialized metabolite accumulation.

4.2 Chamber design

A custom-built and sealed plant growth chamber (300 L volume) was designed for plant labeling studies using $^{13}CO_2$ and constructed. Plants can be labeled starting from seeds or seedlings in the chamber, then pulse-labeled with $^{13}CO_2$ or chased with ambient CO_2 of natural abundance. Detailed construction and operation of this chamber is described first before introducing the method and experiments (Figure 4.2).

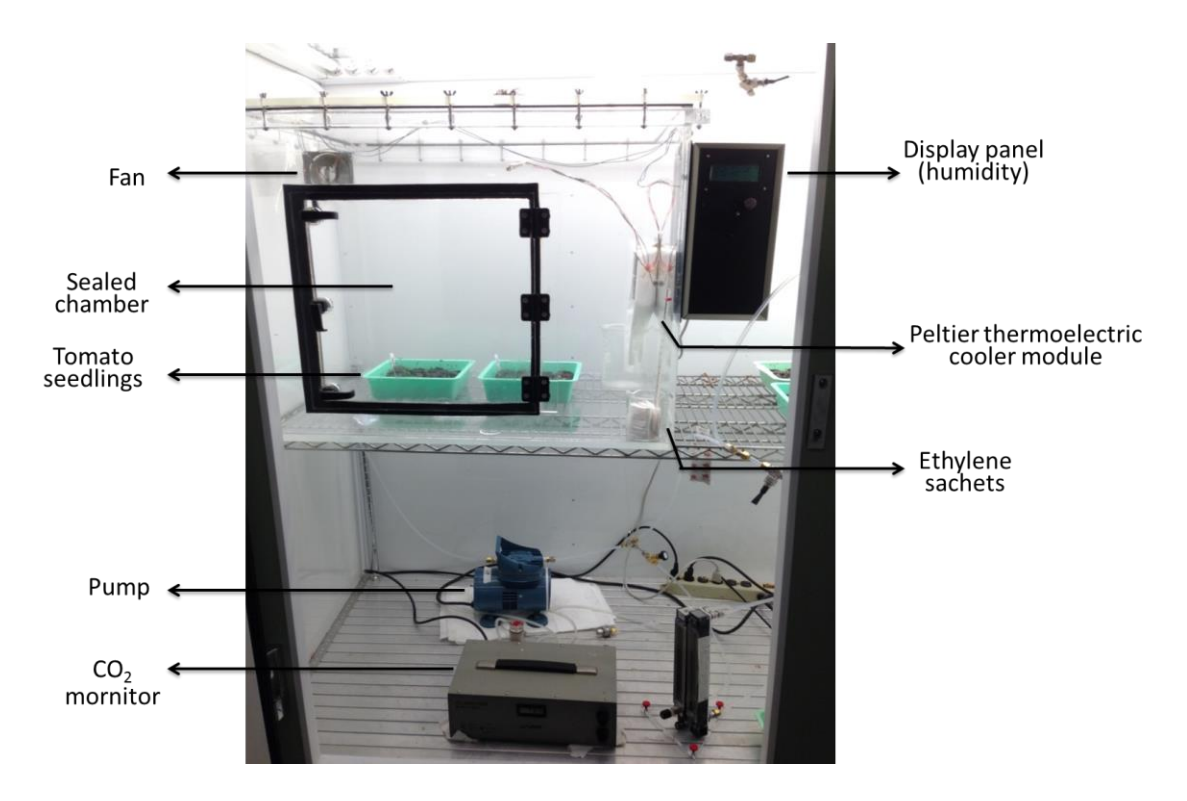


Figure 4.2. Front of the labeling chamber and control system. The sealed plastic chamber and CO₂ monitoring/pulsing system are all seated inside a commercial growth chamber with the light control. The ethylene sachets, Peltier thermoelectric cooler module and circulating fan are inside the major sealed plastic chamber.

4.2.1 Hardware setup

This growth chamber was built with 0.3 inch (7.6 mm) thick plexiglass and has an airtight door sealed with a rubber gasket and a removable top. Airtight rubber strips were attached to the frame of the front door and the top of the main chamber. An internal electric fan provided additional circulation of gases. A Peltier Thermoelectric Cooler Module was mounted on one side of the walls to the main chamber. This cold plate was designed to control the humidity of the main chamber by condensing atmospheric moisture which then drained into a separate reservoir. Several gas inlets and outlets were connected with 0.5 inch (O.D.) fluorinated ethylene propylene (FEP) tubing for purging and pulsing of either CO₂ free air or labeled ¹³CO₂. In addition, humidity and temperature

sensors (Microchip, Chandler, AZ, USA) were installed inside the main chamber and connected to a LCD Character Display Module (Lumex, Carol Stream, IL, USA). A nondispersive infrared CO₂ analyzer (Model L1-6251, LiCOR, Lincoln, NE, USA), a CO₂ scrubber (Soda Lime) and a diaphragm pump (Model 905CA18, Gardner Denver Thomas, Sheboygan, WI, USA) were located outside the chamber for monitoring the CO₂ levels, removing CO₂ or circulating air inside the growth chamber through recirculation of air. Replaceable ethylene sachets (containing potassium permanganate pellets) were placed inside the chamber. Swagelok-connected toggle valves were connected to every inlet and outlet tubing and before the pump and CO₂ scrubber. This multiple valve design allows for easy switching between purging, pulsing, and circulating modes and allow for refilling of the ¹³CO₂ source or replacement of CO₂ scrubber without disturbing plant growth conditions. Either commercial tank of CO₂ free air (< 1 ppm CO₂) or ambient air pumping through CO₂ scrubber column were used to purge the chamber before pulsing labeled ¹³CO₂.

4.2.2 Power setup

A 12 V DC power supply was used to power the thermoelectric cooler (cold plate), the fan inside the chamber for air circulation, the display panel for monitoring and controlling the humidity, and the temperature and humidity sensor. The CO₂ analyzer and pump was powered by 120 V AC. The power supplies were directly plugged into the wall outlet.

4.2.3 System control setup

4.2.3.1 Control of relative humidity in the chamber

The humidity was controlled as described in the hardware setup by directing humid air onto the cold plate. When the chamber humidity is higher than the set value, a relay that controls the temperature of Peltier Thermoelectric Cooler Module switches on. The air in the main chamber where plants grow will be directed into the cold box and excess moisture can be condensed on the surface of the cold plate. The condensed water will accumulate on the plate and drip onto a tray placed under the condenser.

4.2.3.2 The control of light intensity

No lighting system is integrated in the chamber because the system was designed to be sitting inside a commercial growth chamber where the lighting can be set and controlled separately.

4.2.3.3 The control of CO₂ levels

The air from the chamber can be pumped through the CO_2 analyzer and monitored for CO_2 concentration which can be transformed into ppm. A tank of CO_2 free air is seated outside the chamber for reference gas of CO_2 analyzer. The CO_2 analyzer was turned on before starting a new experiment. CO_2 levels were frequently monitored before and after pulsing, purging and during the plant growth before a new experiment to make sure certain concentration of CO_2 is kept inside the chamber for health plant growth.

The CO₂ pulsing reservoir was a sleeve rubber stopper-capped suction flask (100 mL) that was connected to the main chamber through FEP tubing. The generation of

specific amounts of ¹³CO₂ gas was controlled by injecting sulfuric acid into the calculated amount of sodium ¹³C-bicarbonate which was placed in the sealed suction flask. For our experiment where ~800 ppm of ¹³CO₂ was needed, ~850 mg [¹³C]NaHCO₃ (Sigma, 98 atom% ¹³C) was placed in the flask and 5 mL of 1.8 M sulfuric acid was injected into the flask through a needle syringe penetrating into the rubber stopper cap. The generated CO₂ flowed into the sealed chamber through the side arm of the flask which was connected to the chamber using tubing. After pulsing, an equilibration period of ~10 min was allowed, after which the air was circulated to the infrared CO₂ analyzer using the pump, and CO₂ concentrations were monitored. Since the nondispersive infrared CO₂ analyzer doesn't respond equally for ¹³CO₂ and ¹²CO₂, the system was calibrated using ~850 mg of unlabeled NaHCO₃ (Sigma) to provide ~800 ppm of CO₂ after purging. Once checked, same amount of [¹³C]NaHCO₃ was used afterward for labeling experiments. Meanwhile, the corresponding read value for ¹³CO₂ was documented for day to day comparison.

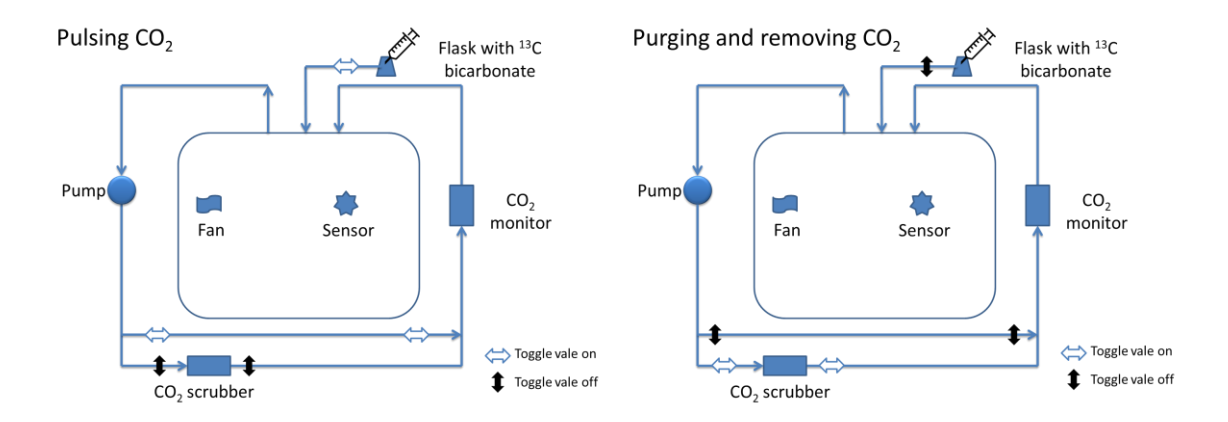


Figure 4.3. Operation of the chamber for labeling experiments. The left figure demonstrates the setup of the system for pulsing ¹³CO₂. The right figure demonstrates the setup of the system for purging the chamber to remove CO₂. Arrows indicate the direction of the air flow inside the system.

4.3 Methods and experiments

To probe acylsugar assembly from sucrose and assess rates of new synthesis of acylsugars, a ¹³C pulse-chase labeling approach was developed. The ¹³C isotope was pulsed into the sealed chamber every 24 h for 5 days duration, after which the plants were returned to ambient atmosphere. To achieve higher percent of labeling, plants were grown using hydroponic conditions to minimize production of unlabeled CO₂ by soil bacteria.

4.3.1 Materials and chemicals

HPLC grade acetonitrile, 2-propanol, methanol, formic acid (88% aqueous solution), and ACS grade sulfuric acid (95%-98%, J.T. Baker) were purchased from VWR Scientific. Sodium [13C] bicarbonate (98 atom% 13C) was obtained from Sigma-Aldrich (St. Louis, MO). Hoagland solution at 1/2 X provided by the Plant Growth Chamber Facility of Michigan State University. Germicidal Bleach (Clorox) was purchased from the Biochemistry and Molecular Biology Research store at Michigan State University.

Seed germination media (200 mL of 1/2 MSO media with 7% agar, no sucrose) was prepared by mixing 4.6 mg MS (Murashige and Skoog) salt, 2 mL stock Gamborg's Vitamin Mixture, and 1800 mL ddH₂O. The pH was adjusted to 5.8 with 1 M KOH, and the total volume was adjusted to 2000 mL with ddH₂O. The above solution was divided into 100 mL aliquots, and 0.8 g agar was added to each.

Tomato (*Solanum lycopersicum* M82; LA3475) seeds were obtained from the UC Davis C. M. Rick Tomato Genetics Resource Center. *Solanum pennellii* IL-5-3 seeds

were obtained from Dr. Dani Zamir (Hebrew University Faculty of Agriculture, Rehovot, Israel). For tomato growth, the lighting condition is usually 16 h light (300 µE m⁻² sec⁻¹) and 8 h dark. For this labeling experiment, 24 h light was used to avoid starch accumulation.

4.3.2 Hydroponic growth of M82 and IL5-3 plants from seeds

Seed germination media, ½ × Hoagland solutions, ddH₂O, capped jars and microcentrifuge tubes for germination were sterilized before use by autoclaving. After autoclaving, poured the media into cleaned jar before the media cooled down to room temperate and solidify. M82 and IL5-3 seeds were treated using 40 mL of 40% bleach (what in the bleach) containing 1 drop of Tween 20 solution for 5 min, and then rinsed with ddH₂O four times. Pots for plant growth were cleaned with 100% bleach and rinsed with water before use.

After cooling to room temperature, 8 to 10 M82 and IL5-3 seeds were kept on seed germination media/agar in capped jars. This was performed in a laminar flow hood to minimize contamination.

The germination of M82 and IL5-3 seeds usually took 6-7 days. After germination, seedlings were transferred into autoclaved vermiculite (medium fine) mixtures pot. Aluminum foil was used to cover the vermiculite from exposure to the light, with an incision in the center to allow the aerial parts of the seedling to be illuminated. Plants were watered with autoclaved 1/2 Hoagland solutions daily and cultivated in the growth chamber for labeling experiments.

4.3.3 ¹³C Pulse-Chase labeling experiment

Before introducing the labeled ¹³CO₂, the sealed chamber was purged for 20 min to remove unlabeled CO₂ through recirculating pumping through a CO₂ scrubber, until the CO₂ monitor reading of CO₂ level dropped below 50 ppm (< 6% within ~80 ppm labeled CO₂). After purging, a valve was closed to switch the CO₂ scrubber off-line and switched a parallel CO₂ pulsing reservoir online to introduce labeled ¹³CO₂. To generate over 800 ppm ¹³CO₂ in the sealed chamber, ~850 mg [¹³C]NaHCO₃ (Sigma, 98 atom% ¹³C) was placed in the sleeve rubber stopper-capped suction flask (100 mL). 5 mL of 1.8 M sulfuric acid was injected into the flask through a needle syringe to start the reaction. The CO₂ then was purged into the sealed chamber through the flask side arm. After pulsing, the chamber was equilibrated for ~10 min, and the chamber air was circulated through the CO₂ monitor to confirm that ~800 ppm ¹³CO₂ was reached.

4.3.4 Leaf dip extract for trichome metabolites

At 24 hours after ¹³CO₂ introduction, the chamber was opened and four M82 and four IL5-3 plants were quickly removed for sampling. The rest of the plants were remaining labeled for four more days by repeating the purging with CO₂-depleted air and pulsing of ¹³CO₂ as described above. For sampling, every leaflet was removed from the stem using a clean razor blade and placed into a separate microcentrifuge tube. A volume of 1.0 mL ACN:isopropanol:H₂O (3:3:2 v/v/v) containing 0.1% formic acid was added to each tube, followed by vortexing for 10 s. Tubes were centrifuged at 1000*g* for 3 min, the supernatants were transferred into new tubes, and solvent was removed under vacuum in a SpeedVac. Each extracted leaflet residue was transferred to a drying oven, and dry

residue masses were measured. Unlabeled control plants were cultivated in the same growth chamber, and tissues were processed following an identical protocol.

Introduction of ¹³CO₂ was performed every 24 hours for 5 days, and plants were removed and sampled every 24 hours at 3pm. After 5 days of labeling, the plants were transferred to grow under ambient atmosphere by opening the chamber door. Leaflet dip extract were sampled every 24 hours for 5 days.

4.3.5 Quantitative LC-MS analysis and data processing

Quantitative LC-MS analysis of acylsugars for quantification of metabolites and ¹³C incorporation followed protocols described in our recent report [33]. Briefly, Waters QuanLynx was used to integrate peak areas for extracted ion chromatograms (XICs) of each isotopologue for an ion. Then, abundance-weighted average of isotopologue masses was calculated based on integrated peak area abundance of all isotopologues, and used for calculation of atom % of ¹³C enrichment and the moles of ¹³C for each acylsugar intact molecules and fragments. According to recently published LC-MS response factors for purified acylsugars [34] we then calculated pmol quantities of each targeted acylsugar metabolite and ¹³C amounts given that the elemental formula for the compound is known. For flux analysis, the concentration of either ¹³C tracers or intact acylsugar molecules was calculated as a function of time for pulse and chase labeling periods. Initial rates of metabolite biosynthesis and subsequent degradation were calculated from the slope of concentration at day zero in the Pulse labeling period or day 5 in the Chase labeling period.

4.4 Results and discussion

4.4.1 Diversity and accumulation of acylsugars in metabolites profiling

Metabolite profiling of leaf-dip extracts from tomato leaf tissue demonstrated accumulation of diverse acylsugar metabolites in young (1-2 weeks post-germination) plants, including acylsucroses containing six-carbon esters extracted from two weeks old M82 plant leaflets that had not been observed in older plant tissues. These findings suggested that biosynthesis and metabolism of acylsugar is dynamic, particularly during early developmental stages (within 3 weeks old). A pilot investigation indicated that acylsugar accumulation in an individual S. lycopersicum M82 leaflet was approximately five-fold higher relative to levels reported in 3-week old plants [3] on a tissue massnormalized basis within a couple of days past emergence of the first true leaf, but in the experiments described here, total peak areas of detected acylsugars normalized to leaf fresh weights exhibited a sharp approximate six-fold decrease after 15 days post germination (Figure 4.4). Levels of all of the most abundant acylsugars (S4:17, S4:24 and S3:22) in M82 tracked total acylsugar accumulation. The sharp drop in acylsugar levels between days 15 and 17 cannot be explained by an increase in tissue weight alone, and suggested that degradation of acylsugar plays an important role in regulating acylsugar accumulation.

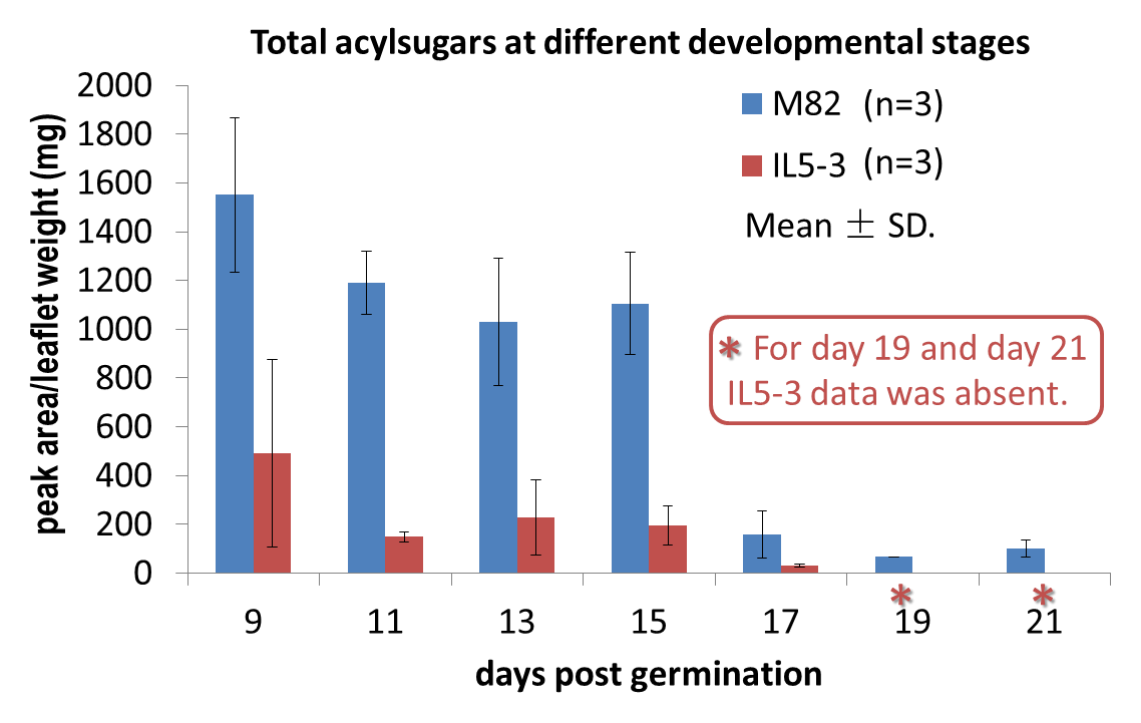


Figure 4.4. Total acylsugar accumulation in M82 and IL5-3 leaf trichomes extracts at early developmental stages. The leaflet A1 was used for M82 and IL5-3 acylsugar quantitation.

4.4.2 Leaf tissues sampled at different developmental stages

To specify the exact leaflet that was sampled for metabolite profiling, the first node developed above the cotyledon of a seedling was designated as node A, and the terminal leaflet growing at the end of the petiole of node A leaflet A1. Accordingly, the two symmetrical primary leaflets next to A1 are named A2. The simplified leaflet spatial distributions for tomato leaf development are shown in Figure 4.5. Leaf tissues sampled at different positions reflect tissues at different developmental stages.

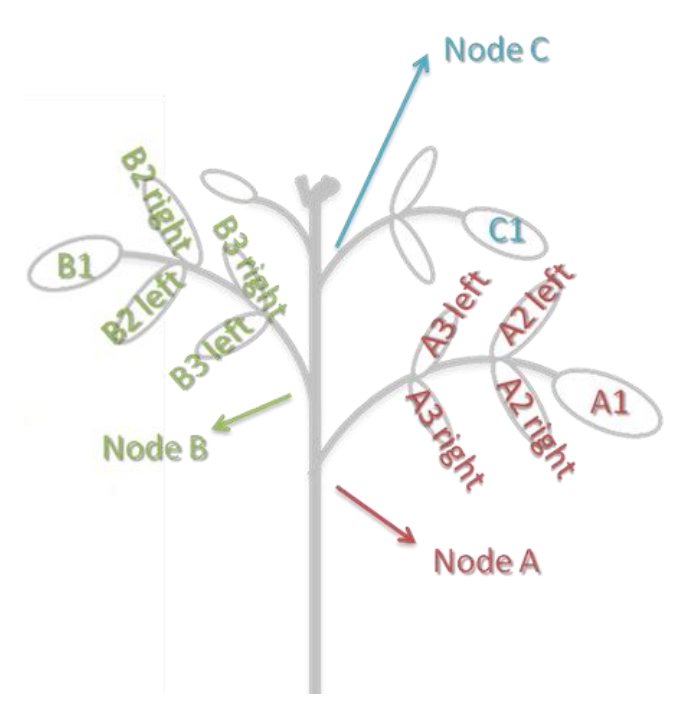


Figure 4.5. Nomenclature for designating compound leaves and individual leaflets.

4.4.3 Rate of acylsugar biosynthesis

We were fortunate to have access to the introgression lines (ILs) developed by the Zamir laboratory which have regions of the *S. pennellii* LA0716 genome substituted in place of the *S. lycopersicum* M82 genome [35]. Each introgression line is nearly isogenic with cultivated tomato, with an average introgression of about 33 cM in a total genome of about 1200 cM. Earlier metabolite profiling of a set of ILs discovered two ILs (IL5-3 and IL11-3) that exhibited substantial reductions in acylsugar accumulation [3]. Exploration of genomic DNA sequences revealed regions on IL11-3 annotated as BAHD acyltransferases, with one gene (named Sl-ASAT3) expressed in tip cells of type I trichomes on chromosome 11 locus [21]. The region of *S. pennellii* chromosome 11 introduced in IL11-3 contained Sp-ASAT3 which did not acylate at the 3 'position on the furanose ring of acylsucroses, and explained the lower levels of acylsugar accumulation

in IL11-3. However, for IL5-3, no tomato genes were annotated as acyltransferases or other proposed acylsugar biosynthetic genes in the chromosome 5 regions that might account for the low acylsugar abundance phenotype. More recently, two genes annotated as acyl hydrolases (*ASH1* and *ASH2*) were discovered to code for <u>AcylSugar</u> acyl<u>Hydrolase 1 and 2 enzymes that remove acyl chains from specific positions of certain tri- and tetra-acylsucroses *in vitro* [38]. Their expression in tomato trichomes suggested that they might play a role in acylsugar degradation.</u>

To explore rates of acylsugar biosynthesis and degradation using an alternative flux analysis approach, a pulse-chase labeling experiment was performed using ¹³C as a tracer, growing plants under labeled ¹³CO₂ for several days, then returning the plants to ambient atmosphere. Plant tissues were harvested each day to assess total acylsugar levels and the extent of ¹³C incorporation into acylsugars. Beginning at 10 days postgermination, 800 ppm of labeled ¹³CO₂ was introduced to the sealed growth chamber every 24 h for 5 days. Acylsugars S3:22 and S4:24 were two of the most abundant AS detected in leaf dip extracts of IL5-3. Both of these metabolites contain two C5 esters and one n-C12 ester, with the latter also having a single acetate ester group at position 2 [3]. Unlike M82 in which acylsugars with only short acyl chains (most notably C5) are abundant, acylsugars with only short acyl chains were only present in leaflet A1 of IL5-3 at barely-detectable amounts if at all (Figure 4.6). This finding suggested either altered biosynthetic rates for the all-short chain esters or perhaps selective degradation of allshort chain acylsugars in IL5-3. The presence of C5 esters in the abundant acylsugars from IL5-3 suggested that availability of C5-CoA esters was unlikely to be limiting.

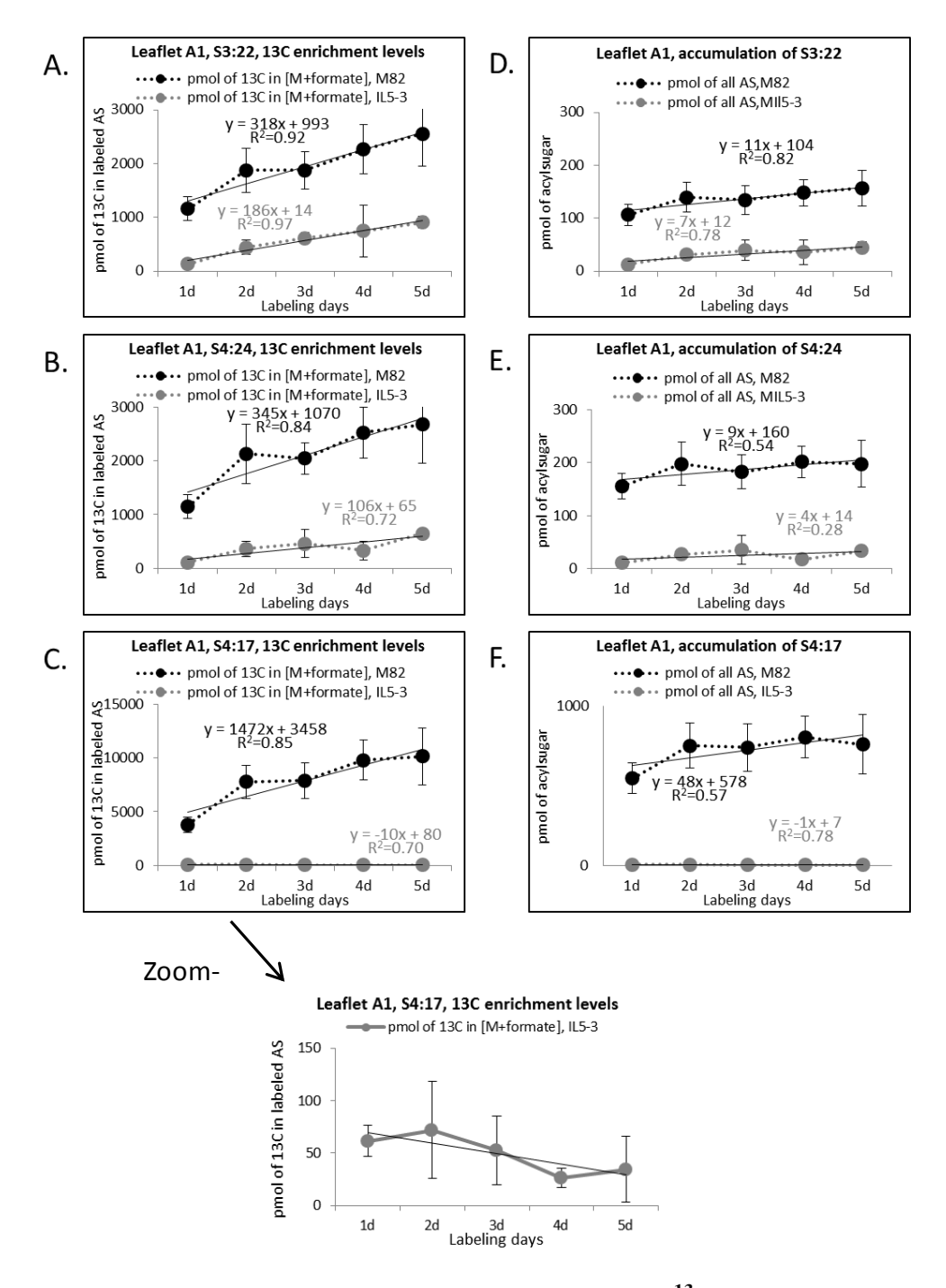
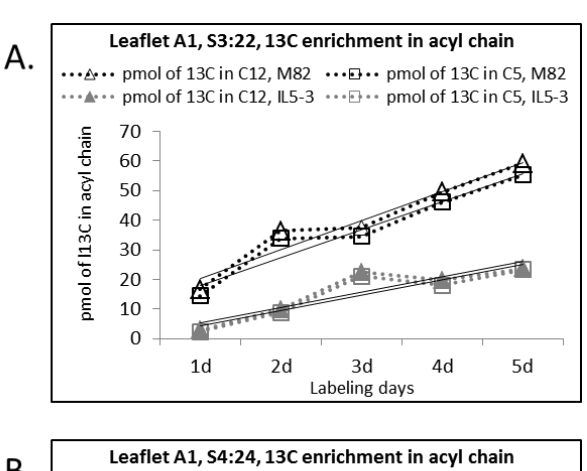


Figure 4.6. The slower biosynthesis rate of acylsugar from ¹³CO₂ in Leaflet A1 from **IL5-3 correlated with lower total accumulation levels relative to M82.** (A), (B) and (C): Picomoles of ¹³C incorporation in labeled acylsugars S3:22, S4:24 and S4:17 during the first five days of labeling; (D), (E) and (F): picomoles of acylsugar accumulation including all isotopologues for each of S3:22, S4:24 and S4:17 within this five days of labeling. For all six figures, black dots indicate result for M82, and grey dots indicate results for IL5-3. For figure C, the zoomed-in figure shows the picomoles of ¹³C incorporation in labeled S4:17 from IL 5-3 leaflet, which was barely detectable.

From the LC/MS data taken from tissues harvested during 1-5 days of labeling with ¹³CO₂, both relative and absolute levels of ¹³C incorporation were calculated from LC/MS data, and the slopes of the relationships between picomoles of ¹³C in acylsugars with labeling time reflect the rates of ¹³C incorporation through the entire pathway. The long chain acylsugars S3:22 and S4:24 accumulated ¹³C 2 to 3 times faster in M82 than in IL5-3 during the labeling period of Leaflet A1 as is evident from the greater slopes (Figure 4.6 A and B), while levels of these acylsugars, including both labeled and unlabeled forms, showed only slight increases (11 and 7 pmol/day for S3:22 in M82 and IL5-3, 9 and 4 pmol /day for S4:24 in M82 and IL5-3) during the same period (Figure 4.6 D and E). The slopes in the total AS levels are low, which suggests that the unlabeled pools for S3:22 and S4:24 in Leaflet A1 were substantial before the labeling began. Linear regression fit informed that the rates of ¹³C accumulation in S3:22 and S4:24 were 1.7- and 3.3-fold greater in M82 than in IL5-3 (318 and 345 vs. 186 and 106 pmol of ¹³C/day). These differences in net biosynthetic rate between M82 and IL5-3 corresponded with the differences in total acylsugar accumulation levels. For S3:22, the total accumulation rate in M82 (11 pmol/day) was 1.6-fold greater than in IL5-3 (7 pmol/day). Accumulation of total S4:24 in IL5-3 increased during the first 3 days of labeling, and then kept constant from 3-5 days (35 to 33 pmol). Since no genes in the introgression region in chromosome 5 were annotated as acyltransferase or CoA synthesis genes, the lower acylsugar and ¹³C accumulation rates of S3:22 and S4:24 in IL5-3 were initially interpreted to result from increased outflow of end product acylsugars within the trichome during this period, via degradation and/or transport to other tissues.

For acylsugar S4:17, which lacks a longer-chain acyl group (having only C5 and C2 esters), the accumulation levels in IL5-3 were barely above the detection limit, which stands in contrast to M82 in which S4:17 is the most abundant acylsugar and has a higher ¹³C accumulation rate (1472 pmol of ¹³C/day) than all other acylsugars (Figure 4.6 C). Other less-abundant short chain acylsugars that were measured in M82 extracts were not detected in IL5-3. The even lower accumulation rate of ¹³C into short chain acylsugars (Figure 4.6 F) is consistent with rapid degradation or export of these molecules from the trichome, given that no acyltransferase alteration is known in this region of the *S. pennellii* chromosome 5.



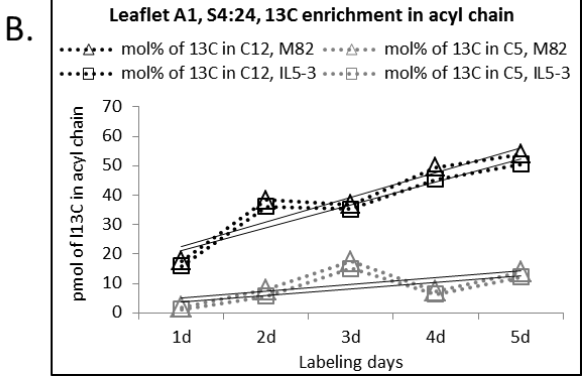


Figure 4.7. Incorporation of ¹³C into long chain (C12) and short chain (C5) esters of acylsugars from M82 and IL5-3. This was determined by measurement of label in fragment ions corresponding to C12 and C5 acid anions, are similar for both M82 and IL5-3 long chain acylsugar.

4.4.4 Rate of biosynthesis in acylsugar substructures

The incorporation of ¹³C into specific substructures of acylsugar metabolites reflects the synthesis rates and pool sizes for that part of the synthetic pathways, and the methods for measuring isotope enrichments in fragment ions using multiplexed CID was described in Chapter 3. For acylsugars containing long chains (e.g. C12), the short chains (e.g. C5) are derived from branched chain amino acid synthetic pathway, and the long chains are presumed to be derived from fatty acid synthesis and elongation pathways (ref). In this study, even though the ¹³C incorporation rates and accumulation levels of long chain and short chain acylsugars were different in IL5-3 and M82, the ¹³C incorporation rate into different acyl chains within a single acylsugar type were similar in both M82 and IL5-3. For instance, slopes of the trend lines for pmol of ¹³C in C12 and C5 group of M82 and IL5-3 in Figure 4.6 A show 9.8 and 9.4 pmol of ¹³C/day incorporated into the C12 and the two C5 acyl groups of S3:22 from M82, but only 5.1 and 5.1 pmol of ¹³C/day into the corresponding C12 and C5 acyl groups in S3:22 from IL5-3 (Figure 4.7 A). Similarly for acylsugar S4:24, slopes of trend lines for pmol of ¹³C in C12 and C5 group of M82 and IL5-3 in Figure 4.6 B show 8.4 and 7.8 pmol of ¹³C/day incorporated into the C12 and the two C5 acyl groups of S4:24 from M82, but only 2.4 and 2.2 pmol of ¹³C/day into the corresponding the C12 and the two C5 acyl groups from IL5-3 (Figure 4.7 B). This indicates that for both M82 and IL5-3, there is no distinguishing difference in the incorporate rates from C5 or C12 to the end product tri- and tetra- long chain acylsugars.

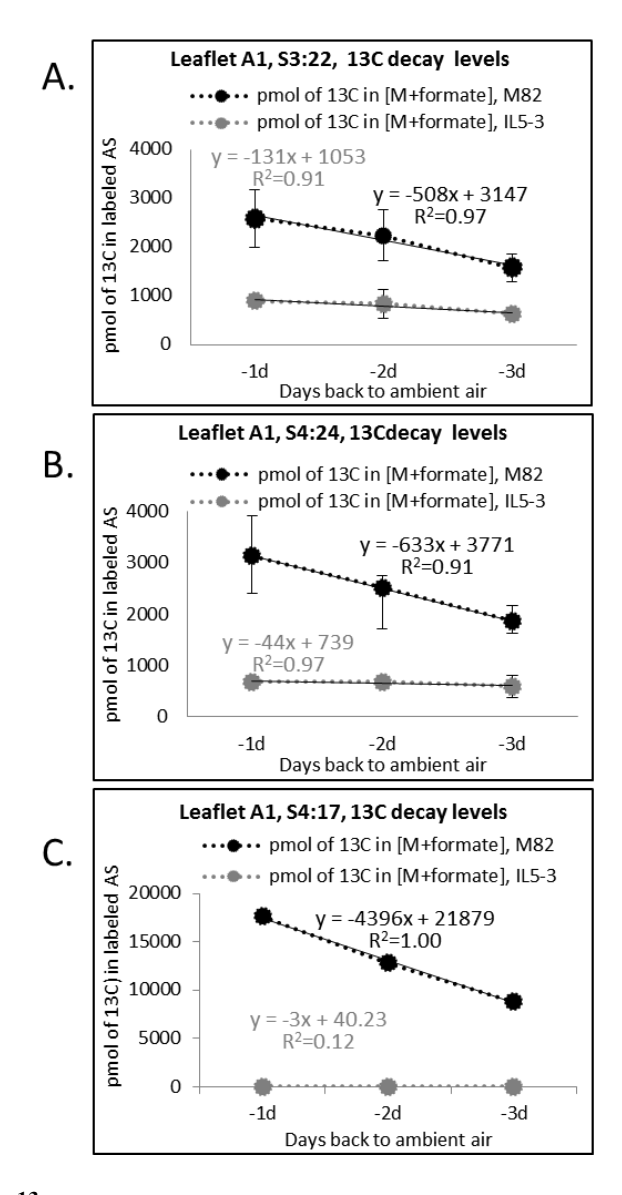


Figure 4.8. Decay of ¹³C content during the chase phase for long chain acylsugar end products S3:22, S4:24 and short chain acylsugar end product S4:17 in M82 and IL5-3. This data was from leaflet A1.

4.4.5 Rate of acylsugar degradation

Given that the accumulation rates of both long chain and short chain acylsugars were approximately 2-fold lower in IL5-3 than M82, we tested whether these differences were consistent with increased rates of degradation of S3:22, S4:24 and S4:17 in IL5-3. However, decay of ¹³C content during the post-labeling (chase) period showed the

opposite result (Figure 4.8). After five days of labeling the plants were returned to ambient air (CO₂ at natural isotope abundance) and leaflets were harvested daily for metabolite profiling. Disappearance rates of ¹³C in the labeled acylsugars reflect metabolite degradation or export at each developmental stage, but we have no evidence yet for acylsugar export to other tissues. As shown in Figure 4.7, the rate of disappearance of ¹³C in labeled S3:22 and S4:24 was ~4-fold lower in IL 5-3 than M82 (-131 vs. -508 pmol of ¹³C/day) for S3:22 and 14-fold lower (-44 vs. -633 pmol of ¹³C/day) for S4:24. As was the case for the accumulation rate, the rate of label disappearance in S4:17 was minimal because the levels of this acylsugar were barely above the detection limit. This indicates that the lower levels of S3:22 and S4:24 in IL5-3 cannot be attributed to more rapid degradation in IL5-3 alone. Based on mass spectrometry response factors for acylsucroses that have been recently reported [34] and trichome diameters observed using light microscopy [36], we estimate that concentrations of these acylsugars in M82 and IL5-3 trichomes are approximately equal to acylhydrolase K_{m} values (~17 $\,\mu\!M$ for hydrolysis of the 3-position ester of S3:22) described in a recent report [38]. At acylsugar concentrations around the $K_{\rm m}$, rates of hydrolysis would be expected to approximate a first-order rate law with the rate of hydrolysis proportional to acylsugar subtracts concentrations. Using this approximation, one obtains similar rate constants ($k_{M82}/k_{IL5-3} =$ 0.7) for hydrolysis of acylsugar S3:22 in M82 and IL5-3. This finding suggests that the corresponding hydrolase enzymes, if present in similar trichome levels in vivo in IL5-3 and M82, hydrolyze S3:22 substrates with almost equal efficiency in the two genotypes. These factors lead to our conclusion that ASH-catalyzed hydrolysis of S3:22 and S4:24 is not directly responsible for their lower levels in IL5-3

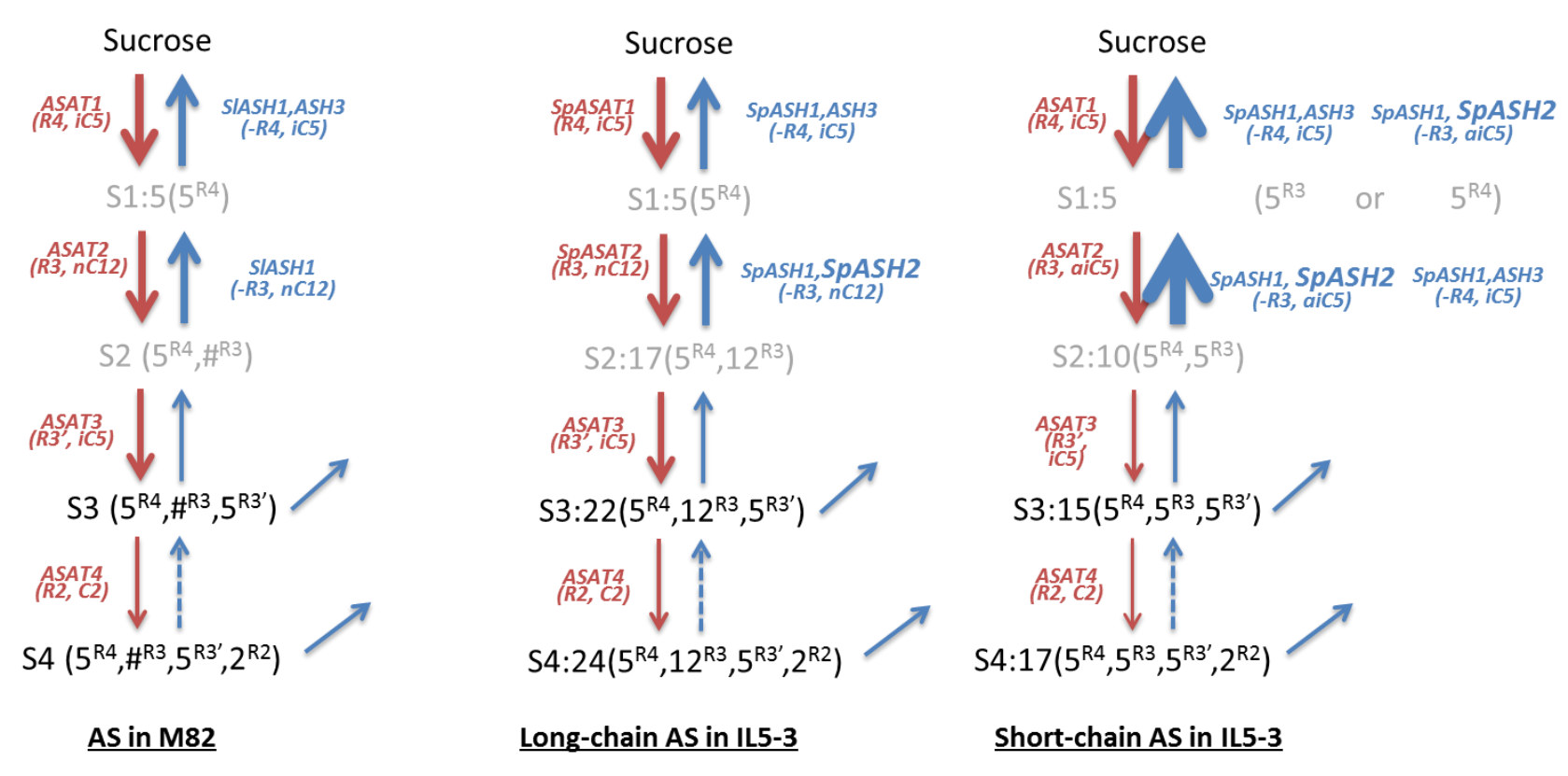


Figure 4.9. The illustration of pathways for synthesis and degradation of long chain and short chain acylsugars from M82 and IL5-3. The lower acylsugar "synthesis rate" in IL5-3 can be explained by higher rates of hydrolysis of mono- and di-acylsugar intermediates by *SpASH2*. The pathways for synthesis and degradation of long chain and short chain acylsugars are illustrated for M82 and IL5-3. Red arrows indicate biosynthesis and accumulation of intermediates and product acylsugars, blue arrows indicate hydrolysis and degradation. Grey S1 and S2 intermediates indicate that mono- and di- acylsugars have not been detected in extracts of *S. lycopersicum* trichomes.

At first glance, our flux analysis result stands in contrast with recent findings from bioinformatics analysis, *in vitro* biochemistry, and gene silencing experiments [37] that suggested highly expressed *SpASH2* (introgression of *S. pennellii* LA0716 genes) replaced *SlASH2* (from M82) in IL5-3 and catalyzed hydrolysis of long- and short-chain acylsugars in trichomes. One hypothesis that might resolve this disagreement proposes that the *S. pennellii* hydrolase (*SpASH2*) has higher catalytic efficiency in degrading mono- and di-acylsugars, which are metabolic precursors of the tri- and tetra-acylsugars, than the wild-type *SlASH2* that it replaces in IL5-3. Unfortunately, catalytic activities toward mono- and di-acylsugars were not reported in this recent paper owing to substrate scarcity. A more efficient hydrolysis of these early intermediates in IL5-3 would be expected to result in lower net rates of end-product synthesis, as was reflected in our labeling results.

The complexity of acylsucrose biosynthesis is reflected in Figure 4.9, which reflects the order in which acylation steps occur [38]. The sequential actions of ASAT1, ASAT2, ASAT3, and ASAT4 on sucrose catalyze acylations at the 4-, 3-, 3-, and 2-position oxygens, with the ability to form a 3-position long-chain ester. Accumulation of measurable amounts of mono- and di-acylsugars has been rare, and would be consistent with either their rapid further acylation or degradation. The acylsugars detected in IL5-3 have same acyl chain composition and positions of esterification as M82 acylsugars. No new acylsugar structure was identified in IL5-3, nor were less-acylated intermediates observed in the LC/MS profiles, which is consistent with no acyltransferase sequence found in corresponding chromosome 5 regions.

The potential substrate preferences of synthesis and degradation activities for chain substitution position and chain length of acyltransferase and/or acyl hydrolase activities add complexity to the IL5-3 phenotype. As showed in recent in vitro enzyme assays [20], the ASH2 enzymes hydrolyze both short chain and long chains esterified at the 3-position of tri- and tetra-acylsucroses, but have preference for short chain esters since no hydrolysis products were detected that had a C5 acyl chain removed and the long acyl chain remaining. We hypothesize that if mono- and di-acylsucroses were poorer hydrolase substrates when a longer chain (e.g. C12) ester was present on position 3, preferential hydrolysis of short-chain position 3 esters would explain the minimal abundance of tri- and tetra-acyl sugars with all short-chain acyl groups in IL5-3. This would also explain the decrease instead of total disappearance of long chain acylsugars in IL5-3, because once a long chain is added to the sucrose ring and formed an di-acylsugar (2nd step of acyl sugar acyl transfer), enzymatic hydrolysis is less efficient so the long chain di-acylsugar is more likely to be processed further downstream into tri- and tetralong chain acylsugars.

Similarly, in the same report which suggested when a long chain is at the 3-position, ASH1 did not hydrolyze acyl esters at the 4-position when tri- and tetra- AS were used as substrates. This indicated that 3-position long chain substitution also hinders the ASH activity on adjacent position (R4). This again resulted in more rigorous hydrolysis of short chain tri-/tetra- acylsugars than long chain tri-/tetra- acylsugars. Our labeling results suggest that this substrate preference is likely also true for mono-/diacylsugars substrates, in which a short-chain 3-position substitution did not protect the 4-

position short-chain from ASH1 hydrolysis, but long chain-3-position substitution did. Thus, limited amounts of short chain acylsugars were formed and accumulated in IL5-3.

4.4.6 The effect of leaflet developmental stage on acylsugar metabolism

Developmental stages of tomato leaflet regulate the accumulation and degradation activities in S. lycopersicum. We found out that younger leaflet (C1) trichomes are more active in acylsugar metabolism by monitoring the pmol of ¹³C incorporated into acylsugars (Figure 4.10) and the total acylsugar accumulation amounts (pmol) at different times using different leaflets which were at different developmental stages (Figure 4.11). At each sampling date, every individual leaflet of a young seedling was collected in separate tubes for extraction and LC-MS metabolite profiling (see Figure 4.5 for leaflet nomenclature). Figure 4.10 shows that for M82, the decay of ¹³C in labeled S3:22 from younger leaflet C1 (slope is -508 pmol of ¹³C/day, Figure 4.10 A) was faster than older leaflet A1 (slope is -637 pmol of ¹³C/day, Figure 4.10 B) during the first 3 days of back into ambient air growth. However in IL5-3, the situation was opposite to M82, with the older leaflet A1 showing a high decay rate (slope is -131 pmol of ¹³C/day, Figure 4.10 A) while the younger leaflet C1 showing a decay rate close to zero (slope is 11 pmol of ¹³C/day, Figure 4.10 B). This indicated that for IL5-3, younger leaflet C1 doesn't synthesis new unlabeled S3:22 nor degrade any existing labeled acylsugar S3:22 during these three days so that he disappearance rate of ¹³C was effectively zero. One plausible explanation for almost zero degradation is the low amount of labeled S3:22 acylsugar was synthesized and accumulated during the first several days of leaflet development, so that unlike in M82, substrates was hardly accumulated for degradation in leaflet C1.

However, we cannot rule out the possibility that acylsugar hydrolase are still capable to degrade end product S3:22 and mono- and di- AS intermediates very efficiently during early developmental stage of IL5-3, given that signal of labeled S3:22 was barely above the detection limit.

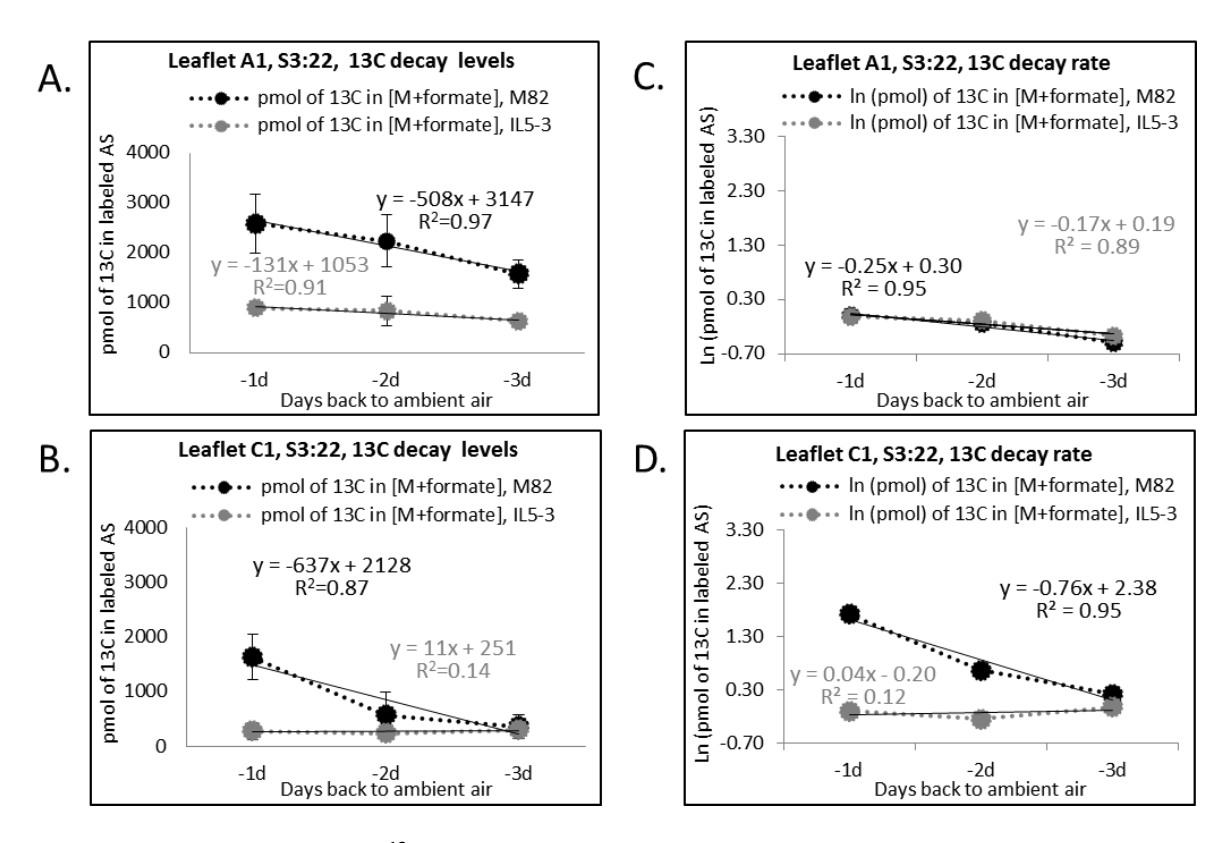


Figure 4.10. Decay of ¹³C **content during the chase phase for S3:22 in S.** *lycopersicum* **M82 and IL5-3 of leaflet A1 and C1.** Figure A and B are the pmol of ¹³C decay in labeled S3:22 during the first three days of chase phase growing in ambient atmosphere, C and D are natural log conversion of ¹³C decay data of A and B in Y-axis, in which the pmol of ¹³C was normalized to time zero (beginning of chase phase, five days of labeling). The slope of trending line in Figure C and D indicate the rate constant of decay in Figure A and B.

For both M82 and IL5-3, the total levels of acylsugar S3:22 in leaflet C1 increased and then reached a steady-state at after three weeks post germination. Figure 4.11 shows the total acylsugar accumulation for S3:22 across 10 days of sampling in

pulse and chase stage of labeling experiment. For leaflet A1, total S3:22 increased during the first 3-5 days and then remained constant afterwards (Figure 4.11 A and C). For leaflet C1, we were not able to collect the data for the first three days of pulse labeling because the leaflet was too small to be sampled. The total accumulation levels in leaflet C1 increased and eventually reached the levels of leaflet A1 at the last day of sampling, which is the case for both M82 and IL5-3, even though total accumulation of S3:22 is three times higher in M82 than IL5-3 (Figure 4.11 B and D). This result indicates that leaflet of different developmental stages synthesize and accumulate acylsugar at dramatically different rates, and reinforces the attention that harvesting time is important for comparative genomics and biochemical analysis when we monitor gene expression levels and enzyme activities for specialized metabolism.

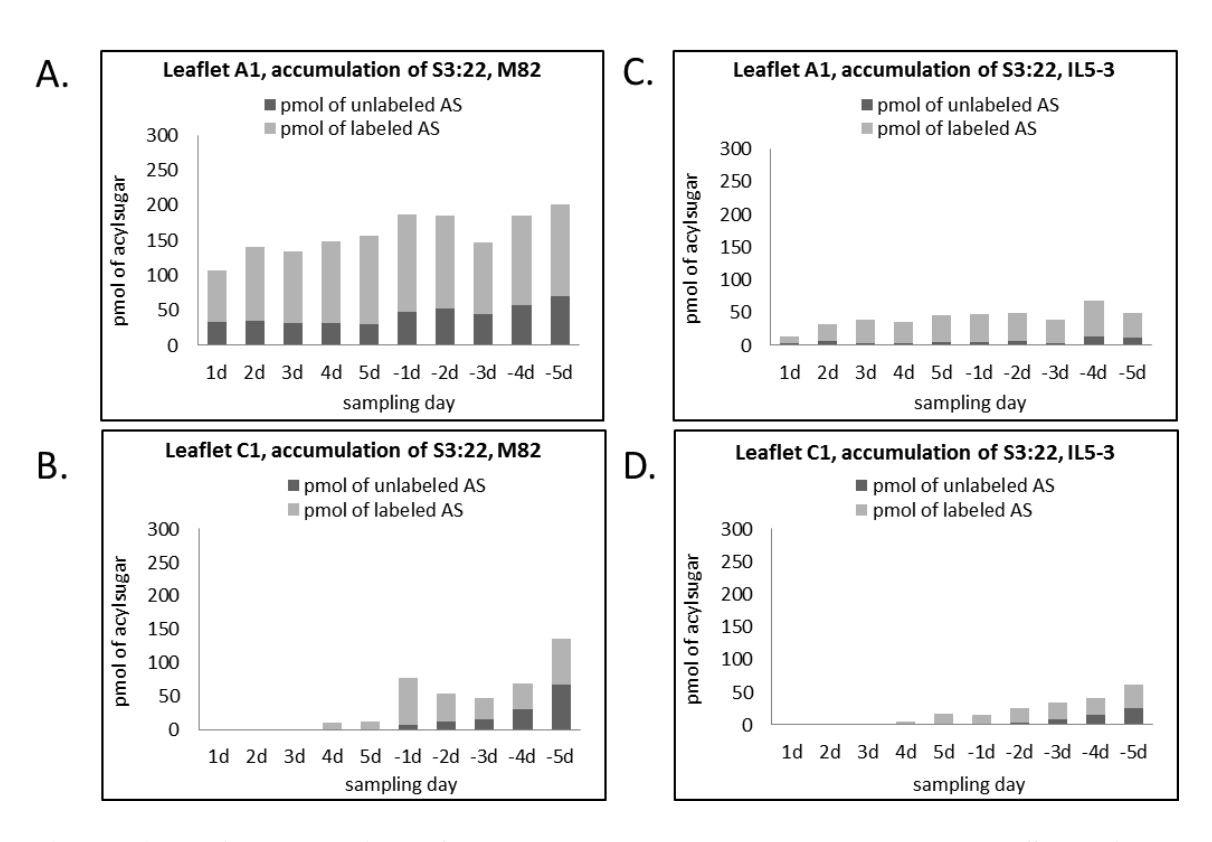


Figure 4.11. Accumulation of labeled, unlabeled and total acylsugar S3:22 in *S. lycopersicum* M82 and IL5-3 showing levels in leaflets A1 and C1.

4.5 Conclusions

The results described above provide a rare example of using ¹³C flux analysis to explain a mechanism that control accumulation of specialized plant metabolites that are synthesized by a complex metabolic network. By virtue of *in vivo* non-invasive tracing and analyzing ¹³C incorporation rates and metabolite quantities, evidence was generated for mechanisms that regulate acylsugar biosynthesis and accumulation in tomato trichome through degradation of intermediates. The concept that degradation of undetected intermediates provides a key regulatory point in the acylsugar metabolic network offers a new standpoint for engineering plant metabolic networks for high levels of end product acylsugars. This work extends our understanding on catabolic activities of specialized metabolites within Solanum trichomes and underscores the importance of metabolic flux analysis as an alternative strategy to fill in the knowledge gaps when the whole pathway is not clear.

Without authentic mono- and di-acylsucrose substrates, it has not yet been feasible to test whether the acylhydrolase actions on these metabolic intermediates are responsible for the IL5-3 metabolic phenotype. The labeling result is consistent with ASH in IL5-3 decreasing the net rate of biosynthesis of acylsugar end products by degrading early pathway acylsugar intermediates, and the slower ¹³C disappearance rates from labeled IL5-3 end products suggests the final biosynthetic steps are not the key determining factors of acylsugar accumulation levels.

REFERENCES

REFERENCES

- 1. Tissier, A. Glandular trichomes: what comes after expressed sequence tags? *The Plant Journal* **70**, 51-68 (2012).
- 2. Schilmiller, A.L., Last, R.L. & Pichersky, E. Harnessing plant trichome biochemistry for the production of useful compounds. *The Plant Journal* **54**, 702-711 (2008).
- 3. Schilmiller, A. *et al.* Mass spectrometry screening reveals widespread diversity in trichome specialized metabolites of tomato chromosomal substitution lines. *The Plant journal: for cell and molecular biology* **62**, 391-403 (2010).
- 4. Wagner, G.J. Secreting glandular trichomes: More than just hairs. *Plant physiology* **96**, 675-679 (1991).
- 5. Glas, J. *et al.* Plant Glandular Trichomes as Targets for Breeding or Engineering of Resistance to Herbivores. *International Journal of Molecular Sciences* **13**, 17077 (2012).
- 6. Schilmiller, A.L., Pichersky, E. & Last, R.L. Taming the hydra of specialized metabolism: how systems biology and comparative approaches are revolutionizing plant biochemistry. *Current opinion in plant biology* **15**, 338-344 (2012).
- 7. Kim, J. *et al.* Striking natural diversity in glandular trichome acylsugar composition is shaped by variation at the Acyltransferase2 locus in the wild tomato Solanum habrochaites. *Plant physiology* **160**, 1854-1870 (2012).
- 8. Simmons, A.T. & Gurr, G.M. Trichomes of Lycopersicon species and their hybrids: effects on pests and natural enemies. *Agricultural and Forest Entomology* **7**, 265-276 (2005).
- 9. Weinhold, A. & Baldwin, I.T. Trichome-derived O-acyl sugars are a first meal for caterpillars that tags them for predation. *Proceedings of the National Academy of Sciences of the United States of America* **108**, 7855-7859 (2011).
- 10. Hill, K. & Rhode, O. Sugar-based surfactants for consumer products and technical applications. *Lipid/Fett* **101**, 25-33 (1999).
- 11. Dembitsky, V.M. Astonishing diversity of natural surfactants: 1. Glycosides of fatty acids and alcohols. *Lipids* **39**, 933-953 (2004).
- 12. Chortyk, O.T., Kays, S.J. & Teng, Q. Characterization of Insecticidal Sugar Esters of Petunia. *Journal of agricultural and food chemistry* **45**, 270-275 (1997).

- 13. Ovenden, S.P. *et al.* Physaloside A, an acylated sucrose ester from Physalis viscosa. *Journal of natural products* **68**, 282-284 (2005).
- 14. Lerk, P.C., Sucker, H.H. & Eicke, H.F. Micellization and solubilization behavior of sucrose laurate, a new pharmaceutical excipient. *Pharmaceutical development and technology* **1**, 27-36 (1996).
- 15. Mutschler, M. & Wintermantel, W. Reducing Virus Associated Crop Loss Through Resistance to Insect Vectors, in *Natural Resistance Mechanisms of Plants to Viruses*. (eds. G. Loebenstein & J. Carr) 241-260 (Springer Netherlands, 2006).
- 16. Leckie, B., De Jong, D. & Mutschler, M. Quantitative trait loci increasing acylsugars in tomato breeding lines and their impacts on silverleaf whiteflies. *Mol Breeding* **30**, 1621-1634 (2012).
- 17. Leckie, B. *et al.* Quantitative trait loci regulating the fatty acid profile of acylsugars in tomato. *Mol Breeding* **34**, 1201-1213 (2014).
- 18. Ghosh, B., Westbrook, T.C. & Jones, A.D. Comparative structural profiling of trichome specialized metabolites in tomato (Solanum lycopersicum) and S. habrochaites: acylsugar profiles revealed by UHPLC/MS and NMR. *Metabolomics* **10**, 496-507 (2014).
- 19. D'Auria, J.C. Acyltransferases in plants: a good time to be BAHD. *Current opinion in plant biology* **9**, 331-340 (2006).
- 20. Schilmiller, A.L. & Moghe, G.D. Functionally divergent alleles and duplicated Loci encoding an acyltransferase contribute to acylsugar metabolite diversity in Solanum trichomes. **27**, 1002-1017 (2015).
- 21. Schilmiller, A.L., Charbonneau, A.L. & Last, R.L. Identification of a BAHD acetyltransferase that produces protective acyl sugars in tomato trichomes. *Proceedings of the National Academy of Sciences of the United States of America* **109**, 16377-16382 (2012).
- 22. Ning, J. *et al.* A feedback insensitive isopropylmalate synthase affects acylsugar composition in cultivated and wild tomato. *Plant physiology* (2015).
- 23. Ratcliffe, R.G. & Shachar-Hill, Y. Measuring multiple fluxes through plant metabolic networks. *The Plant journal : for cell and molecular biology* **45**, 490-511 (2006).
- 24. Shachar-Hill, Y. Metabolic network flux analysis for engineering plant systems. *Current opinion in biotechnology* **24**, 247-255 (2013).

- 25. Hall, R.D. Plant metabolomics in a nutshell: Potential and future challenges, in *Annual Plant Reviews Volume 43* 1-24 (Wiley-Blackwell, 2011).
- 26. Nagegowda, D.A. Plant volatile terpenoid metabolism: Biosynthetic genes, transcriptional regulation and subcellular compartmentation. *FEBS Letters* **584**, 2965-2973 (2010).
- 27. Bowsher, C.G. & Tobin, A.K. Compartmentation of metabolism within mitochondria and plastids. *Journal of experimental botany* **52**, 513-527 (2001).
- 28. Schellenberger, J. et al. Predicting outcomes of steady-state (1)(3)C isotope tracing experiments using Monte Carlo sampling. BMC systems biology 6, 9 (2012).
- 29. Boatright, J. *et al.* Understanding in vivo benzenoid metabolism in petunia petal tissue. *Plant physiology* **135**, 1993-2011 (2004).
- 30. Matsuda, F., Morino, K., Miyashita, M. & Miyagawa, H. Metabolic flux analysis of the phenylpropanoid pathway in wound-healing potato tuber tissue using stable isotope-labeled tracer and LC-MS spectroscopy. *Plant & cell physiology* **44**, 510-517 (2003).
- 31. Matsuda, F. *et al.* Metabolic flux analysis of the phenylpropanoid pathway in elicitor-treated potato tuber tissue. *Plant & cell physiology* **46**, 454-466 (2005).
- 32. Heinzle, E., Matsuda, F., Miyagawa, H., Wakasa, K. & Nishioka, T. Estimation of metabolic fluxes, expression levels and metabolite dynamics of a secondary metabolic pathway in potato using label pulse-feeding experiments combined with kinetic network modelling and simulation. *The Plant journal: for cell and molecular biology* **50**, 176-187 (2007).
- 33. Wang, Z. & Jones, A.D. Profiling of stable isotope enrichment in specialized metabolites using liquid chromatography and multiplexed nonselective collision-induced dissociation. *Anal Chem* **86**, 10600-10607 (2014).
- 34. Ghosh, B. & Jones, A.D. Dependence of negative-mode electrospray ionization response factors on mobile phase composition and molecular structure for newly-authenticated neutral acylsucrose metabolites. *The Analyst* **140**, 6522-6531 (2015).
- 35. Eshed, Y. & Zamir, D. An introgression line population of Lycopersicon pennellii in the cultivated tomato enables the identification and fine mapping of yield-associated QTL. *Genetics* **141**, 1147-1162 (1995).

- 36. Li, C., Wang, Z. & Jones, A.D. Chemical imaging of trichome specialized metabolites using contact printing and laser desorption/ionization mass spectrometry. *Anal Bioanal Chem* **406**, 171-182 (2014).
- 37. Schilmiller, A.L., Gilgallon, K., Ghosh, B., Jones, A.D. & Last, R.L. Acylsugar acylhydrolases: carboxylesterase catalyzed hydrolysis of acylsugars in tomato trichomes. *Sumited to Plant Journal* (2015).
- 38. Fan, P. *et al.* In vitro reconstruction and analysis of evolutionary variation of the tomato acylsucrose metabolic network *Sumited to PNAS* (2015).

Chapter 5. Perspectives for Future Research

Modern research holds the promise to deliver fundamental knowledge that will guide molecular engineering of plants for higher yields of renewable resources including food, medicinal compounds, fibers and energy-related materials. To address the challenge of uncovering complex systems that control biological processes, multidisciplinary cooperation between plant biochemistry, physiology, genetics, chemistry and ecology can provide stepping stones to further the way of exploration. The hidden mechanisms coordinating and controlling plant specialized metabolism are extremely sophisticated pieces of art designed by nature and polished by evolution. To unveil these delicate networks among plant cells and tissues, novel high-throughput technologies in characterization of genes, transcripts, proteins and metabolites are leading the way by generating tremendous amounts of information that represent the functions of cellular metabolic machinery. To summarize and integrate all the information and use it to deduce comprehensive understanding of how plants synthesize and store bioactive compounds is one of the systematic challenges in plant biology.

To move such research efforts forward, this dissertation has presented advances in the development and application of techniques to investigate the dynamics, distribution and development of specialized metabolism in glandular trichomes of tomato and its wild relatives as part of the National Science Foundation-funded 'Solanum Trichome Project' (https://trichome.natsci.msu.edu/). The long term goal of this project has been to understand the regulation of developmental and metabolic activities of a variety of secreting and glandular trichomes within the genus *Solanum* and to rigorously test their biological functions. Previous research achievements on metabolic profiling and gene discovery answered some of the 'What' questions about trichome specialized metabolites

and synthetic pathways, and have led to the following 'When', 'Where', and 'Regulation' questions, which were partially answered by this dissertation in Chapters 2, 3 and 4.

Chapter 2 addressed the 'Where' question of trichome metabolites by employing a matrix-free mass spectrometry imaging technique. This chapter described a simple sample preparation method that transfers the trichomes and their metabolites onto a graphite plate by contact printing and avoids damaging the integrity of metabolite localization. Trichome metabolites are then profiled and visualized using carbonsubstrate-assisted laser desorption/ionization (LDI) mass spectrometry. Various specialized metabolites including terpenes, alkaloids and acylsugars are detected at single-gland resolution. This LDI imaging of leaf trichome is applied to explore the heterogeneous distribution of trichome metabolites across the surface of Solanum leaf tissues. Because single-ion abundance maps for acylsucroses are achieved using this micro-collection of compounds, imaging data can support the consistency between reduced expression of the acyltransferase (SIASAT4) and the absence of specific gene functions (absence of tetraacylsucrose products). One limitation in this approach is the massive amount of data generated for each image, which often consists of tens of thousands of individual mass spectra. There is a need for continued development of software tools that can facilitate more detailed analysis of MS imaging data.

Chapters 3 and 4 together address the dynamics and regulation of specialized metabolism, the 'When' and 'Regulation' questions. Chapter 3 describes a stable isotope labeling and measurement methodology for tracing specialized metabolite fluxes in trichomes. In general, an integrated approach combining whole plant ¹³CO₂ labeling and data-independent LC-MS quantitative profiling was developed to monitor the dynamic

flux and turnover rate of protective plant specialized metabolites. For accurate quantitative analysis of ¹³C incorporation into the substructure of the metabolites, multiplexed nonselective collision induced dissociation (CID) was applied for assessment of ¹³C enrichment in both molecular and fragment ions. For data analysis, the time dependent label enrichments were calculated based on mass isotopologue abundances and isotopologue ratios. This analytical strategy is applicable to a wide range of specialized metabolites as well as alternative techniques for ion activation, since ¹³CO₂ is a universal tracer incorporated through photosynthetic carbon fixation and the entire plant metabolome is labeled within an experiment growth. Application of this mass spectrometric profiling and ¹³C tracing method to trichome metabolite investigation is then described in Chapter 4. In this chapter, the quantification of stable isotope incorporation and fluctuations during different tomato leaf developmental stages were measured for M82 and one introgression line IL5-3. This study demonstrated that total acylsugar accumulation reaches a steady state at an early stage of development (within three weeks old). However, the steady state is dynamic at the same time, meaning biosynthesis, reassembly and degradation was also happening. Evidence was generated to support the concept that degradation of undetected metabolic intermediates provides a key regulatory point in the acylsugar metabolic network offers a new viewpoint for engineering plant metabolic networks for high levels of end product acylsugars. This novel regulation mechanism extends our understanding of catabolic activities of specialized metabolites. Perhaps more important, this work underscores the importance of metabolic flux analysis as an alternative strategy to fill knowledge gaps when the whole metabolic pathway is not clear. Together, Chapter 3 and 4 demonstrate that improved

understanding of the biochemical basis for plant specialized metabolic networks demonstrate that there are still significant challenges for future metabolic engineering of crop plants.

The achievement of this dissertation is just the beginning of tempo-spatial dynamics investigation on specialized trichome metabolites and the regulation mechanisms of different genotypes. For instance, the research results in Chapter 4 identify the need to generate authentic mono- and di-acylsucrose standards as subtracts for hydrolase activity and enzyme kinetics testing. The scarcity of authentic substrates makes it difficult to test whether the acylhydrolase actions on these metabolic intermediates are responsible for the IL5-3 metabolic phenotype. Given the important roles in both synthesis and turnover of metabolites, a systematic analysis of gene families involved will be essential for rational engineering of biosynthetic pathways of valuable products in plants.